DETERMINATION OF THE DISTRIBUTION OF WATER DROPLET SIZES IN BUTTER AND MARGARINE USING PULSED FIELD GRADIENT–NMR AND CONFOCAL SCANNING LASER MICROSCOPY

This thesis was presented in partial fulfillment of the requirements for degree of Master of Science in Chemistry at Massey University

吕　明

Ming Lu

1999

献给：

我的父母，

姐妹，

毛毛，

爱我的人.

Abstract

PFG-NMR has been used to determine the distribution of water droplets in emulsions. Especially, it has been used to measure the samples with high optical dense systems and highly viscous systems Butters and Margarines).

To refine the method, the optimum measuring condition was investigated. It included delay time (Δ) between the field gradient pulses, τ null (τ_0), gradient strength (G), water self-diffusion coefficients (D) and sampling techniques. Under the optimum conditions the water droplet size distributions of commercial butters, experimental butters and margarines were measured.

Experimental results showed that PFG-NMR is an accurate, fast method to determine the water droplet size distributions of the butters and margarines. Also, it is can be used to investigate the properties of dispersed phase in emulsions. Especially, the method is suitable not only in the laboratory but also in the factory environment. The method was able to distinguish different distributions in butters of the same water content but with different manufacturing techniques. Differences in the distributions of water droplets were also obtained when comparing butters made by the same manufacturing technique but with different water contents.

To confirm the results from PFG-NMR, confocal scanning laser microscopy (CSLM) was chosen to determine the droplet size distributions and the moisture contents of samples. Comparison between PFG-NMR and CSLM shows limitations in the latter techniques and its uses are limited.

Acknowledgments

I would like to thank the following people who gave me great assistance when undertaking my studies at New Zealand Dairy Research Institute (NZDRI) and Massey University.

The biggest thanks go to my co-supervisors for their supervision and enthusiasm during the research of this project: Associate Professor Ken Jolley (Massey University) and Principle Research Scientist Alastair H MacGibbon (NZDRI).

Special thanks go to the Professor Andrew Brodie (Massey University).

If there are not their kind encouragement and assistance, I would not have finished my study in Massey University.

I wish to further thank the following people. Much of the work would not have been possible without the gratefully acknowledged contributions from the these people:

Yvonne van der Does (NZDRI) for her kind assistance in the project.
Tony McKenna (NZDRI) for help in the study of Confocal Scanning Laser Microscopy (CSLM).
Robyn L Hisrt (NZDRI)for help in the sample preparations of CSLM.
Dr. Pat W M Janssen (NZDRI) for introducing me to use the VIPS program of image analysis and refine the program.
Susan Lane (NZDRI) for separation of the aqueous phase and the milkfat phase from butters.
Dr. Sarah L Codd (Massey University) for high resolution NMR measurements (Bruker AMX 300).

Dr. Pat J B Edwards (Massey University) for high resolution NMR measurements (JOEL-GX 270).

My Chinese friends: Dr. Yinqu Wu, Dr. Fuguang Cao and Yuming Li.

Thanks also to members of the Food Science Section of NZDRI and the Institute of Fundamental Sciences for their assistance and help.

Thanks to other who have helped me directly and indirectly, thank you.

My thanks to the Studentship Fund from NZDRI.

I would finally like to thank the members of my family:
I great thank my older sister for her encouragement and assistance honestly, thank my parents for their support and thank Pinlei Lu – my son.

TABLE OF CONTENTS

List of Figures

List of Tables

1.0 Introduction

Eating is one of the most pleasurable activities in our life. When you think about the safety, the nutrition and the taste of foods, you may realise that many factors contribute to them. These factors are mainly caused by components in foods, though there are effects from environmental factors. Among the components, water is probably the most common and also the most important component of foods because it affects food texture, quality, microbiological safety and nutritional status and digestibility.

Butter is one of the most delicious, flavourful and also powerful of all food. The power for good or evil is beyond compare. Their good can be enjoyed every day and their evil power can be controlled by limited consumption, not by their elimination from the diet. Thus, the horrors of heart disease as well as other serious health afflictions – and complications – of evil design can be well thwarted without giving up one of nature's most mystic of all foods. No one can escape from its taste and fragrance [1].

Margarine mimics butter in composition and texture, but has a less complex flavour profile.

Butters and margarine are " water in oil " emulsions, but as the oil phase is partially solid, they have a plastic nature in the continuous phase. The structures of butter and margarine have similarities and differences. When butter is made, the first basic step is that milkfat is crystallised by holding the cream at low temperature [2], and the churning step involves a phase inversion from a fat-in-water emulsion (cream) to a water-in-fat emulsion (butter). In this process, some of the membranes of the fat globules are

disintegrated, and the fat coagulates into grains of butter. The crystalline fat can form three dimensional networks with liquid fat intermeshed between the fat crystals. Both products contain water in the form of water droplets. In addition, butter also contains intact fat globules and globule fragments which are not found in margarine [3]. Butter contains about 80 wt% fat as the continuous phase and about 16 wt% water as the disperse phase. Salt, protein and lactose are dissolved in the aqueous phase. Margarine has a similar composition if it uses skim milk as part of the aqueous phase, as is the case in New Zealand. The continuous milkfat phase is stabilized by the fat crystal network (see Figure 1 and Figure 2).

Figure 1. General view of the fine structure of butter. Water droplets (W) are dispersed in the continuous fat phase (C), which contains a varying amount of more or less undistorted fat globules (G).

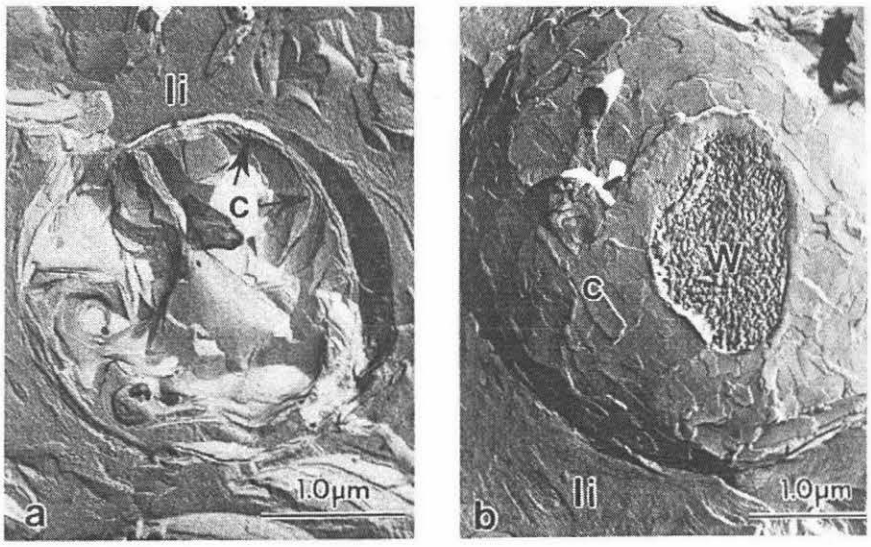

Figure 2. Detailed views of the structure of butter showing (a) a cross-fractured largely intact fat globule within the continuous fat phase (c: crystalline shell, li: liquid fat); (b) a peripherally fractured water droplet covered with a layer of fat crystal (c: crystalline fat, li: liquid fat, W: water phase).

(Figure 1 and Figure 2 are reprinted from Wolfgang Buchheim and Petr Dejmek, Food Emulsions: Milk and Dairy-Type Emulsions, Third Ed, edited by Stig E. Friberg and Kåre Larsson (1997) 235~278)

Water-in-oil (W/O) emulsions (butter, margarine, spreads) are not stabilised simply by forming an adsorbed layer of surfactant which minimises the effects of the interfacial energy. Other important factors in stabilising these emulsions are the crystallinity of the oil phase, and the presence of agents that increase the viscosity of the aqueous phase in the droplets.

In butter and margarine, the moisture dispersion is critical as it influences the microbiological stability of the product because the growth of pathogenic micro-organisms in food materials is determined by the local availability of water to the bacterial cells. Bacteria require certain nutrients for their growth, and the need for nutrients varies widely among different bacteria. The main sources of food are organic compounds. e.g. proteins, fats, carbohydrates, trace elements and vitamins. The micro-organism, saprophytes, can live on dead organic matter. The other micro-organism, parasites, can live on living organic matter. As well as material for cell formation, organic matter also contains the energy necessary for micro-organism growth. Such matter must be soluble in water and have a low molecular weight in order to be able pass through the cytoplasmic membrane of the bacteria (semi-permeable membrane which performs many vital functions, including regulation of the exchange of salts, nutrients and metabolic products between the cell and its environment) and be digested by the bacterium. Consequently bacteria need access to water and small droplets (<20 μm diameter) are desirable so as to minimise this access.

In addition, for desired texture and appearance the droplets need to be small enough (<30 μm) to prevent the formation of channels and lakes. These affect the appearance and texture of the product. However, the taste and flavour release requires large enough droplets to allow phasery inversion (from W/O to O/W) and flavour release in the mouth. Small droplets are stable and more difficult to invert. So droplet sizes should not be too small. Quite small water droplets and uniform droplet sizes lead to a lighter and more even colour distribution and loss of water changes in colour, a phenomenon known as "primrosing".

Because the size and distribution of the water droplet is closely linked with the shelf–life of the butter, the International Organization for Standardization laid down the international standard for water dispersion in 1985 [4]. This is a very crude method which only shows very large droplets ("lakes"). Special indicator paper was used to bring in contact with a freshly cut plane of butter to determine the water dispersion. Moisture occurring in large drops causes spots on the indicator paper which indicates number, shape and size. Estimation of the dispersion is made by comparison to a standard scale. However, only large drops are observed. In general, a closed W/O structure with a small droplet size can be influenced by the mixing during manufacture and the interactions of the components [5-7]. In summary, many properties of butter are affected by the water droplet size distribution in the butter and a quick, accurate and reliable method to determine the droplet size distribution in emulsions is needed..

The particle size distribution in water-in-oil emulsions is more difficult to characterise than in oil-in-water emulsions. Several methods pre-suppose a dilution of the emulsion with the continuous phase which is difficult for butter or margarine because coalescence of the droplets is rapid when the crystal network is broken down during dilution [8].

Optical methods that have been used to determine droplet size distribution are limited in the sense that only the surfaces of the butters or the margarines are seen and sample preparation and treatment tend to be time-consuming and may introduce artefacts [9]. In addition, the resolution is rather limited (> 10 μm) and undisturbed observation of the sample is difficult, especially when deeper layers must be probed.

Electron microscopy [10] has the advantage of a high resolution (~ 1 nm) and it can be used to determine the number-average size distribution, providing that a fully representative sample of the emulsion is prepared, fixed, mounted, sectioned and stained without distortion, a sufficient number of particles are measured to ensure statistical accuracy of the distribution, and that proper account is taken of the effects of two–dimensional sectioning on the apparent droplet diameter. However, it is generally very laborious and requires elaborate sample preparation that may lead to artefacts. In addition, transmission electron microscopy provides static two–dimensional images that are difficult to reconstruct three-dimensionally from serial sections. This is not a technique to be used routinely to determine size distribution. Confocal scanning laser microscopy (CSLM) can be also used [11 ~ 14]. The basic principle of the confocal microscope is that a point in the object is optimally illuminated and also optimally imaged in the detector pinhole. This leads to an increased resolution and a reduced depth of field because off-focus levels in the specimen will hardly contribute to the image. Confocal scanning laser microscopy has advantages over conventional light microscopy and electron microscopy in that optical sectioning can be undertaken, so that a disturbance-free observation of the three-dimensional internal structure can be achieved. CSLM techniques have been applied to the study of emulsion systems [15 ~ 17] and dairy products [18 ~ 23].

It has long been recognized that NMR can be of use to the food scientist and food processor. One of the earliest references to the use of NMR in foods for moisture measurement is dated 1957 [24]. However, it is only within the last 10 to 12 years that there has been consistent and widespead growth of the use of NMR for this purpose. This is probably the result of three factors. The first is the increasing sophistication and relative ease of use of NMR instrumentation. This has meant that, for example, multinuclear and solid-

state methods have become much easier to apply. The second is the increasing need of the food industry to understand and innovate in its products and process. Finally, there is the pressure for new methods to enforce legislation and control quality.

The nature of food has led to the choice of NMR as an investigative method for the same reason that NMR is being increasingly used for the study of biological system. The requirement in both cases is to have a non-invasive technique that can extract useful information from a chemically complex and highly heterogeneous system. In foods the requirement for non-invasiveness stems not from any ethical consideration but from the need to preserve and examine the food structure [8].

Low resolution NMR can be used to study the bulk properties of food emulsion systems. For example, determining the droplet size distribution of spreads such as margarines and butters. Because of the modest price and the relative simplicity of the low resolution NMR equipment, this method can be used in a factory environment. When using this method all protons, originating from oil and water, resonate at the same position of the spectrum. Because we are only interested in the contribution of the protons of the discontinuous phase (water, in case of an W/O emulsion), the contribution of the ^{1}H nuclei in the continuous phase (the oil phase in a W/O emulsion) has to be selectively eliminated. A technique that will enable this to be done is pulsed field gradient nuclear magnetic resonance spectroscopy (PFG– NMR).

PFG-NMR technique was first described by Stejskal and Tanner [25 ~ 27]. In addition to their work on unrestricted diffusion they also performed

theoretical analyses of restricted diffusion and tested their results on octanol-in-water emulsions stabilized by surfactants.

Packer and Rees [28] extended the work of Stejskal and Tanner by the development of a theoretical model using a log-normal size distribution function. Measurements made on two water-in-oil emulsions were used to obtain the self-diffusion coefficient. D of the water in the droplets and σ and ξ, the width and median diameter of an assumed log-normal distribution of droplet radii. Since then, NMR has been widely used for studying the configuration and dynamics of molecules in a variety of systems. For example, PFG-NMR has been used to measure self-diffusion coefficients of water in plant cells [29] but NMR studies on emulsions are sparse.

In 1983 Callaghan et al. [30] presented a paper about the diffusion of fat and water in cheese as studied by PFG-NMR. The water diffusion coefficients found were one-sixth of that of bulk water at the same temperature. The authors suggested that water diffusion is confined to surfaces within the protein matrix. The fat is present in the form of small droplets within the cheese. The size distribution of fat droplet was obtained by fitting the data to a Gaussian distribution of sphere volumes.

Fleisher et al. [31] studied the self-diffusion of oil and water in rape seeds. The self-diffusion of oil was found to be restricted. The experiments could be explained in terms of the model of diffusion within spherical droplets and a Gaussian mass distribution of the droplet radii.

Van den Enden et al. [32] gave a rapid method for the determination of water droplet size distributions in spreads by using low resolution pulsed field gradient NMR in 1990. This was same technique with Fleisher's report.

Cory and Garroway [33] introduced the NMR pulsed gradient stimulated echo method to study compartments which are too small to be observed by conventional NMR imaging. They showed so-called proton displacement profiles of bulk water and dimethyl sulfoxide. The displacements are due to free diffusion and are Gaussian shaped. The profile of water in yeast cell showed restricted diffusion with a characteristic cell width of approximately 5 μm.

Lönnqvist et al. [34] performed NMR experiments on emulsions stabilized by surfactants to obtain information about the droplet size and size distribution and whether a particular emulsion is of the O/W or the W/O type. Murday and Cotts' equation [35] was used with different droplet radii, each radius being weighted by its normalized volume fraction.

Söderman et al. [36] have published an overview of NMR self-diffusion studies of emulsion systems. They concluded that a log-normal distribution function gives a better fit than a normal distribution. Several examples are given including margarine and hydrocarbon gel emulsions.

Hills and Snaar [37] used PFG-NMR to study cellular tissue and related multicompartment systems. They showed how to obtain dynamic information about membrane permeability and intend to use the given strategy to study plant tissue and food preparations.

Li et al. [38] performed PFG-NMR experiments on oil-in-D_2O emulsions. D_2O, with similar chemical properties as H_2O, was chosen because the NMR resonance frequency of deuterium is quite different from that hydrogen. Therefore they could select the experimental parameters so that only NMR signals from oil molecules are observed. In their calculations

they assumed a log-normal distribution. Because of the very different diffusion coefficients of the two oils used (n-hexadecane and n-octane), they were only able to obtain stable converged distribution parameters for the n-octane sample during the non-linear fitting procedure.

Balinov et al. [39] applied PFG-NMR to a system with permeable barriers. The system used was a highly concentrated emulsion consisting of 97 % water with an internal structure of closely packed water droplets that are separated by thin oil films. These oil films belong to the general class of porous systems. They reported that under certain conditions one may actually detect diffraction-like effects when the PGSE experiment is applied to an emulsion system. From the experiment the mean droplet size may be determined. PFG-NMR was discussed and applied to some low calorie spreads and margarines ranging in fat content from 40 to 80 %. The results showed that the droplet size distribution is fairly polydisperse, at least for the solid margarines studied. The parameters of the log-normal function were determined by a least square fit directly on the experimental raw data for all the systems studied. The uncertainties in the obtained parameters are judged by means of a Monte Carlo technique [9].

The principles of magnetic resonance imaging (MRI) have been covered in a number of textbooks [40 ~ 42] and reviews [43~ 44]. In clinical applications MRI is invaluable in providing high-resolution images revealing anatomical features in a non-invasive way. However, this is not usually the case with food imaging since high-resolution "anatomical" or structural information is most simply obtained by visual or microscopic examination after physically slicing the food sample. There are, of course, advantages in being able to examine foods non-invasively with MRI, but the unique value of food imaging lies in the information not readily obtainable by any other physical

technique. This information is contained in the spatial dependence of the NMR parameters determining image contrast. Food imaging by NMR is still in its infancy [45 ~ 46]. So far most work has merely explored the feasibility of using imaging methods to investigate topics of interest in food science such as drying or crystallization. Ruan et al. [47] obtained separate magnetic resonance images of water and fat in oil-in-water emulsions and cheese blocks by the use of the chemical shift selective suppression technique.

The aim of this research is to refine a methodology using PFG-NMR, so that it can be used as a routine analytical method to determine the water droplet size in New Zealand butter and spreads and to compare and confirm the results obtained with these obtained from high resolution PFG-NMR experiments and with confocal scanning laser microscopy.

2.0 Background theories and techniques

2.1 Pulse field gradient NMR method (PFG-NMR)

2.1.1 Basic theory of pulse field gradient NMR method

Low resolution PFG-NMR is unable to resolve the individual proton environment so all protons, originating from oil and water, resonate at the same position of the spectrum. Because we are only interested in the contribution of the protons of the discontinuous phase (water, in case of an W/O emulsion), the contribution of the ^{1}H nuclei in the continuous phase (the oil phase in a W/O emulsion) has to be selectively eliminated. However, because of the modest price and the relative simplicity of the low

resolution NMR equipment, there are advantages in that this method can be used in a factory environment.

A high resolution NMR spectrometer is built around a superconducting magnet with a very strong and homogeneous magnetic field and, consequently, is very expensive. Furthermore, high resolution spectrometers require air conditioned environments which make that unsuitable for use within a factory environment. Nevertheless, high resolution NMR spectroscopy has some important advantages over low resolution NMR. By changing magnetic field strengths (e.g. from 0.47 T when using a spectrometer operating at a 20 *MHz* proton frequency to 6.35 T for a 270 *MHz* spectrometer) the sensitivity can be increased to a great extent, since the quanta absorbed are larger and the resonance is correspondingly stronger [48~49]. Secondly, the high resolution method is much more selective. The acquired free induction decay can be Fourier transformed and the peaks in the spectrum, originating from the oil and water are very well separated. In this way one can obtain information about the continuous as well as the discontinuous phase at the same time. An example is given in Figure 3. which shows experimental proton spectra of butter we obtained. These advantages allow its use as a standard against which to compare low resolution measurements.

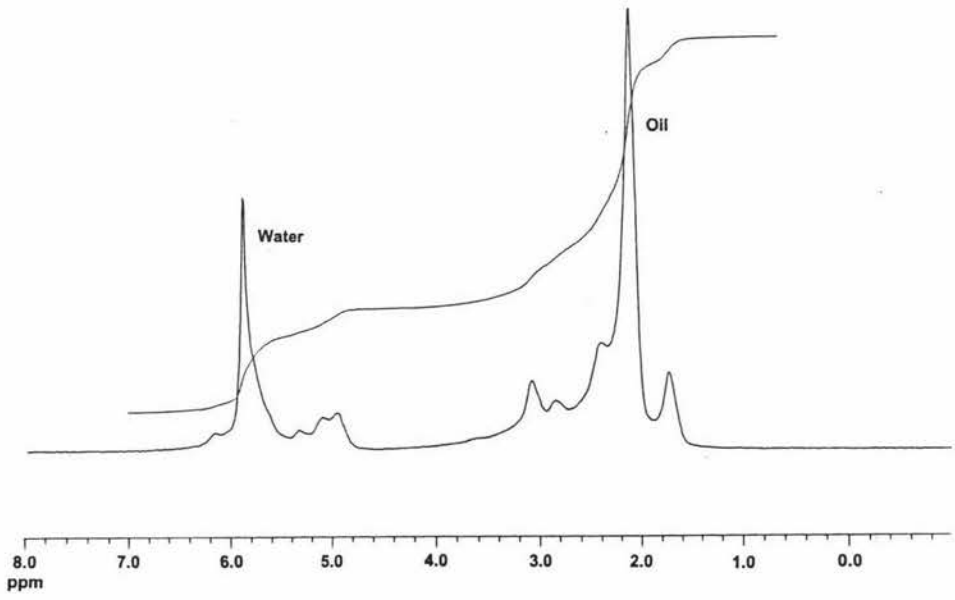

Figure 3. High resolution proton NMR spectra of butter. Measurement was performed on a JOEL GX-270 spectrometer, operating at 270 MHz. The water and oil protons are clearly distinguished.

The PFG – NMR technique can provide self-diffusion coefficients with good precision in a few minutes, without the need for isotopic labelling. Self-diffusion data provide unique, detailed and easily interpreted information on molecular organization and phase structure. However, in most heterogeneous food materials, water diffusion is restricted by the presence of solid inclusions, fat or oil phases, cell wall or lipid membrane barriers. Simple analytical expressions for the distribution do not exist and the relationship between the microstructure and the distribution is far from straight forward. Much work remains to be done both theoretically and experimentally to explore this relationship. The difficult nature of this problem probably accounts for the relatively few reports of PGSE measurements of water in complex food materials since its inception in

1965. However, this situation may well change with the reformulation of the PGSE experiment as " q-space microscopy " by Callaghan et al. [50 ~ 53].

Recently, the principles of self-diffusion measurements by pulsed gradient spin echo techniques have been reviewed [8] [45] [54 ~ 57].

Nuclei such as ^1H in water and fat molecules behave as charged bodies with a magnetic moment, and will precess about an externally applied magnetic field (B_0) (see Figure 4). The frequency of procession (the Larmor frequency, ν_0) is proportional to the strength of the external magnetic field, i.e.

$$\nu_0 = \gamma (B_0 / 2\pi) \qquad (1)$$

where γ is gyromagnetic ratio ($= 2.675 \cdot 10^8$ (T s)$^{-1}$ for protons).

NMR experiments essentially involve labelling molecules using the characteristic Larmor frequencies of the component nuclei (Figure 4). The labels may, in addition, be given a spatial dependence by the imposition of a well-defined magnetic field gradient over the sample space.

Very sensitive precessional phase displacements may be detected in an NMR spin-echo experiment and the echo signals may be used to measure molecular translational motion (Appendix 1). The magnetic field gradient may be applied in the form of pulses between the transmission and receiving periods of the NMR spin-echo experiment.

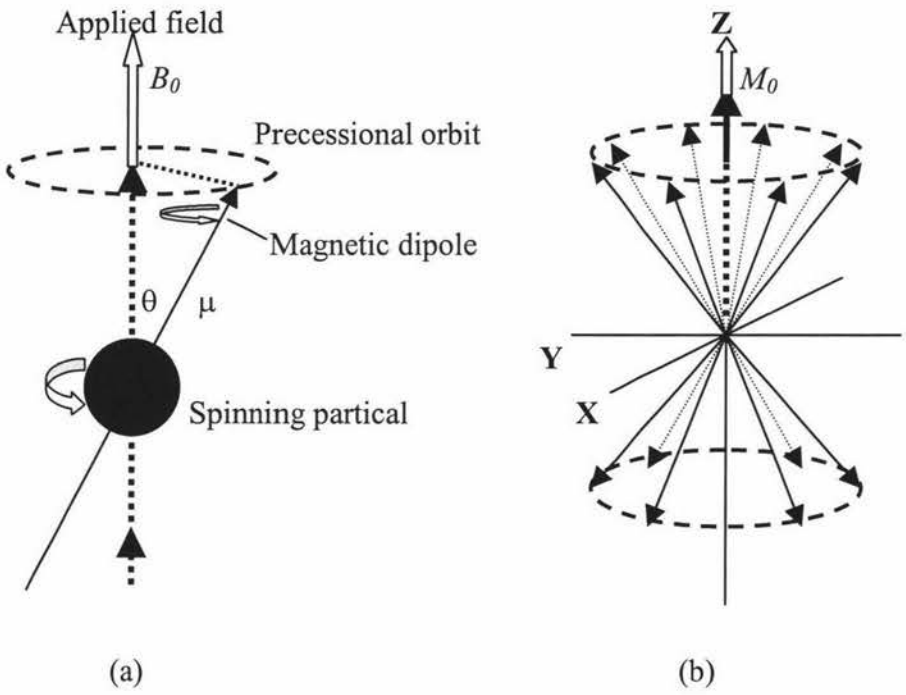

Figure 4. (a) Precession of a magnetic moment μ about a fixed magnetic field B_0. (b) Precession of an ensemble of identical magnetic moments of nuclei with I = ½ (for example: protons). The net macroscopic magnetization is oriented along B_0 (the Z-axis) and has the equilibrium value M_0 [58].

The PFG-NMR method in its simplest form consists of a spin-echo experiment using two radio frequency (r.f.) pulses and a magnetic field gradient pulse applied, respectively, during the dephasing and rephasing segments of the echo cycle (Figure 5).

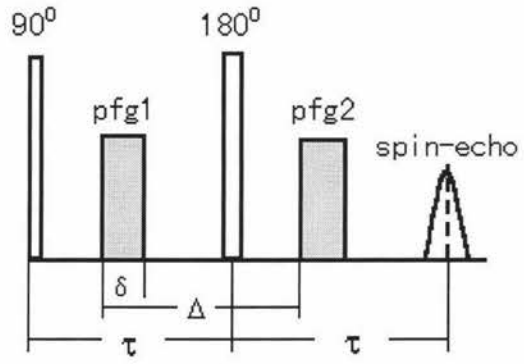

Figure 5. The pulsed field gradient spin-echo pulse sequence.

When a magnetic field gradient, G, of duration δ is imposed across the sample, a rapid precessional phase shift (dephasing) takes place because the nuclei process with different frequencies depending on the position of each nucleus in the sample. In the time interval (Δ) between the first and second gradient pulse (pfg1 and pfg2), the molecules containing the nuclei change position because of diffusion. The greater the change of position in the gradient field, the greater the reduction in the spin-echo peak.

In order to measure the water droplet size in emulsions, we need to use a variation on the Hahn spin-echo experiment (Appendix 1) in which the 180^0 refocusing pulse is divided into two pulses of 90^0 (Figure 6). This is done because Δ in this measurement is quite long compared to the T_2 value of the water. After such a long time at the end of the experiment hardly any echo signal would be observable. In addition, the oil proton signals need to be eliminated. To do this, a 180^0 pulse first inverts M_o. The first 90^0 pulse is then applied at the "crossover" point for the oil protons. i.e. the point at which M_t for the oil proton is zero. At this point there is still and significant water signal, as can be see in Figure 7.

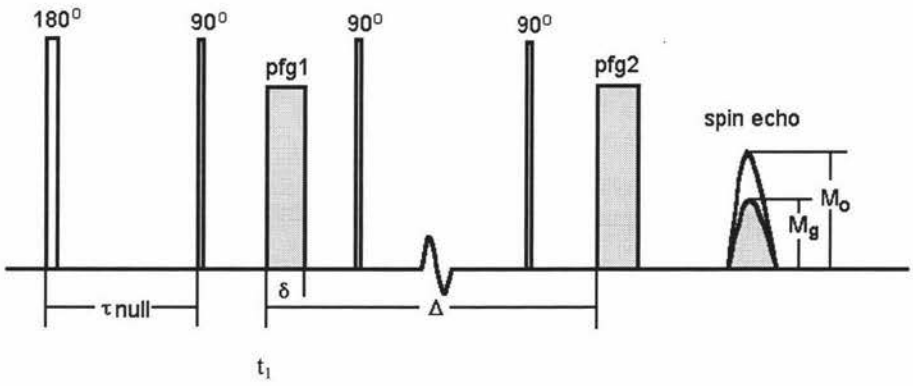

Figure 6. It is improved that the pulsed field gradient stimulated spin-echo pulse sequence.

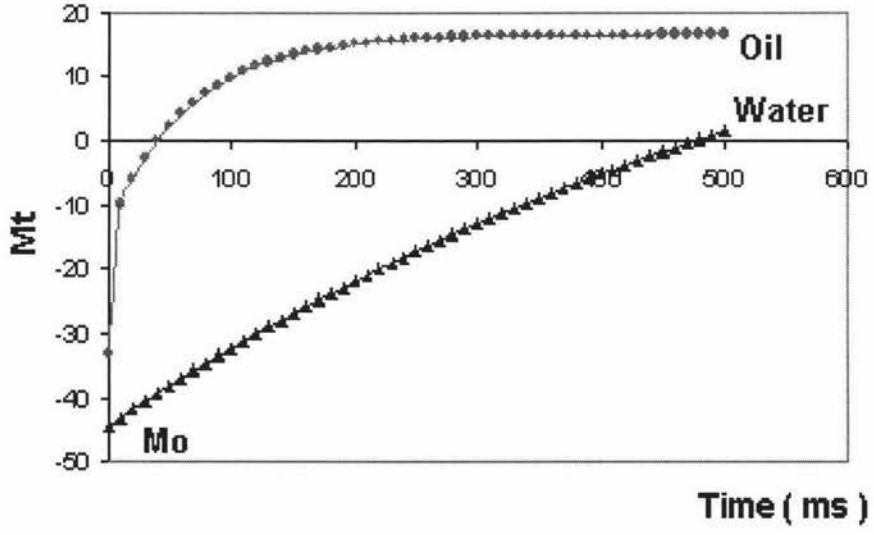

Figure 7. The recovery of M_t following inversion by the application of a 180^0 pulse at time t = 0.

The two 90° pulses between the two field gradient pulses invert all prior phase shifts which has the effect of refocusing the signal. In the same way that a 180^0 pulse will. However, the first pulse rotates M_t, so that it is along the Z-axis and the relaxation of the magnetisation is now determined by T_1 which is between 5 to 10 times larger than T_2 depending on the water content of the butter. The second 90^0 pulse rotates the magnetisation into the XY plane and T_2 relaxation is restored. Refocusing of the magnetisation is only complete where no diffusional motion has occurred. The degree of 'failure' of refocusing results in attenuation of the spin-echo signal ($R = M_g/M_o$, where M_g is the amplitude of the signal at the echo with gradient applied and M_o is the amplitude of the signal at the echo without gradient applied). R is given by [59]:

$$R = \int_{-\infty}^{\infty} \left\{ \int_{-\infty}^{\infty} p\,(z_0/z, \Delta) \cos\left[\gamma\,\delta\,G\,(z - z_0)\right] dz \right\} dz_0 \qquad (2)$$

Where p is the conditional probability for the arrival at point z, at time Δ, of nuclei that originated at point z_0, and γ is the gyromagnetic ratio. For molecules undergoing unhindered isotropic Brownian motion, p must be Gaussian and R is given by [59]:

$$R = exp\left[-\gamma^2\,\delta^2\,G^2\,D\,(\Delta - \delta/3)\right] \qquad (3)$$

where D is the self-diffusion coefficient. Equation 3 has been validated in experiments on simple liquids [26] [60], and has been applied to studies of solutions, gels and solid foods.

2.1.2 Droplet size application for NMR-minispec

The ratio R of echo amplitude with gradient pulses (M_g) to echo amplitude without gradient pulses (M_o) is a function of Δ, δ, D, G and the droplet radius d (Equation 5) [59].

$$R(\Delta,\delta,D,G,d) = \exp\left[-2\gamma^2 G^2 \sum_{m=1}^{\infty} \frac{\frac{2\delta}{\alpha_m^2 D} - \frac{2 + e^{-\alpha_m^2 D(\Delta-\delta)} - 2e^{-\alpha_m^2 D\Delta} - 2e^{-\alpha_m^2 D\delta} + e^{-\alpha_m^2 D(\Delta+\delta)}}{(\alpha_m^2 D)^2}}{\alpha_m^2(\alpha_m^2 d^2 - 2)}\right] \quad (5)$$

Where α_m is the m'th positive root of the Bessel function equation; $J_{3/2}(\alpha d) = J_{5/2}(\alpha d)$ [61]. The above function is valid for uniform droplets for each class.

For the purpose of determining the droplet size distribution by PFG-NMR, δ is varied and all other parameters are constant. The parameters of the droplet size distribution can then be calculated from the measured data $R(\delta)$ by a nonlinear regression fit (Levenberg-Marquart).

2.1.3 Droplet size distribution

Water droplet size distribution in water-in-oil emulsions like butters and low-calorie spreads are assumed to be log-normal. Experimental data show that this mathematical function is most suitable to describe particle size distributions of these products.

As an example, consider Figure 8. In this figure the droplet diameter d is plotted on the abscissa and the relative frequency of a droplet $q(d)$ with a

specific diameter is shown on the ordinate. Integration of frequency distribution leads to the sum distribution $Q(d)$ that gives the fraction of droplets being smaller than or equal to the diameter d.

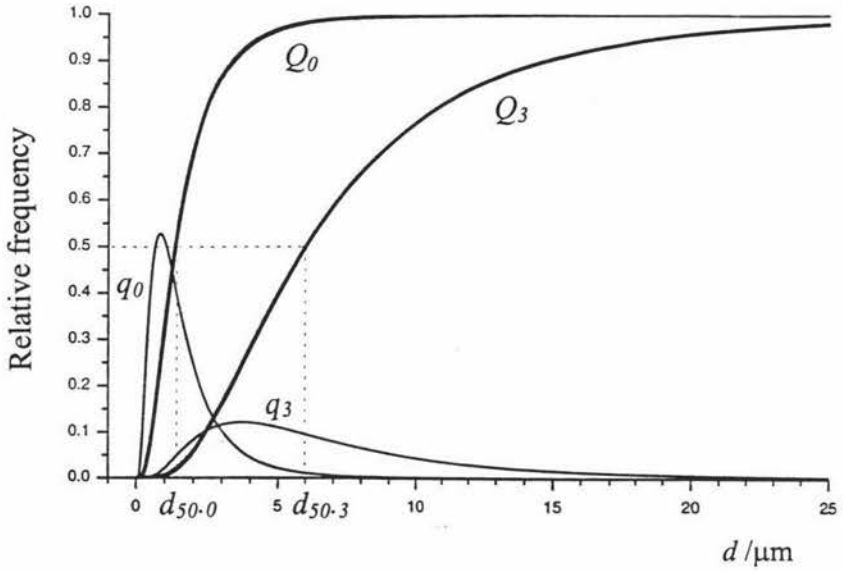

Figure 8. Droplet size distributions for a log-normal distribution.q_0 and q_3 are the relative frequencies of droplets with diameter d based on a number and volume distribution respectively. Q_0 and Q_3 are the respective accumulated frequencies. $d_{50,0}$ and $d_{50,3}$ are the geometric mean diameters. In the number distribution, for example, 50% of the total number of droplets will have a diameter < $d_{50,0}$.

Obviously the small droplets make a large contribution to q_0 but a much smaller contribution to q_3. While small droplets do not make a large contribution to the total water volume, the fewer large droplets (high diameters) represent a major part of the total water volume. For example, one droplet with a diameter of 10 μm occupies the same volume as 1000 droplets with a diameter of 1μm. since for most purposes the number of the

larger droplets is more important, the q_3 distributions are more useful. The geometric mean diameters $d_{50.0}$ and $d_{50.3}$ are related by the equation [59]

$$d_{50.0} = d_{50.3} / exp\ (\ 3\sigma\ )^2$$

where σ is standard deviation of the log normal distribution (equation 4).

A log-normal distribution is not symmetric, because, on one hand, droplets will never be smaller than 0 μm, and on the other hand, the natural limit at large droplets is uncertain. However, if the relative frequency is plotted against the logarithm of the diameter as shown in Figure 9, the frequency distribution turns into the symmetric bell-shaped Gaussian normal distribution.

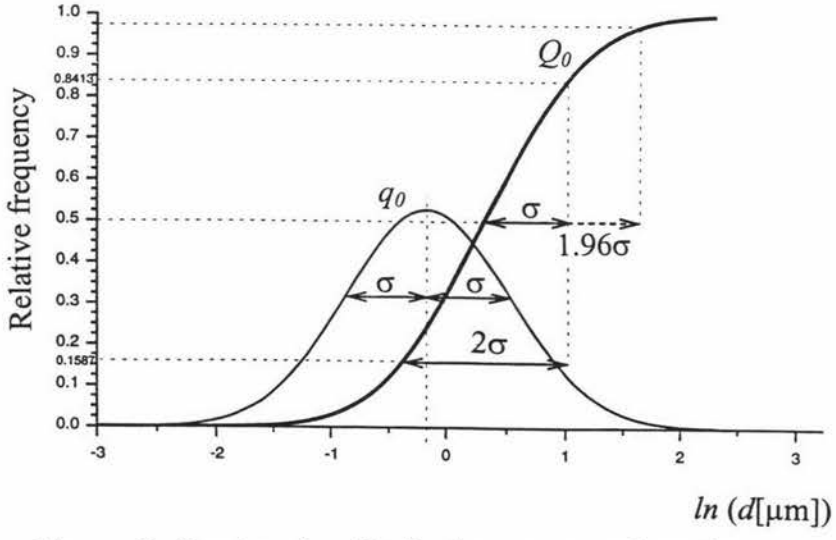

Figure 9. Droplet size distributions, expressed as the relative frequency vs the *ln d* the droplet diameter, for a sample with $d_{50,0}$ = 1.4μm and σ = 0.7 μm.

Mathematically log-normal distributions are described as follows:

$$q_i(d) = [d \cdot \sigma \cdot (2\pi)^{0.5}]^{-1} \cdot exp\ \{-[\ln(d) - (\ln(d_{50,i})]^2 / 2\sigma^2\} \qquad (4)$$

So this particle size distribution is characterized by two parameters (σ and $d_{50,i}$). The first is geometric mean diameter $d_{50,i}$, i.e. 50% of droplets are smaller and 50% large than this diameter, so the area under the distribution curve is divided into equal halves by the geometric mean diameter. The second is the standard deviation σ of the normal distribution which is a measure of the width of the distribution.

For microbial keeping properties the width of the volume distribution is important. So it is useful to determine distribution intervals. They are derived from the graph in log-scale using values of standardised normal distribution.

2.2 Confocal scanning laser microscopy (CSLM)

2.2.1 The basic theory of confocal scanning laser microscopy

The confocal microscope is based on the principle that image of a light source is focused on a well-defined depth in the specimen and that information from this focal point is projected onto a pinhole in front of a detector. Light source and detector pinhole are both located in the focal plane of the imaging lens (Figure 10). This principle of confocality was first described by Minsky [62] and adapted for use in a microscope by Petran et al. [63] (the tandem scanning microscope, TSM). Sheppard et al. [64] and

Brakenhoff [65] have developed confocal scanning laser microscopes equipped with a scanning table. In most commercially available CSLMs the sample is kept stationary and scanned with the laser beam.

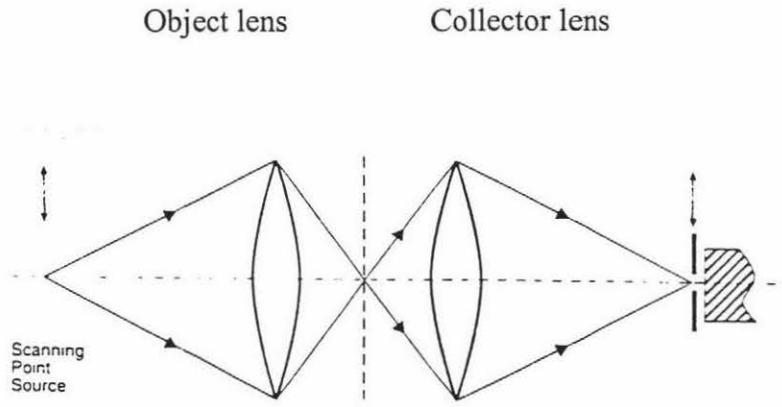

Figure 10. Optical arrangement of the confocal microscope. The object lens focuses the beam in the sample and the collector lens is used to make an image of the probed region on the point detector (after Minsky, 1957).

In confocal microscope a point light source probes a very small region of the specimen and the point detector ensures that only light from that small region is detected. This allows images to be obtained from a small volume element in the focal plane in the specimen (Figure 11).

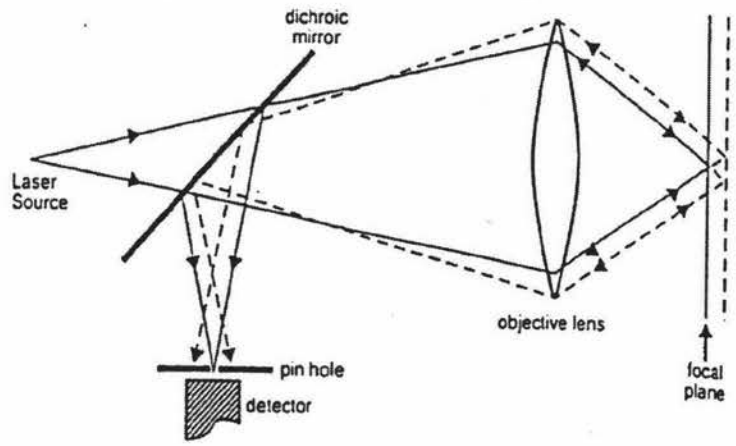

Figure 11. Diagram of the excitation beam and the reflected and fluorescent light in an incident light confocal system. The lens acts as condenser as well as collector lens. Solid lines: infocus light; dashed lines: out-of-focus light (after Minsky, 1957).

By synchronously scanning the image of the point source in the specimen with the pinhole of the detector, an image is built up in a computer frame store. The magnification in CSLM is determined by the ratio of the image screen and the scanned area in the sample. A zoom facility in the software of the confocal microscope makes it possible to decrease the scanned area resulting in a final higher magnification. The resolution of the confocal microscope is determined by the size of the volume element in the specimen from which light is collected in the detector and depends on the magnifying power and numerical aperture (N.A) of the objective lens. The optical sectioning or depth discrimination (Δz) depends on the size of the pinhole as well as on the N.A. of the objective lens (Figure 12).

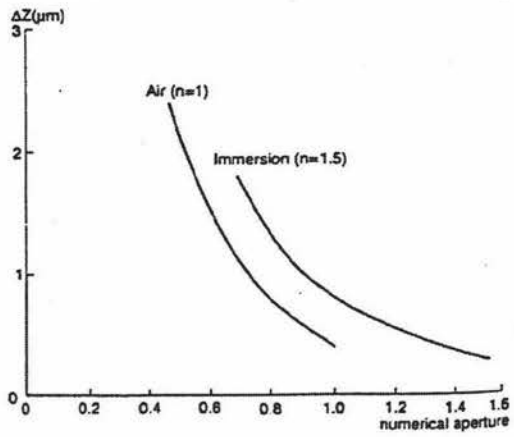

Figure 12. Optical scanning sectioning length (Δz) as function of the numerical aperture N.A. (λ = 632.8 nm) (after Wilson, 1990).

Above N.A. = 1 the depth discrimination becomes smaller than 1 μm. When the aperture of the pinhole in front of the detector is increased the optical sectioning degrades and at a fully open pinhole the microscope is no longer confocal and becomes a conventional scanning microscope. In CSLM the lateral resolution is improved by a factor of 1.4 compared to conventional microscopy.

The depth resolution in CSLM is much better than in the conventional microscopy, because in the latter the contribution from out-of-focus light blurs the image to a great extent. This improvement in depth resolution is the most important advantage of confocal microscopy. Optical sectioning in bulk specimen images, together with calibrated stepping control of the fine focus of the microscope, allows collection of series of optical sections having a thickness of less than 1μm at well-defined distances in the specimen. The data set of this series of optical sections can be used to prepare are construction of the three-dimensional (3-D) microstructure of the sample.

2.2.2 Z Series experiment

Confocal microscopy offers a powerful means to address food systems, given new understanding of microstructure and processes. To obtain three–dimensional information from the specimen, it is common practice to acquire a series of optical sections, referred to as a z series, taken at successively higher or lower focal planes along the Z-axis. Optical sections are normally constructed from x-y planes perpendicular to the laser beam, which is in the z-direction. For example, using the stepping principle CSLM has the ability to construct x-z sections at different y-positions (Figure 13) [66 ~ 67]. Each two–dimensional scan of the specimen is called an optical slice or section, and all the slices together comprise a volume data set (see Figure 14).

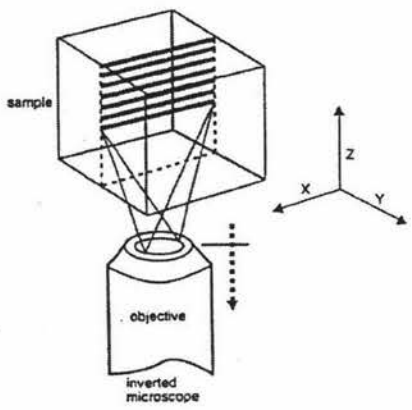

Figure 13. Schematic diagram of the construction of a x-z image in an inverted microscope. After each scanned line the objective is moved in the z-direction with respect to the objective, resulting in a x-z image.

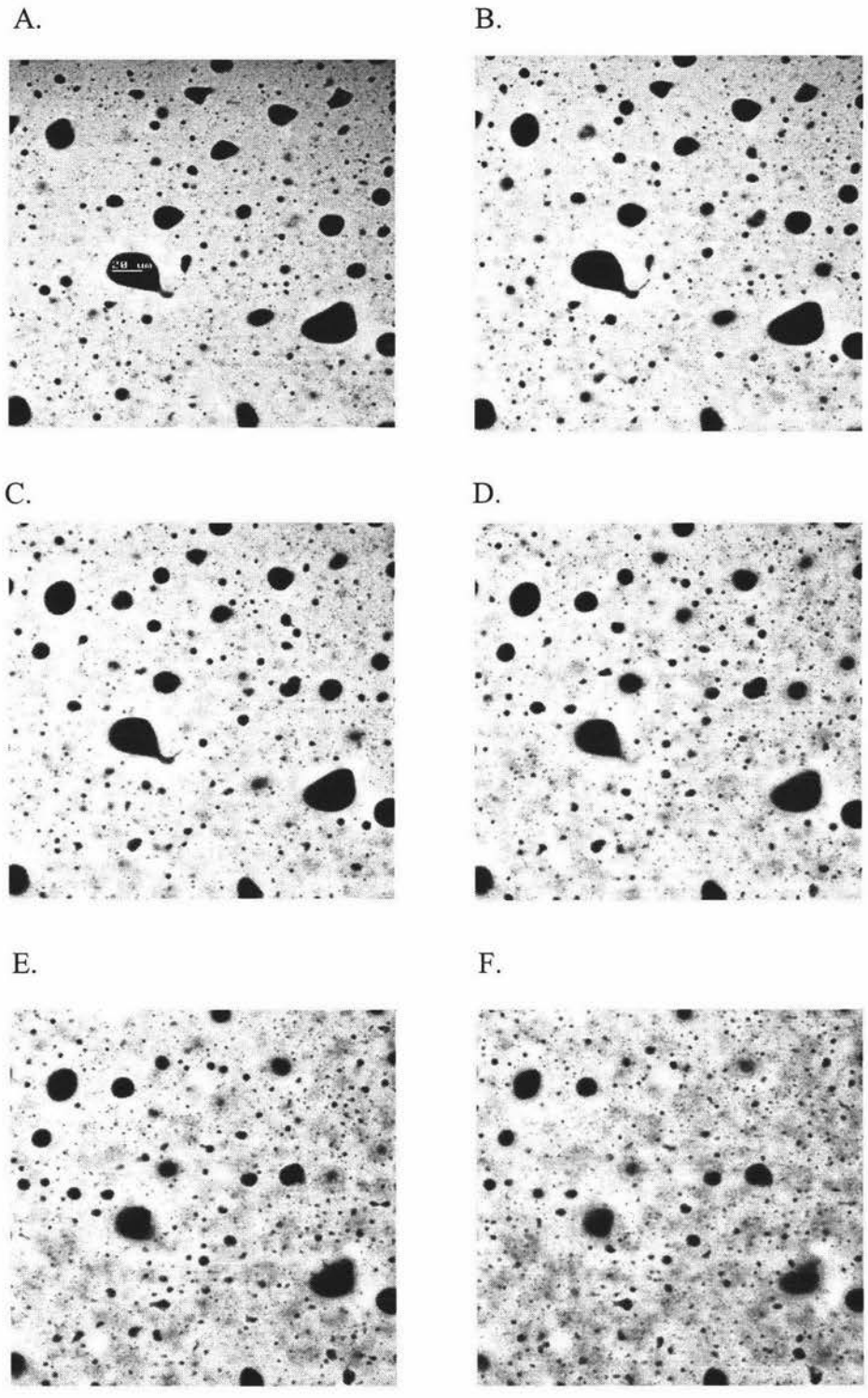

Figure 14. Serial confocal optical sections (from A to F) of a z-series through a butter (40x object). Optical sections were taken at 1.63 μm intervals. There is a scale bar (20 μm) in the A optical section.

3.0 Experimental methods and materials

3.1 Instrumentation

3.1.1 NMR Spectrometer

• Low resolution instrument:

Bruker NMS 120 Minispec (NMR Analyzer) with Bruker GU 200 pulsed gradient unit (Bruker Analytik GmbH, Silberstreifen, Germany) and Bruker NMS Soft-EDM 'droplet' pulse sequence routine. Samples were placed in a 10 mm diameter glass tube in the NMR probe with a 2 T/m field gradient and variable temperature control. The usual experimental temperature was 5^0C.

• High resolution instrument:

Bruker AMX-300 with Bruker BAFPA 40 and Bruker BAFPA 30 pulsed gradient units (Germany). Samples were placed in a 10 mm diameter glass tube in the NMR probe with a 0.99 T/m and field gradient and variable temperature control. The experimental temperature was 5^0C.

3.1.2 Confocal scanning laser microscopy (CSLM)

Leica TCS 4D laser scanning confocal microscope (Germany) with RSP580/LP515 detector and 60 pinhole. Magnifications were 16x object, 40x object and 100x object.

3.2 Samples

Descriptions of the samples used in this study are given in the following table.

Samples	Moisture (%)	Remarks
STD-1	16	A standard commercial butter
SEP-1	24	A specialty butter made using a modified technique
SPE-2	24	A specialty butter made using traditional Fritz technique
DRI-8	8	An experimental butter
DRI-16	16	An experimental butter
DRI-24	24	An experimental butter
DRI-32	32	An experimental butter
MAR-1	16	A commercial margarine

3.3 Sample preparation

3.3.1 NMR samples

The butter sample was prepared as shown in Figure 15. The sample was cut at the middle with a sharp knife. A thin septum was set on the freshly cut

surface. Then, the sample probe was inserted into the freshly cut surface. The probe gave samples with a diameter of 7.5 mm. The low resolution sample was 1 cm in length while the high resolution sample was 2 cm long. All operations were carried out in a cold room at a temperature of 4^0C.

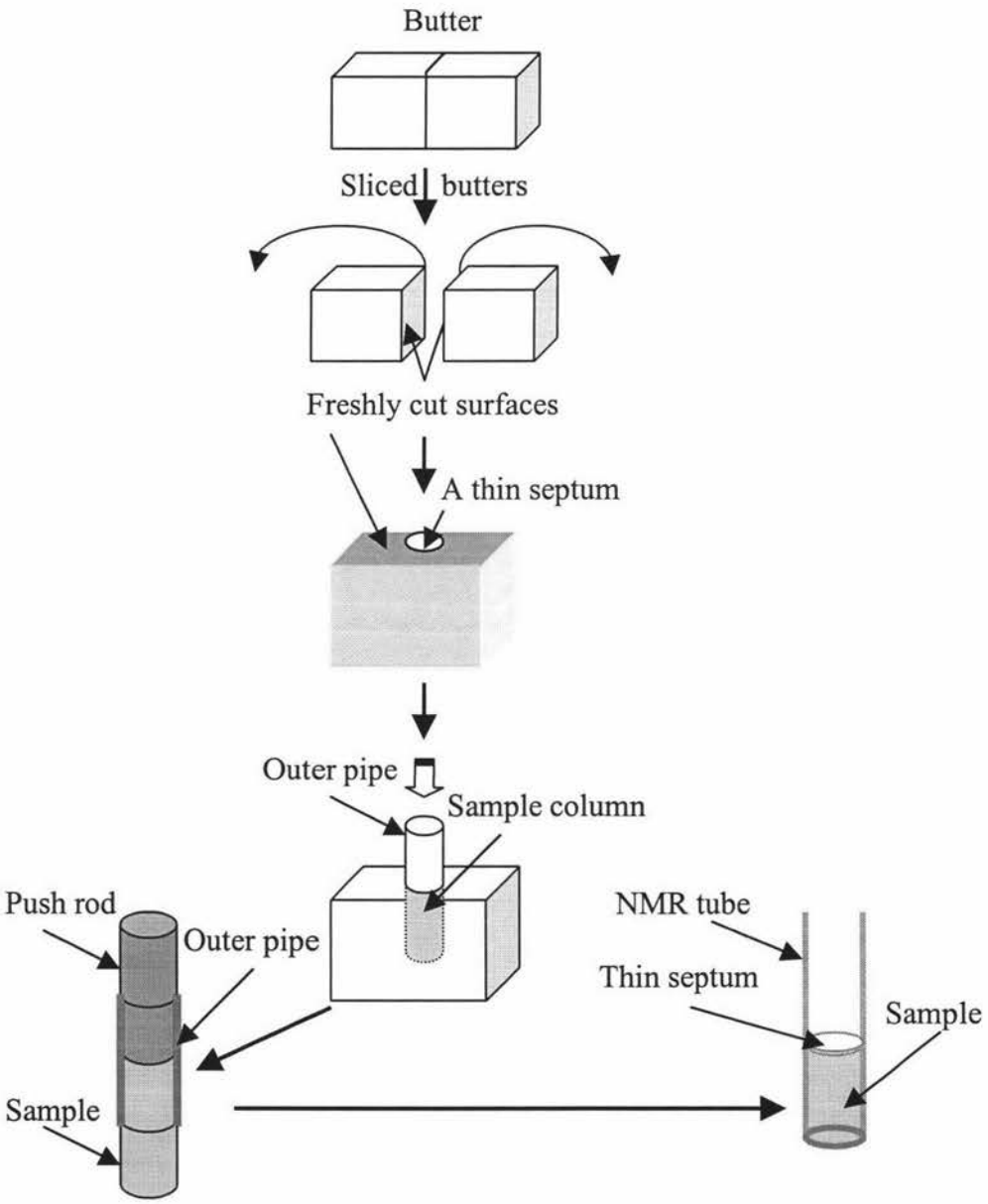

Figure 15. Butter sampling in NMR measurement

3.3.2 Confocal scanning laser microscopy (CSLM)

3.3.2.1 Dye preparation

Nile Red powder (a fat soluble fluorescent dye) was added to propylene glycol. Then the solution was mixed and stirred until the powder was completely dissolved.

3.3.2.2 Preparation of CSLM sample

In a cold room (4^0C), the sample was placed into a copper dish (see Figure 16), and a razor blade was used to smooth the surface of the sample. Then the dye was dropped on the smooth surface and allowed to diffuse into the fat. Next day, the surface of the stained sample was washed by Milli-Q water and a coverslip was placed over it.

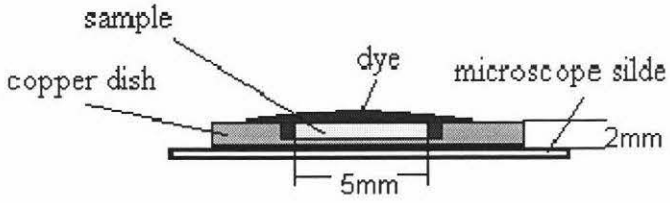

Figure 16. Butter sampling in CSLM exploration

3.4 Data analysis

The confocal data was analysed by an image analysis program (VIPS, Massey University) with algorithm written by Dr Pat Janssen, NZDRI. The application of this program is discussed in detail in section 4.2.6.

4.0 Results and discussions

4.1 NMR measurements

4.1.1 Pulse sequence used in diffusion measurements

The low resolution machine was used to determine the distribution of water droplet size in butter and margarine. In the classical Hahn spin-echo experiment (Appendix 1), the water signal and fat signal can't be separated. And because the decay time Δ (the interval between two pulsed field gradients) is quite long in this experiment, the echo signals are hardly observed. To get water signals, we used a variation on the Hahn spin-echo experiment. One change is that the 180° pulse is divided into two pulses of 90°. Another change is that a 180° pulse is put before the first 90° pulse. It can be used to eliminate the effect of fat signal (see page 16). It is necessary to optimise the various experimental variable to the samples, *i.e.* to the butters.

4.1.2 Choice of optimum measuring conditions

4.1.2.1 The delay time Δ between the field gradient pulses

There are two possible diffusion processes in proton diffusion. One is free diffusion, another is restricted diffusion (Figure 17). If the proton containing molecular have unrestricted motion during the time Δ then free diffusion is said to occur. A plot of the echo amplitude against Δ will yield a straight line. If the molecules are contained within boundaries, such as water molecules in the water droplets in butter or margarine, the protons will be able to move but only within the limits of the droplet in which they are

present. In this case for a large enough value of Δ, *R* does not decrease anymore, *i.e.* it reaches a "plateau" in the curve. To get a certain R value a Δ large enough have to be chosen. The value used here is a value suitable for margarines, butters and low-calorie spread [59].

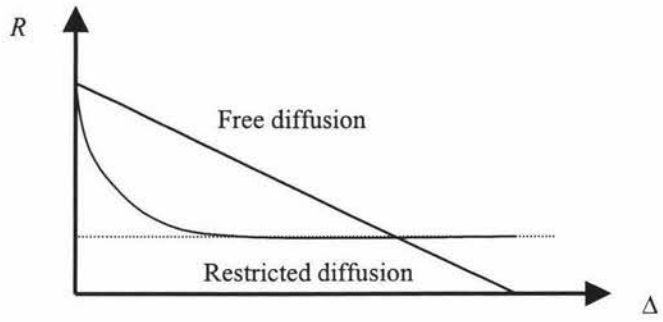

Figure 17. The relationships between the spin-echo amplitude (*R*) and the interval (Δ) between two pulsed field gradients under condition of free diffusion and restricted diffusion (see figure 6).

4.1.2.2 τ null (τ_0)

The optimum value of τ_0 depends on the T_1 relaxation line of the fat protons. The relaxation of protons following a 180^0 inverting pulse is given by the equation:

$$\ln (A_0 - A_t) = - t / T_1 + \ln 2A_0$$

Where A_0 is the amplitude of the signal from the protons in question at time (t) zero, and A_t is the amplitude of the signal at time t.

At the crossover point, *i.e.* When $A_t = 0$

$$\ln A_0 = -t / T_1 + \ln 2A_0$$

$$i.e. \qquad t = \ln 2 \cdot T_1 = 0.693 \cdot T_1$$

Table 1. T_1 and T_2 results

Sample	T_1(ms)	T_2 (ms)	τ_0 (ms)
16% H2O butter a (fat)*	62.0 (9)	8.6 (3)	43
16% H2O butter b (fat)*	61.0 (8)	8.7 (2)	42
STD-1 butter-1 (fat)	58.6 (10)	8.9 (2)	40.6
STD-1 butter-2 (fat)	57.6 (10)	8.7 (2)	39.9
STD-1 butter (water)	688.5 (10)	N/A	477.1

* Values measured by James Stephenson [68].

Table 1 gives T_1 values for various butters. From this table the optimum value of τ_0 is, therefore, about 40 ms, In practice, however, the echo amplitudes and water droplet distributions are found to be insensitive to the value of τ_0 (Table 2). This is because both the T_1 and T_2 value for fat in butter are roughly seven times smaller than the corresponding water values (Table 1). Thus, at the time of the echo from the water molecular, no signal remains form the fat molecules. In addition at 5^0C only 35% of the fat is in the liquid form. The default value used by Bruker for τ_0 is 85 ms.

Table 2. The distributions of water droplet sizes in STD-1 butter with different τ_0

τ_0 (ms)	Distribution (μm)		
	$d_{2\cdot5,3}$	$d_{50,3}$	$d_{97.5,3}$
1.00	0.5 (1)	1.9 (2)	7.0 (6)
85.0	0.4 (1)	1.7 (2)	8.1(6)

4.1.2.3 Gradient strength (G)

According to equation (5), the echo amplitude is a function of the Δ, δ, D, d and G (G is gradient strength). With changing the gradient strength, the echo amplitude will be changed. Hence, the R versus δ (the echo amplitude versus the gradient pulse width) curve will be changed.

With different gradient strengths (0.99 T/m and 2.00 T/m) used, the water droplet size distributions of Margarine, experimental better and commercial butter have been determined. The R versus δ curves for the MAR-1 margarine and DRI-24 butter are given in Figure 18 and 19 respectively and the corresponding distribution in Table 3.

Table 3. The water droplet size distributions by volume of Margarine, experimental butter and commercial butter obtained from R vs δ curves using two gradient amplitudes

samples	Distribution (μm)					
	G = 0.99 T/m			G = 2.00 T/m		
	$d_{2\cdot5,3}$	$d_{50,3}$	$d_{97.5,3}$	$d_{2\cdot5,3}$	$d_{50,3}$	$d_{97.5,3}$
MAR – 1	*1.3* (4) *1.7* (4)	***4.6*** (2) ***4.8*** (2)	*16.3* (26) *13.7* (26)	*1.6* (2) *1.8* (2)	***4.8*** (2) ***4.6*** (2)	*14.1* (20) *12.1* (20)
DRI – 24	*0.1* (1) *0.1* (1)	***2.8*** (1) ***2.9*** (1)	*59.9* (26) *62.5* (26)	*0.1* (1) *0.1* (1)	***2.7*** (1) ***2.7*** (1)	*65.2* (3) *65.5* (3)
STD – 1	*0.7* (1) *0.7* (1)	***2.2*** (1) ***2.2*** (1)	*6.7* (5) *7.2* (5)	*0.4* (1) *0.4* (1)	***1.7*** (1) ***1.7*** (1)	*7.9* (8) *7.1* (8)

From the data in Table 3 we can see that the distributions of water droplet sizes of the margarine (MAR-1) and the experimental butter (DRI-24) are not affected when the gradient strengths were changed.

For the MAR-1 and DRI-24 samples (Figure 18 and Figure 19) there was a significant echo attenuation which is associated with larger droplet sizes. For samples with smaller droplet sizes the attenuation is smaller. This is illustrated by Figure 20 which shows the R versus δ curves for STD-1 butter at the two field gradients. Because the attenuation is small it is best to use as high a value of G as possible.

The importance of maximising the echo attenuation is shown by the distributions for STD-1 use the two field gradients (Table 3). Unlike the MAR-1 and DRI-24 samples the $d_{2.5,3}$ and $d_{50,3}$ values obtained from the G = 0.99 T/m and G = 2.00 T/m experiments are significantly different. With changing δ from 1.00 to 5.00 ms R was changed about 20% when G was 2.00 T/*m*. The stronger echo attenuation can be obtained because noise was a little comparing with echo amplitude. However, the range of R was about 7% with increasing δ from 1.00 to 5.00 ms when G was 0.99 T/*m*. It is clear that the effects from noise were bigger than G was 2.00 T/*m*.

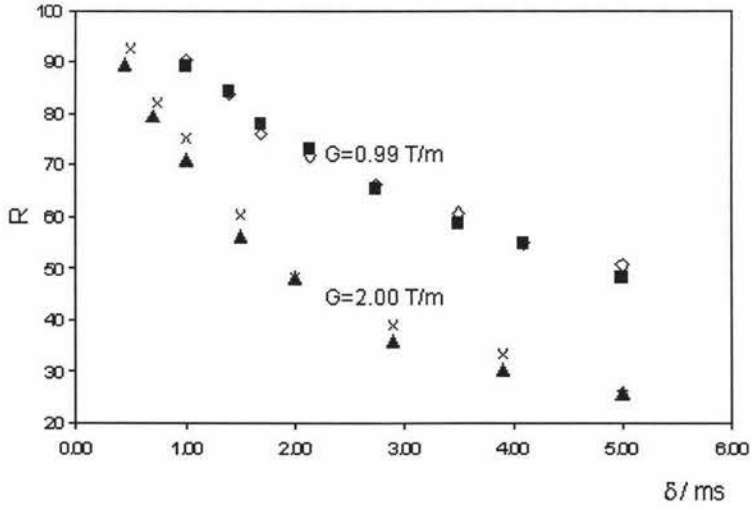

Figure 18. The relationship between the echo height ratio R and the pfg width δ with different gradient strength for MAR–1. Two experiments were performed at each field gradient amplitude.

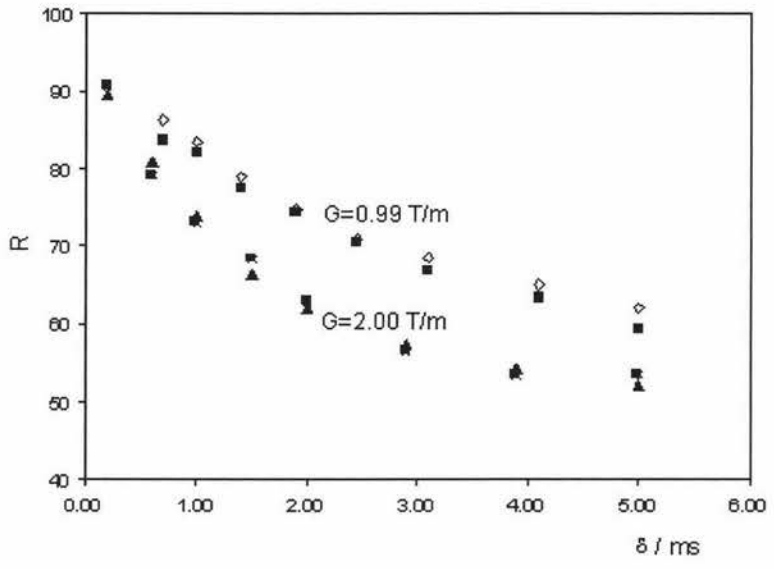

Figure 19. The relationship between the echo height ratio *R* and pfg width δ with different gradient strength for DRI– 24. Two experiments were performed at each field gradient amplitude.

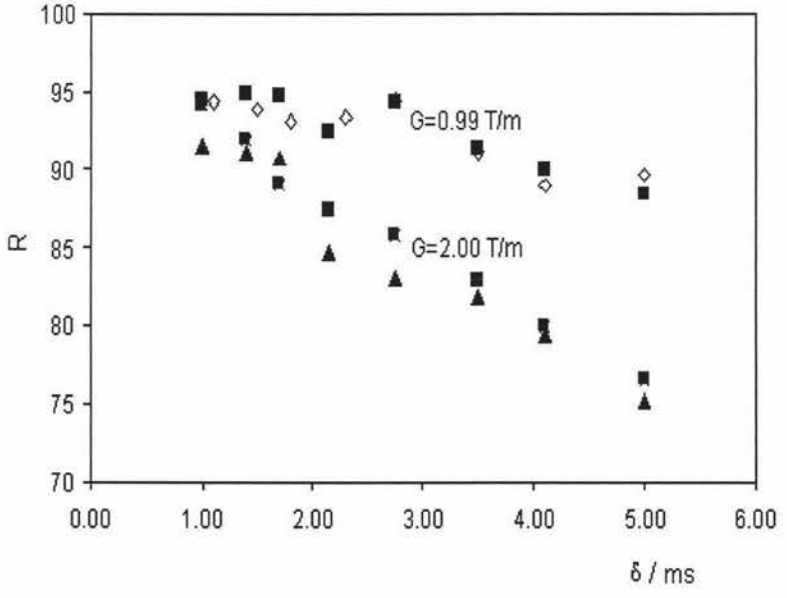

Figure 20. The relationship between the echo height ratio *R* and pfg width δ with different gradient strength for STD-1 butter. Two experiments were performed at each field gradient amplitude. Note the data is much more scattered than it is for the sample shown in Figure 18 and 19.

The maximum value of G that can be obtained on the Bruker NMS 120 Minispec (NMR Analyzer) is 2.00 T/m and this value was used for all the samples considered in these study.

4.1.3 Choice of water diffusion coefficient

The Bruker default setting for the water self-diffusion coefficient is that of pure water at 5^0C (1.31×10^{-9} m^2/s). However, protein, salt and lactose in water droplets in butters will result in a lower value for this parameter, which is used in equation (5). Such a decrease in the water self-diffusion coefficient may affect the R versus δ curves in such a way that the distribution of water droplet sizes will be changed.

The diffusion coefficients of water in aqueous phase samples extracted from STD-1, DRI-16 and MAR-1 were measured and the effects of changes in the water self-diffusion coefficients on the droplet distribution investigated.

4.1.3.1 Determinations of water self-diffusion coefficients

Samples were placed in a beaker which was transferred into an oven (60^0C) to melt the sample. After one and half hours, milkfat and aqueous phase were separated. The aqueous phase was left in a cold room (4^0C) overnight to congeal the dispersed fat present in the warm sample. The remaining liquid was then centrifuged at 2000 rpm for 10 minutes. The aqueous phase was collected and the self-diffusion coefficients determined at 5^0C. The results are shown in Table 4 and Appendix 2.

Table 4. Diffusion coefficients in aqueous phase extracted from samples

Sample	$D \times 10^{9}/m^{2}s^{-1}$
Pure Water	1.31 (2)
STD –1	0.78 (2)
DRI-16	0.95 (2)
MAR-1	1.13 (2)

Because the protein, salt and lactose were solved in aqueous phase, the viscosity of water phase product extracted from butter or margarine is higher than in the pure water. So that the diffusion speeds of protons in aqueous phase are slower than the pure water. The values of diffusion coefficients of real aqueous phase of samples are smaller than the pure water. The proton diffusion in MAR-1 margarine is faster than in butters. Hence, the diffusion speeds of protons in water droplets of the butter are different from the pure water.

4.1.3.2 Effect of choice of D on the water droplet size distribution

The MAR-1 sample was chosen to investigate the effect of changes in the water droplet size distribution. The effect of changing D in equation (5) as the distribution of water droplet size in MAR-1 is given by in Table 5.

Table 5. The distributions of water droplet sizes in MAR-1 using standard water and real aqueous phase to calibrate low instrument

D x $10^9/m^2s^{-1}$	Distribution by droplet volume		
	$d_{2.5,3}/\mu m$	$d_{50,3}/\mu m$	$d_{97.5,3}/\mu m$
1.31	<1.6 <1.7	<5.0 <4.9	<15.6 <13.9
1.20	<1.7 <1.7	<4.7 <4.8	<13.3 <13.7
1.13	<1.7 <1.6	<4.9 <4.9	<14.5 <14.8
1.00	<1.4 <1.6	<4.6 <4.6	<15.0 <12.9

0.90	<1.6 <1.4	<4.6 <4.6	<13.2 <15.3
0.80	<1.5 <1.5	<4.4 <4.4	<12.9 <13.1

It is clear from Table 5 that there isn't any significant change of water droplet distribution on changing the D value, ie. the choice of D is not critical.

4.1.4 Sampling techniques

Initial experiments gave curves for the distribution of water droplet size with long tails (Figure 21 and Table 6).

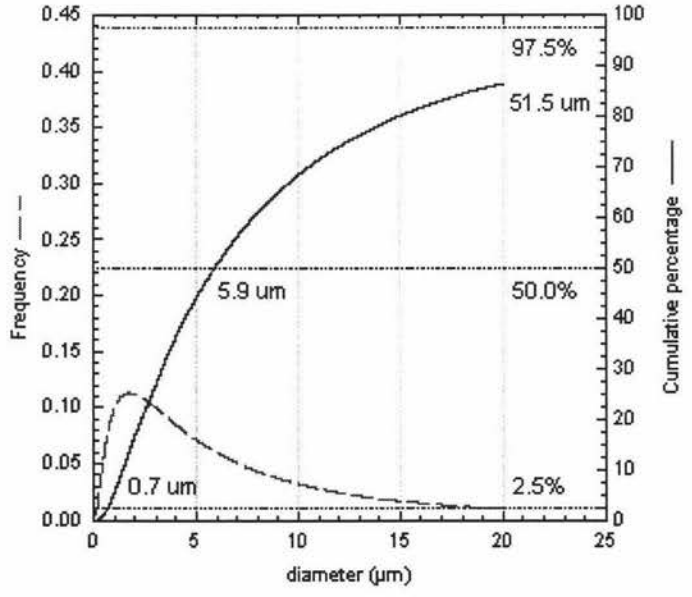

Figure 21. The distribution curve of water droplet size in STD-1 butter

Table 6. The distributions of water droplet sizes in butters

Sample	Droplet size distribution / μm		
	$d_{2.5,3}$/μm	$d_{50,3}$/μm	$d_{97.5,3}$/μm
STD-1	<0.7	<5.9	<51.5
STD-4	<0.5	<8.5	<141.6
STD-5	<0.9	<9.0	<92.5

The presence of such large droplets is unexpected and far exceeds the literature value [3] [12]. If these data in Table 6 are correct, the largest water droplet in the sample could be seen by optical microscopy, but no such droplets could be seen. So these results can not represent the properties of original samples.

After various tests, it was found that the butter samples had been squeezed when taking samples. The original butter sampling probe had been designed with a shortcoming which was causing distortion and aggregation of water drops. The probe was therefore modified as shown in Figure 22.

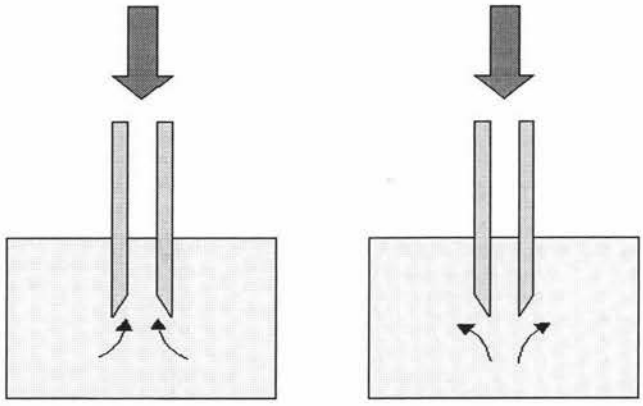

A B

Figure 22. The butter sampling probes.
A. The old sampling probe. B. The new sampling probe

In the new sample probe the compression force is minimised and this prevents the "squeezing out" of water into larger droplets. This can be seen by the improved distribution obtained using the new sample probe (Table 7 and Figure 23).

Table 7. The distribution of water droplet sizes in butters by new sampler

Sample	Droplet size distribution (μm)		
	$d_{2.5,3}$/μm	$d_{50,3}$/μm	$d_{97.5,3}$/μm
STD-1	<0.4	<1.5	<6.3
STD-4	<0.15	<2.0	<25.7
STD-5	<0.4	<2.0	<10.3

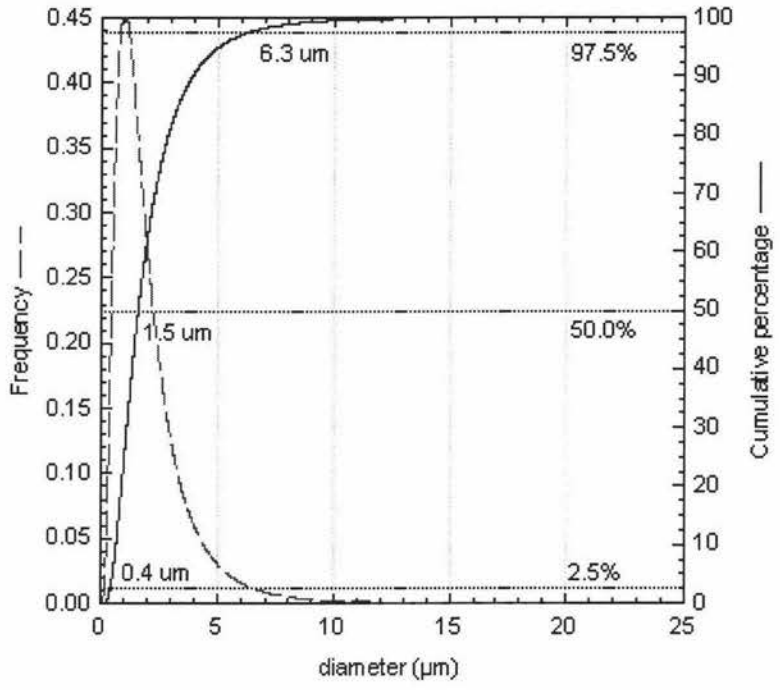

Figure 23. The distribution of water droplet size in STD-1 butter using new sample probe.

4.1.5 Distribution of water droplet size in commercial and experimental butters

Under optimum conditions, the water droplet size distributions of commercial butter, experimental butters and margarine were measured. Also, the distributions of water droplet size in experimental butters with different moisture contents were determined, and determined the moisture contents in these samples obtained by chemical analysis. At the same time, the water droplet distributions of butters with similar water contents but made by different techniques were determined.

4.1.5.1 Distribution curves of water droplet sizes by volume

The results of STD-1 butter, DRI-24 butter and MAR-1 margarine were shown in Figure 24, Figure 25 and Figure 26. In these figures only one experimental distribution is shown. It has been establish in a previous study [69], however, that the reproducebility is excellent. In this study the distribution was measured ten times for a particular sample and no changes in the distribution were observed within experimental error.

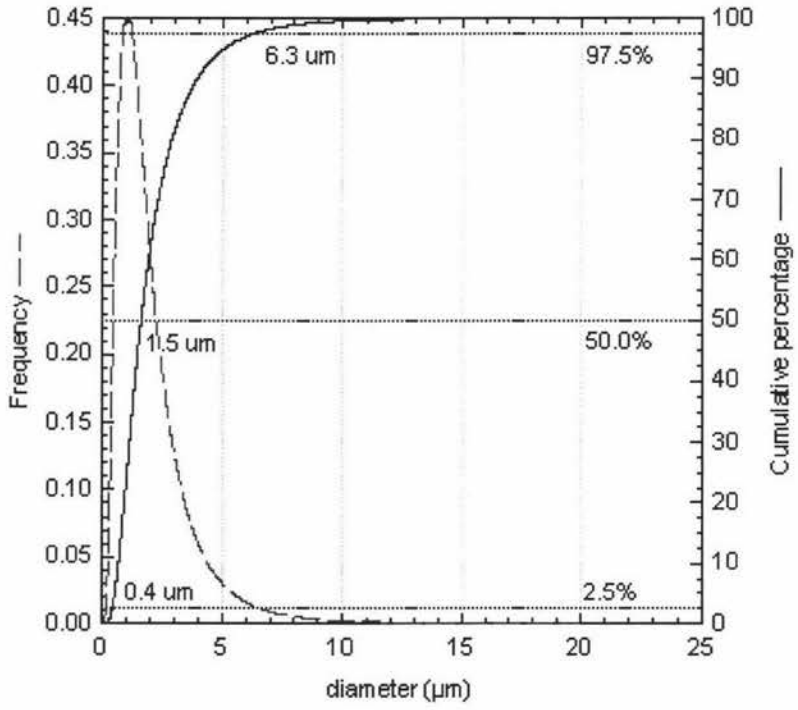

Figure 24. The distribution curve of water droplet sizes by volume of STD-1 butter at 5^0C.

For the STD-1 butter (Figure 24), the peak in frequency curve occurs at 1 μm. From the cumulative percentage curve, it is clear that 97.5% of the water droplets in the STD-1 butter are smaller than 6.3 μm in diameter, 50.0% droplets are below 1.5 μm and 2.5% are smaller than 0.4 μm.

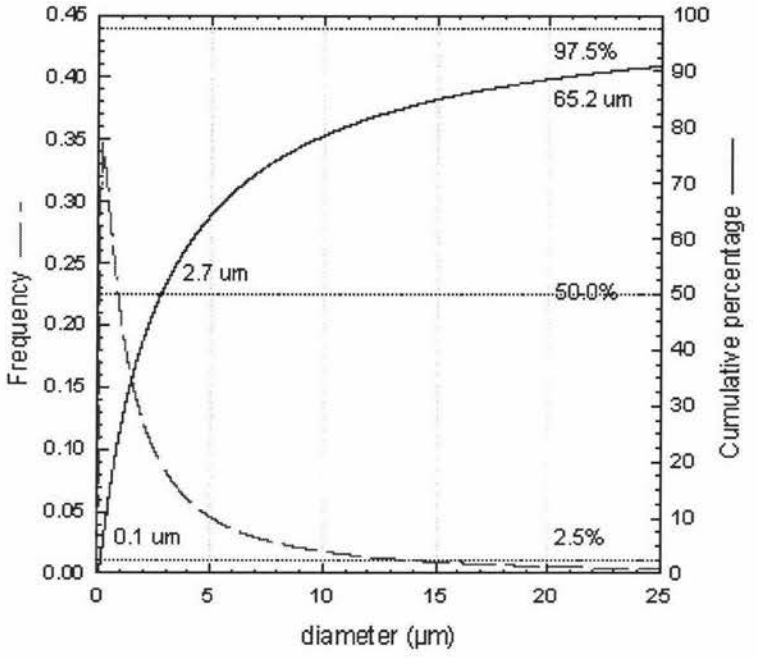

Figure 25. The distribution curve of water droplet sizes by volume in DRI-24 butter at 5^0C.

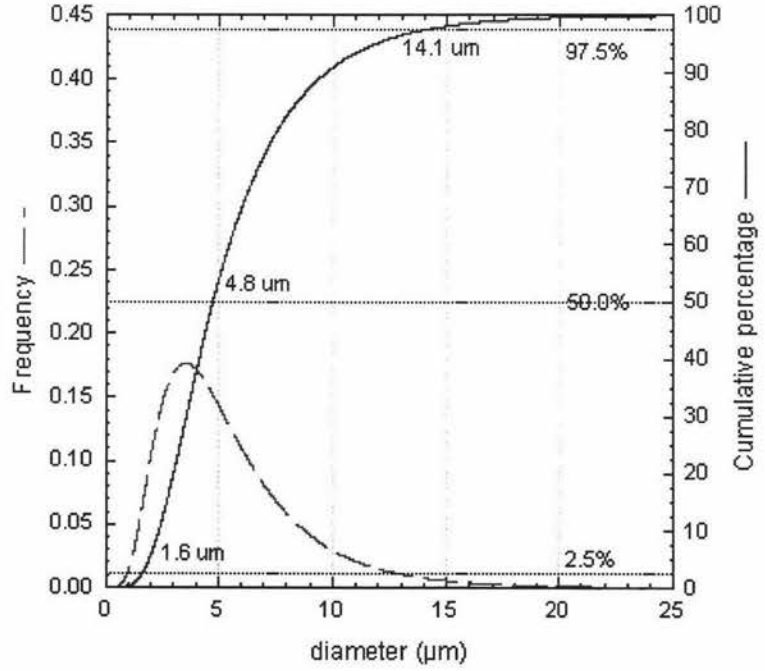

Figure 26. The distribution curve of water droplet sizes by volume of MAR-1 margarine at 5^0C.

For the MAR-1 margarine (Figure 26), 50% of the droplets have a diameter below 4.8 μm. For the DRI-24 butter (Figure 25), 50% of the droplets have a diameter smaller than 2.7 μm. The respective peaks in the distributions of MAR-1 and DRI-24 are at 3.1 and 0.1 μm. The DRI-24 sample has a long tail in the distribution curve indicative of droplet with larger diameters. These larger droplets in DRI-24 sample are larger than in margarine. It is clear that there is a much larger range of water droplet sizes in the DRI-24 sample than in both the STD-1 and MAR-1samples.

4.1.5.2 The distributions of water droplet sizes in experimental butters with different moisture contents

The distributions for experimental butters with different moisture contents are plotted in Figure 27 and their water contents listed in Table 8.

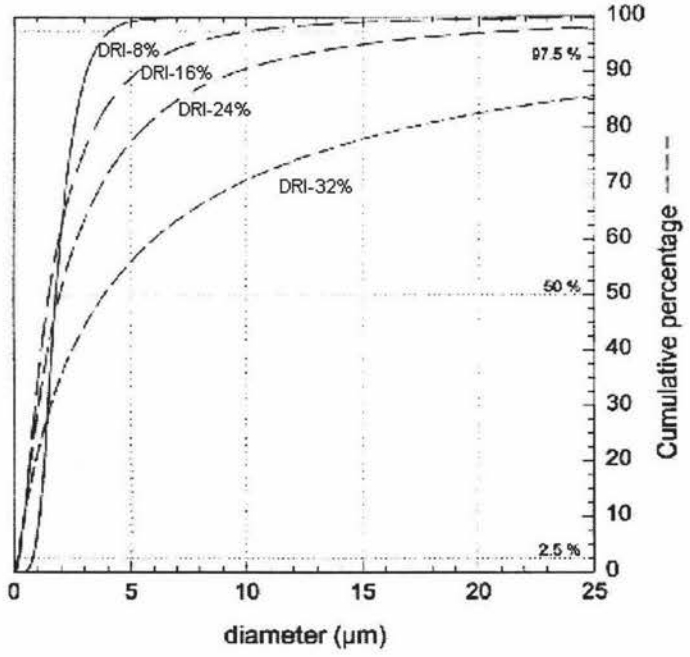

Figure 27. The distributions of water droplet sizes by volume in experimental butters with different moisture contents.

Table 8. Moisture contents of NZDRI experimental butters

Sample No.	Moisture content (%) (Kohman Moisture)
STD-1 butter	**14.6**
MAR-1 margarine	**15.5**
DRI-8 butter	**6.9**
DRI-24 butter	**23.2**
DRI-32 butter	**29.8**

The water droplet size distribution is clearly dependent on the water content (Figure 29). With increasing the moisture content in sample, the amount of larger droplets in sample is increased. It means that the probability that larger droplets are formed in the high moisture sample is bigger than in the low moisture sample. This gives rise to the possibility of determining the

moisture content from the distribution. However, the distribution alsodependent on the method used to manufacture the butter. This is clearly shown in the next section.

4.1.5.3 Distributions of water droplet sizes in butters made using different manufacturing techniques

SPE-1 and SPE-2 samples have been investigated. Both butters have similar water contents (Table 9). Their distributions of water droplet sizes, however, are quite different (Figure 28) because they were made by different techniques.

Table 9. The Moisture contents of SPE-1 and SPE-2 butters

Sample No.	Moisture content (%) (Kohman Moisture)
SPE-1 butter	**22.4**
SPE-2 butter	**25.0**

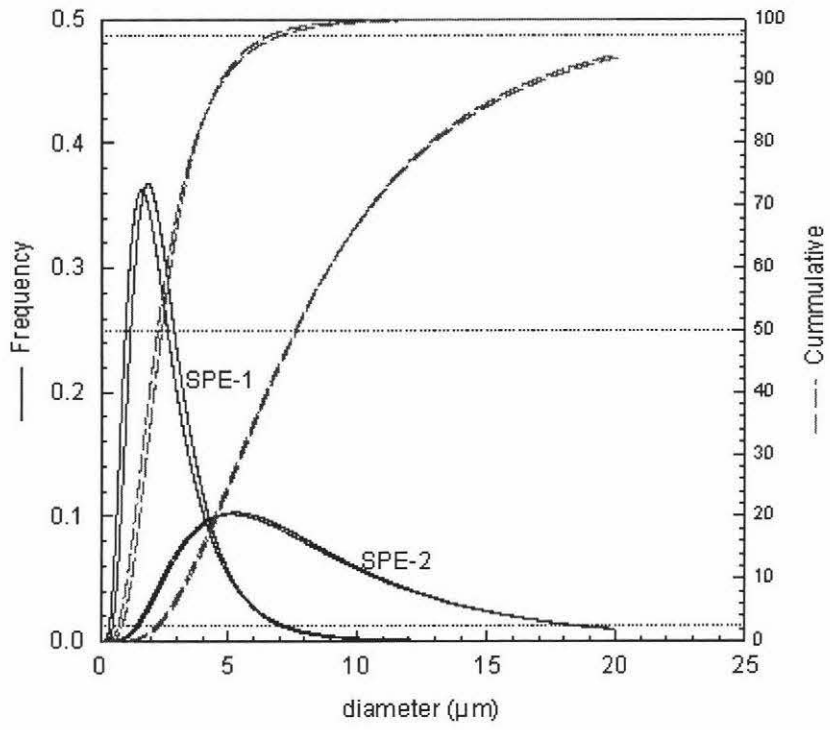

Figure 28. The droplet distributions by volume of the SPE-1 and the SPE-2 butters with close moisture contents.

In SPE-1 butter, most droplets are small sizes, and the distribution is tight. It is benefit to control bacterial growth and to extend the shelf life of commercial butters. However, there is a large proportion of droplets with larger sizes in SPE-2 butter. And the distribution is wider because there are some bigger droplets that show us a long tail in the distribution curve. So the PFG-NMR is a very useful tool helping to chose different techniques to service the requirements of markets and customs.

4.2 Confocal scanning laser microscopy

Confocal scanning laser microscopy was used in an attempt to confirm the results of the water droplet size distribution by visible observation of the droplet sizes.

Before useful comparisons could be made methods had to be devised to optimally observe the water droplets in butter. The optimisation involved the dyeing technique, dye type, dye solvent and magnification. This involved analysis of about 100 images.

4.2.1 The sampling

To investigate the effects of different sampling techniques, we have tried three sampling methods:

- Sample slice was set on a microscope slide to stain.
- Sample was cut into a small cube and stained in a beaker.
- Sample was set into a copper dish to stain.

As discussed below confocal images of samples are the best when the copper dish was used.

4.2.1.1 Use of microscope slide in dyeing sample

Butter sample was cut into a slice. The slice was placed on a microscope slide and dye was dropped on sample slice. The sample was stored in a cold room (4^0C) overnight (Figure 29).

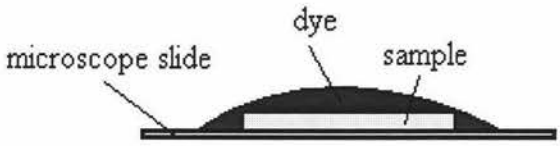

Figure 29. The sampling technique of CSLM using a microscope slide.

Observing the images of samples, It is clear that the dyeing effects of the samples are not ideal. There are some residual dye crystals in the pictures showing up as dark areas in images of the samples (Figure 30 and Figure 31). Two problems were observed, firstly the dye crystal may not be completely dissolved in solvent, and secondly the diffusions of dyes in the samples were not uniform. The latter leads to little useful information below the surface layer.

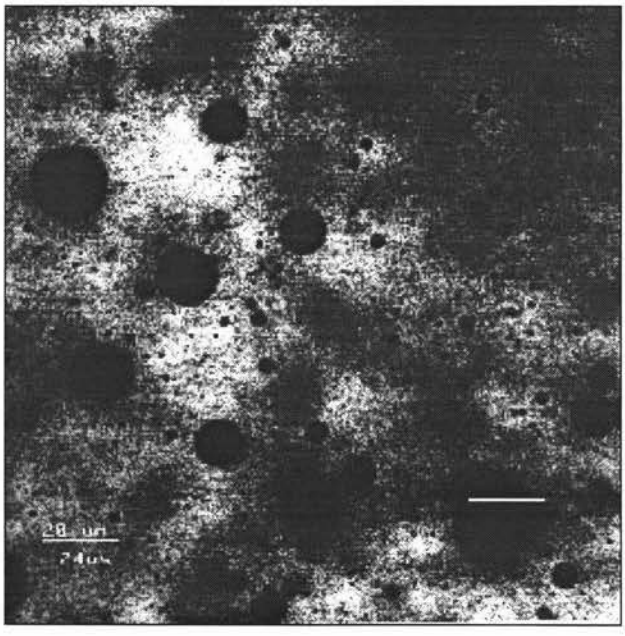

Figure 30. The microstructure of DRI-24 butter obtained from a sample prepared using a microscope slide. Lipids stained with Nile Red in corn oil. Dark holes are water droplets. Bar = 20 μm (24% moisture).

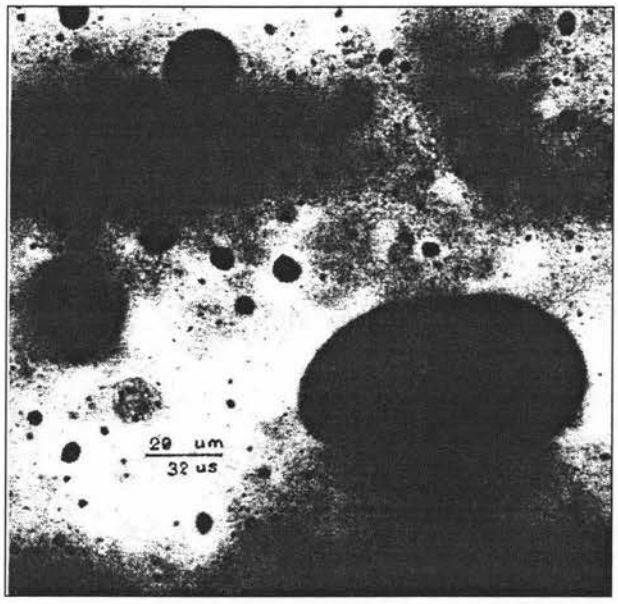

Figure 31. The microstructure of DRI-32 butter obtained from a sample prepared using a microscope slide. Lipids stained with Nile Red in corn oil. Dark holes are water droplets. Bar = 20 μm. (32% moisture).

4.2.1.2 Small cube of sample stained in a beaker

In the cold room (4^0C), the sample was cut into a small cube, and it was set into a beaker with dye solution to stain the sample overnight. Next day, the stained cube was filled into a copper dish by stainless steel sampler, and the surface of sample was smoothed by a razor blade. Then, the surface was washed by Milli-Q water (4^0C). The observed images are shown in Figure 32 and Figure 33.

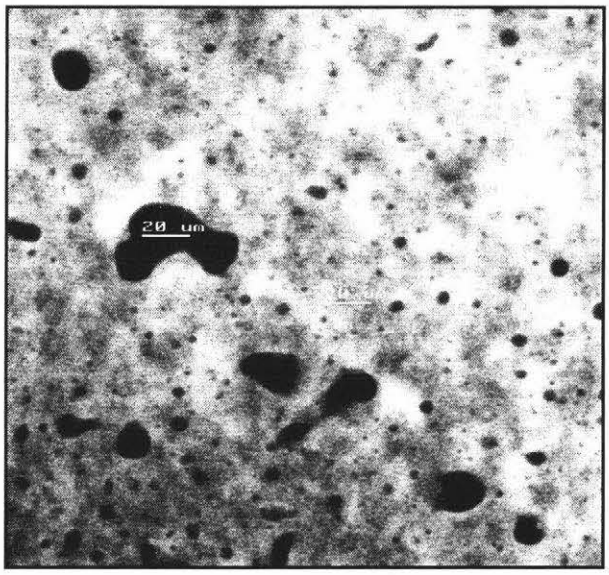

Figure 32. The microstructure of STD-1 butter obtained from a sample prepared by stained a cube of butter in a beaker. Lipids stained with Nile Blue in Milli-Q water. Dark holes are water droplets. Bar = 20 µm.

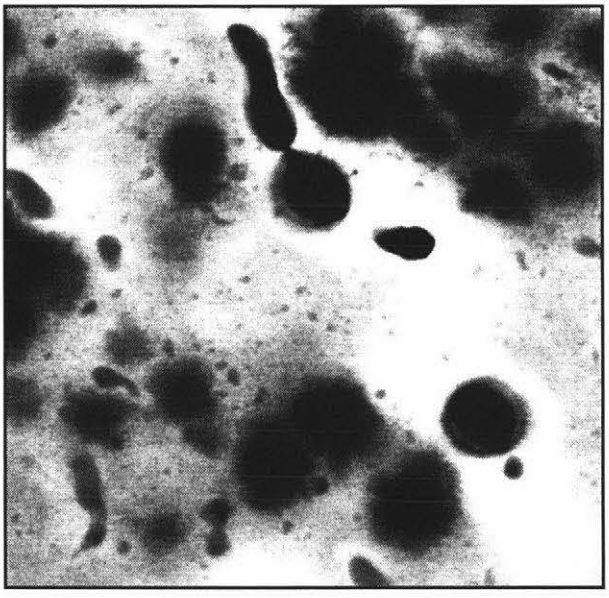

Figure 33. The microstructure of DRI-24 butter obtained from a sample prepared by stained a cube of butter in a beaker. Lipids stained with Nile Blue in Milli-water. Dark holes are water droplets.

In Figure 32 and Figure 33, the dissolved dye crystals are still present. The boundaries between water phase and fat phase are fuggy. It is hard to calculate the volume of droplet size and to obtain the distribution of droplet sizes.

4.2.1.3 Uses of copper dish

The copper dish was tried as it acts as a heat sink and protects the sample against changes in temperature dewing sample transferred from the fridge to the microscope. Also, it is easier to get a parallel surface for the coverslip. This is important for good resolution and depth control.

In the cold room (4^0C), the sample was filled from stainless steel sampler

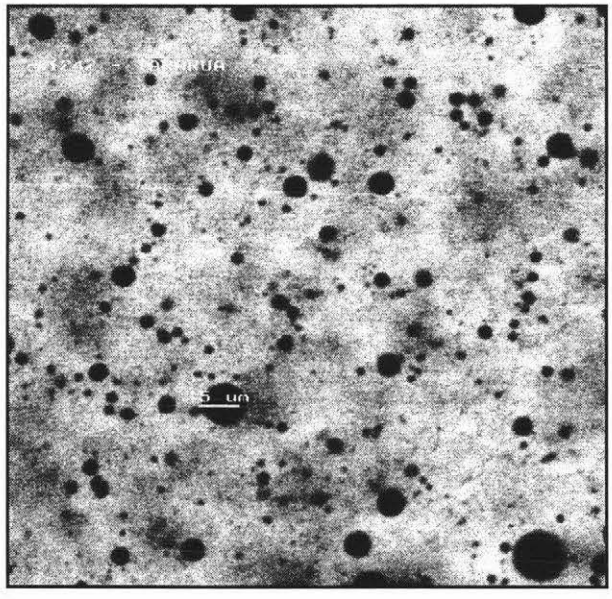

Figure 34. The microstructure of STD-1 butter obtained using a sample prepared in a copper dish. Lipids stained with Nile Blue in Milli-Q water. Dark holes are water droplets. Sample holder is copper dish. Bar = 5 µm.

into a copper dish (4^0C), and a razor blade was used smooth the surface of the sample. Then, the dye (4^0C) was dropped on the smooth surface to stain the sample (Figure 16). Next day, the surface of sample was washed by Milli-Q water and a coverslip was placed onto the sample. The images of samples, which are stained in copper dishes, have shown in Figure 34 and Figure 35.

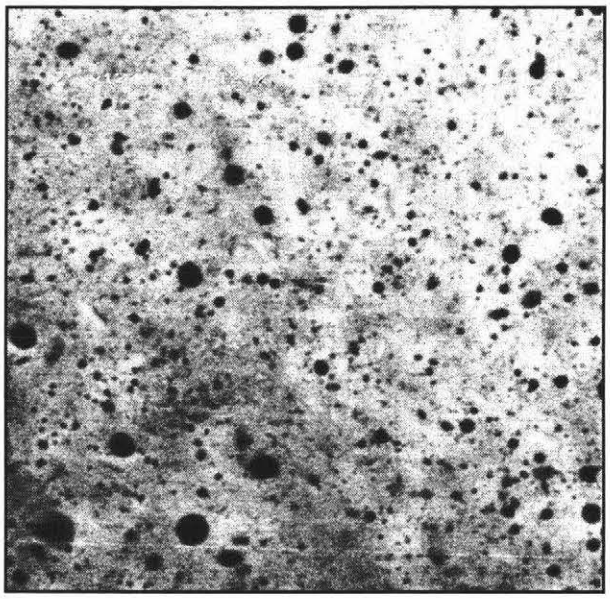

Figure 35. The microstructure of DRI-24 butter obtained using a sample prepared in a copper dish. Lipids stained with Nile Blue in Milli-Q water. Dark holes are water droplets. Sample holder is copper dish.

From Figure 29 to Figure 35, it is clear that the best result is obtained when a copper dish is used to stain the sample.

4.2.2 Dyeing techniques

Two available fluorescent dyes were Nile Blue and Nile Red. Both these dyes dissolve in the fat layer. To obtain clear confocal images of samples, the confocal images of samples were investigated with different dyes and different solvents (glycerol, Corn oil, Milli-Q water and Propylene glycol) to stain samples. As discussed below the best dyeing effect was obtained when Nile Red in propylene glycol was used.

4.2.2.1 Comparisons between Nile Blue in glycerol and Nile Red in corn oil

Dye mixtures that had previously used on dairy products were used for the first experiment. These were: Nile Blue dissolved in glycerol and Nile Red is dissolved in corn oil.

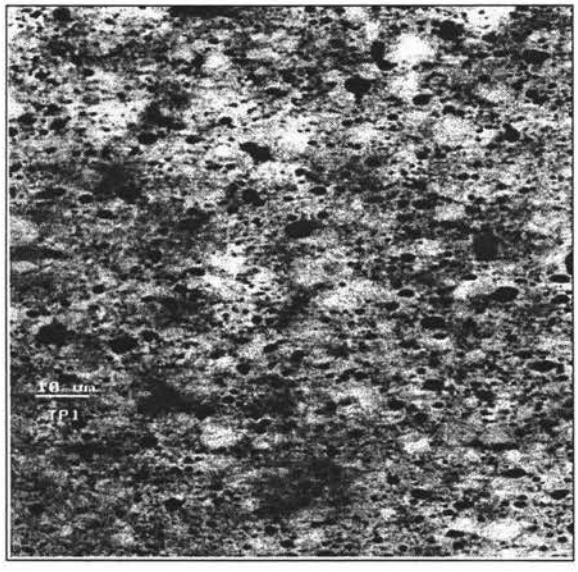

Figure 36. The microstructure of STD-1 butter obtained from a sample prepared using a microscope slide. Lipids stained with Nile Blue in glycerol. Dark holes are water droplets. Bar = 10 μm. (16% moisture).

The results of the experiments are shown in Figure 29, Figure 30 and Figure 36 where the fluorescent fat phase shows up light and the water droplets (with no dye) are dark.

It is clear that Figure 36 (Nile Blue) is much clearer than Figure 29 (Nile Red) and Figure 30. In the Figure 36, water droplets are clearly seen. However, in Figure 29 and Figure 30, it is hard to obtain clear images because some dye crystals did not dissolve.

4.2.2.2 Nile Blue

Literature reports [14] used Nile Blue dissolved in Milli-Q water and this dye was also trialed. Three samples were observed and shown in Figure 37, Figure 38 and Figure 39.

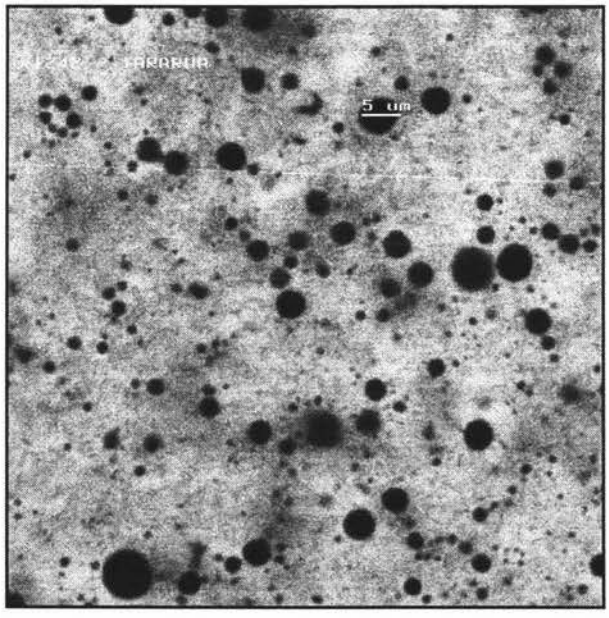

Figure 37. The microstructure of STD-1 butter. Lipids stained with Nile Blue. Dark holes are water droplets. Bar = 5 μm (16% moisture).

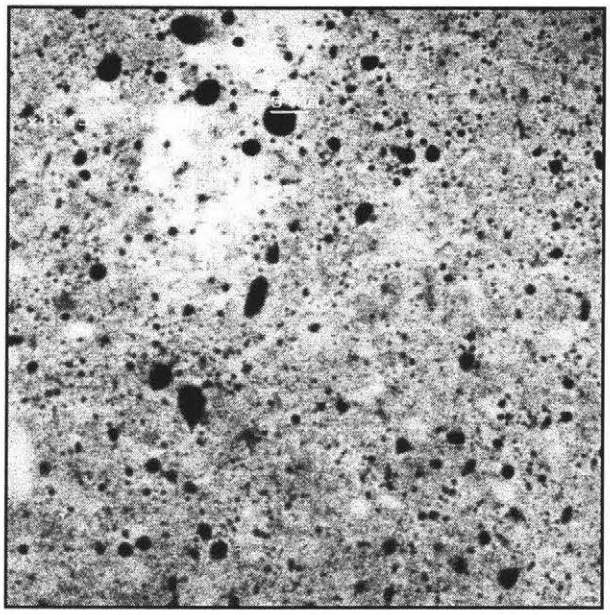

Figure 38. The microstructure of DRI-24 butter. Lipids stained with Nile Blue. Dark holes are water droplets. Bar = 5 μm. (24% moisture).

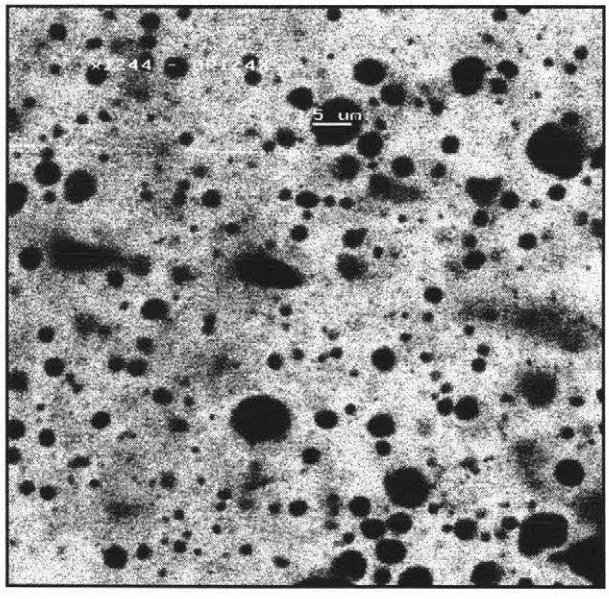

Figure 39. The microstructure of MAR-1 margarine. Lipids stained with Nile Blue. Dark holes are water droplets. Bar = 5μm. (16% moisture).

From Figure 37 and Figure 39, clear boundaries between milkfat phases and aqueous phases are seen, but, at the same time, some undissolved crystals are present (even after centrifugation). Also the contrast at the boundaries are not sufficiently sharp for a good determination of droplet sizes.

4.2.2.3 Comparisons between Nile Blue in Milli-Q water and Nile Red in propylene glycol

To attempt to improve the quality of the image Nile Red in propylene glycol was tested and compared to Nile Blue.

In this comparing experiment, two samples are examined (Figure 40, Figure 41 and Figure 42).

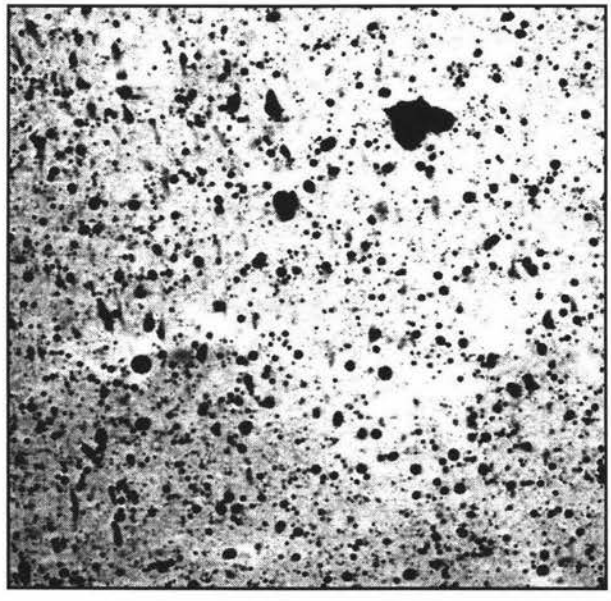

Figure 40. The microstructure of MAR-1 margarine. Lipids stained with Nile Red dissolved in propylene glycol. Dark holes are water droplets. Bar = 5 μm. (16% moisture)

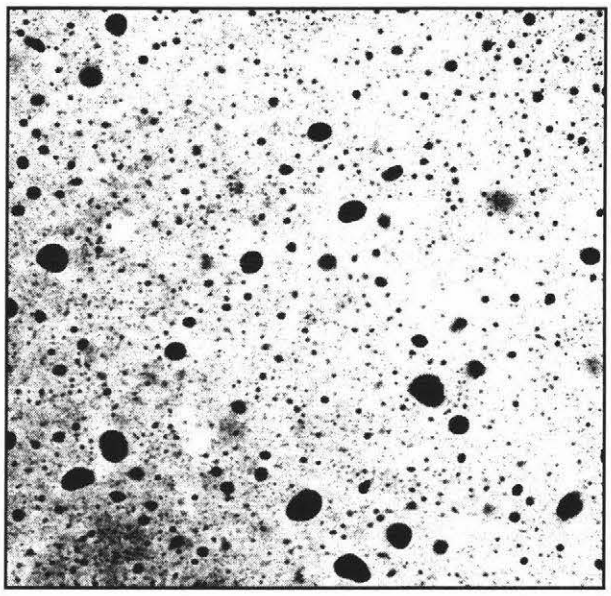

Figure 41. The microstructure of DRI-24 butter. Lipids stained with Nile Red dissolved in propylene glycol. Dark holes are water droplets.

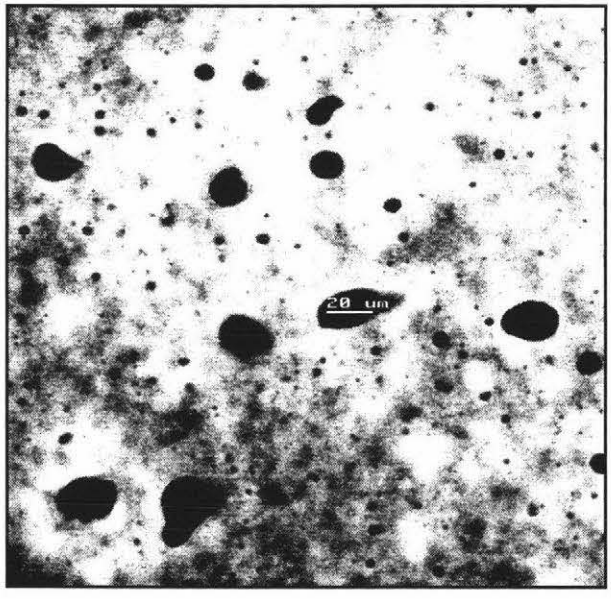

Figure 42. The microstructure of STD-1 butter. Lipids stained with Nile Blue dissolved in Milli-Q water. Dark Holes are water droplets. Bar = 20 μm. (16% moisture)

Observing these images, the Nile Red in propylene glycol is far superior than to of Nile Blue in Milli-Q water when the milkfat phases were stained because the boundaries between milkfat and aqueous phase are clear. The resolving power is better and the backgrounds are uniform. After experiments, Nile Red in propylene glycol was chosen as the dye to stain the milkfat phase of butter or margarine sample in CSLM because satisfactory images are obtained. Therefore Nile Red in propylene glycol using copper dishes was used in subsequent experiments.

4.2.2.4 Butter samples

Using confocal scanning laser microscope, the confocal images of commercial butter (STD-1), experimental butter (DRI-24), margarine (MAR-1) and specialty butters (SPE-1 and SPE-2) have been obtained. They are shown in Figures 43, to 47 and in APPENDIX 3.

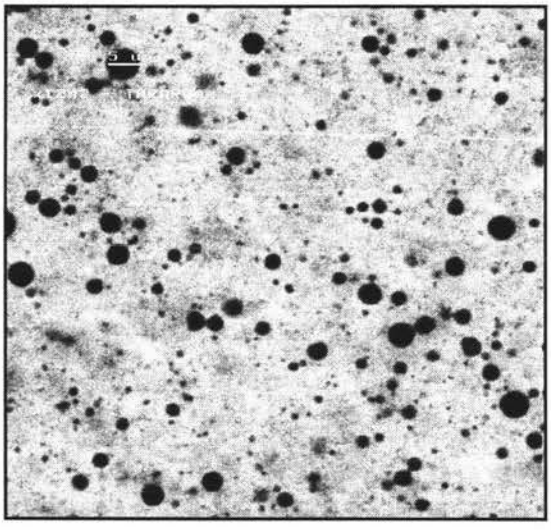

Figure 43. The microstructure of STD-1 butter. Lipids stained with Nile Red dissolved in propylene glycol. Dark holes are water droplets. Sample holder is copper dish. Bar = 5 μm. (16% moisture).

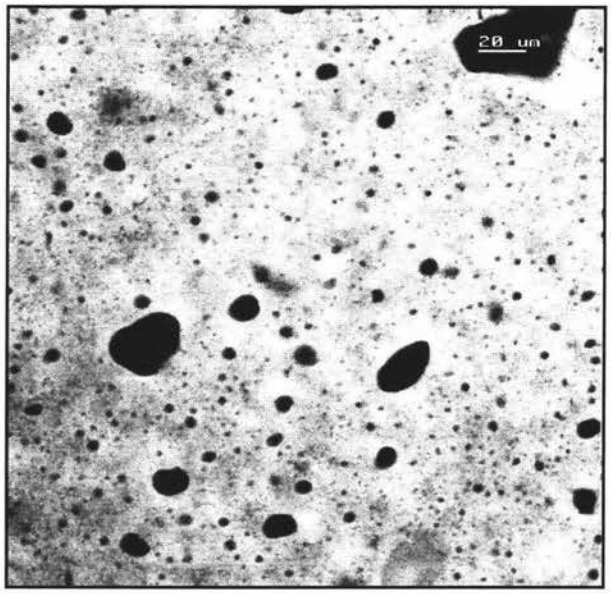

Figure 44. The microstructure of DRI-24 butter. Lipids stained with Nile Red dissolved in propylene glycol. Dark holes are water droplets. Sample holder is copper dish. Bar = 20 μm. (24% moisture)

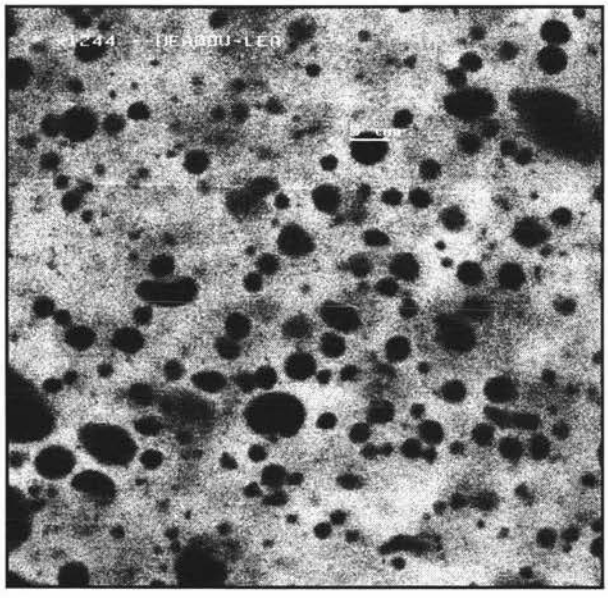

Figure 45. The microstructure of MAR-1 margarine. Lipids stained with Nile Red dissolved in propylene glycol. Dark holes are water droplets. Sample holder is copper dish. Bar = 5 μm. (16% moisture)

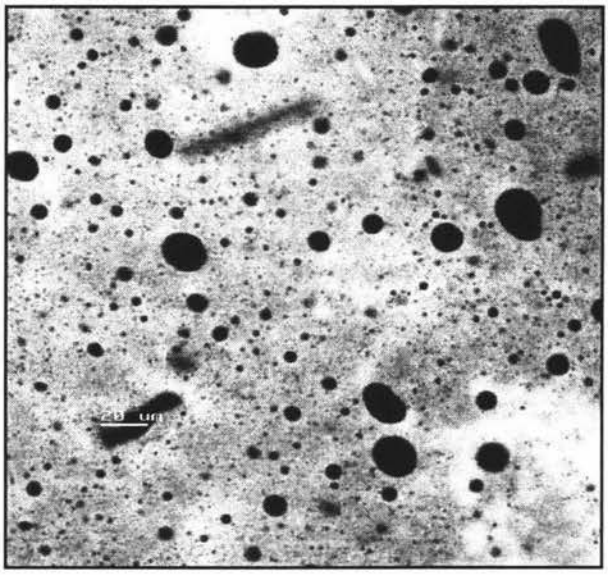

Figure 46. The microstructure of SPE-1 butter. Lipids stained with Nile Red dissolved in propylene glycol. Dark holes are water droplets. Sample holder is copper dish. Bar = 20 μm. (24% moisture).

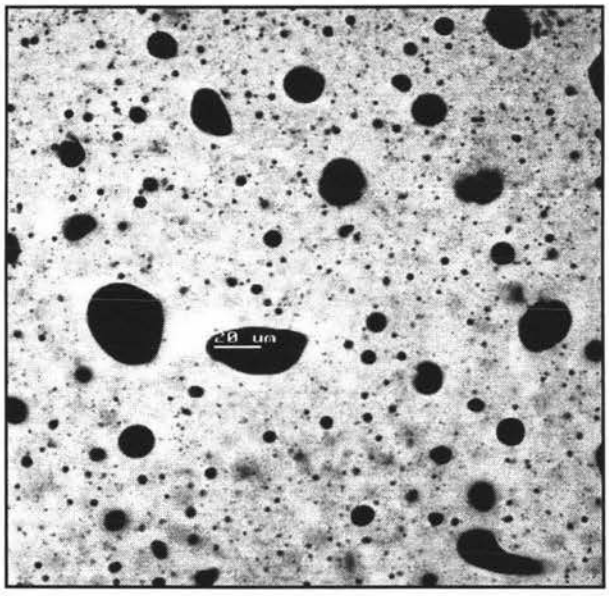

Figure 47. The microstructure of SPE-2 butter. Lipids stained with Nile Red dissolved in propylene glycol. Dark holes are water droplets. Sample holder is copper dish. Bar = 20 μm. (24% moisture)

Observing microstructures of the SPE-1 and the SPE-2 butters (Figure 46 and Figure 47), it is easy to see that there are some irregular shaped droplets and a wide range of droplet sizes.

From these pictures, (Figure 43 to Figure 47), droplet distributions, moisture contents and droplet shapes of samples can be obtained. These can provide original data to compare with the results of PFG- NMR method.

4.2.3 Choosing the magnification of images

To find most of water droplets in sample, images of some samples with different magnification have been obtained. Most of the water droplets in the sample are small size droplets with their diameters below 5 μm, but bigger size droplets are also very important because one bigger size droplet may be equal to several hundred small size droplets in volume. So it is important to observe both large number of small size droplets and the small number of large size droplets at the same time.

Two speciality butters (SPE-1 butter and SPE-2 butter) were studied using different magnification (16x, 40x and 63x). Their images are shown in Figures 48 to 53.

Figure 48.
Microstructure of SPE-1 butter
Magnification: **16x** object
Scale bar: 50 μm
Explored area: 623 x 623 $(\mu m)^2$
Dye: Nile Red in propylene glycol
Sample holder: Copper dish

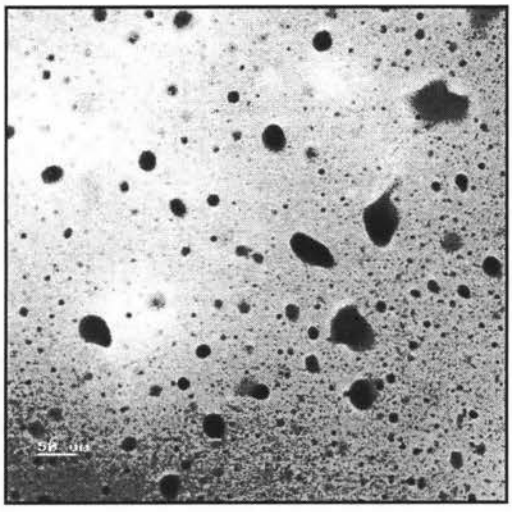

Figure 49.
Microstructure of SPE-1 butter
Magnification: **40x** object
Scale bar: 20 μm
Explored area: 248 x 248 $(\mu m)^2$
Dye: Nile Red in propylene glycol
Sample holder: Copper dish

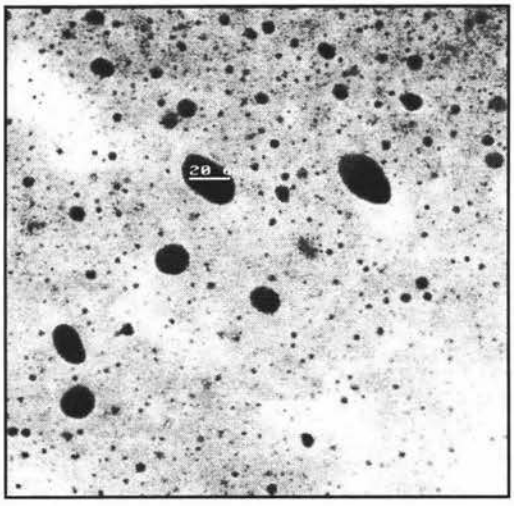

Figure 50.
Microstructure of SPE-1 butter
Magnification: **63x** object
Scale bar: 20 μm
Explored area: 158 x 158 $(\mu m)^2$
Dye: Nile Red in propylene glycol
Sample holder: Copper dish

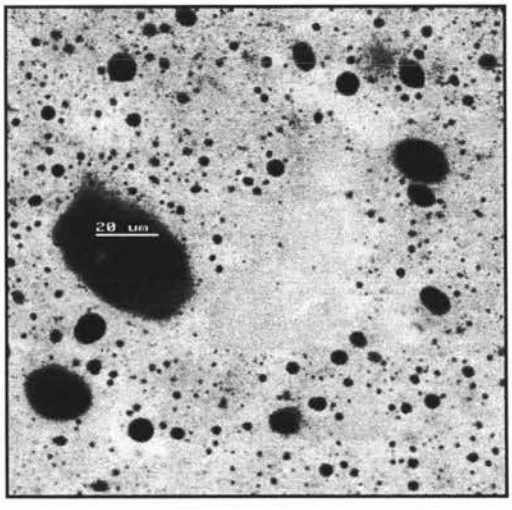

Figure 51.
Microstructure of SPE-2 butter
Magnification: **16x** object
Scale bar: 50 μm
Explored area: 623 x 623 $(\mu m)^2$
Dye: Nile Red in propylene glycol
Sample holder: Copper dish

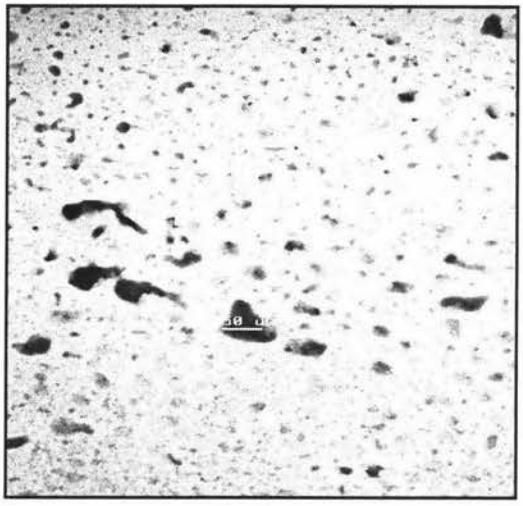

Figure 52.
Microstructure of SPE-2 butter
Magnification: **40x** object
Scale bar: 20 μm
Explored area: 248 x 248 $(\mu m)^2$
Dye: Nile Red in propylene glycol
Sample holder: Copper dish

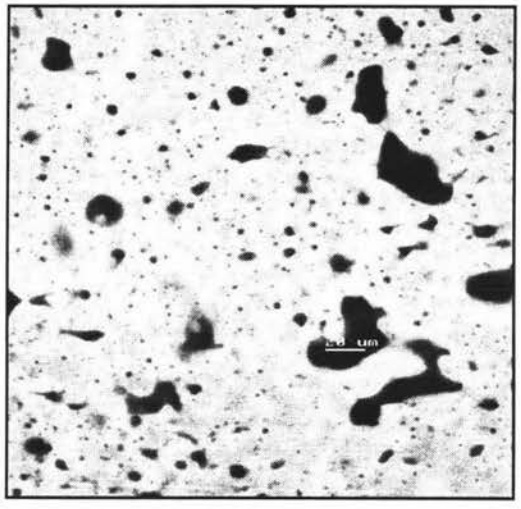

Figure 53.
Microstructure of SPE-2 butter
Magnification: **63x** object
Scale bar: 20 μm
Explored area: 158 x 158 $(\mu m)^2$
Dye: Nile Red in propylene glycol
Sample holder: Copper dish

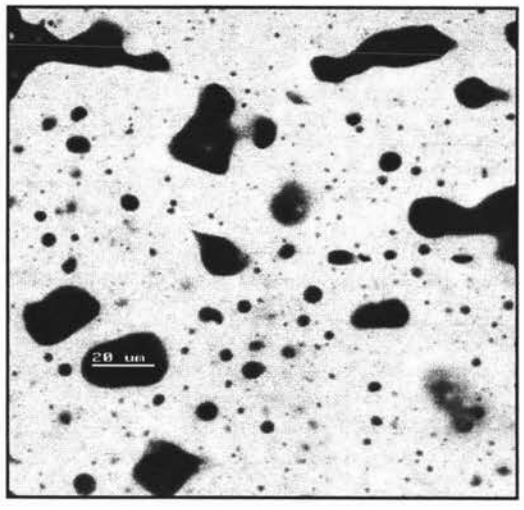

The low magnification images (16x object) cover a larger explored area (623 x 623 μm). Hence, large droplets are visible in the sample, but some smaller sized droplets may be lost. If a high magnification (63x object) is used to study the microstructures of samples, most of small size droplets are found, but some larger size droplets may be lost because the explored area is smaller (158 x 158 μm) than that of the low magnification images. To observe both larger size droplets and smaller size droplets, a middle magnification (40x object) is preferable. Image analysis using the VIPS program allowed the determination of the droplets size distribution into diameter bands. The curves of droplet distributions give same answer (Figure 54 and Figure 55), particularly in that 40x magnification gave the best compromise in observing large and small droplets.

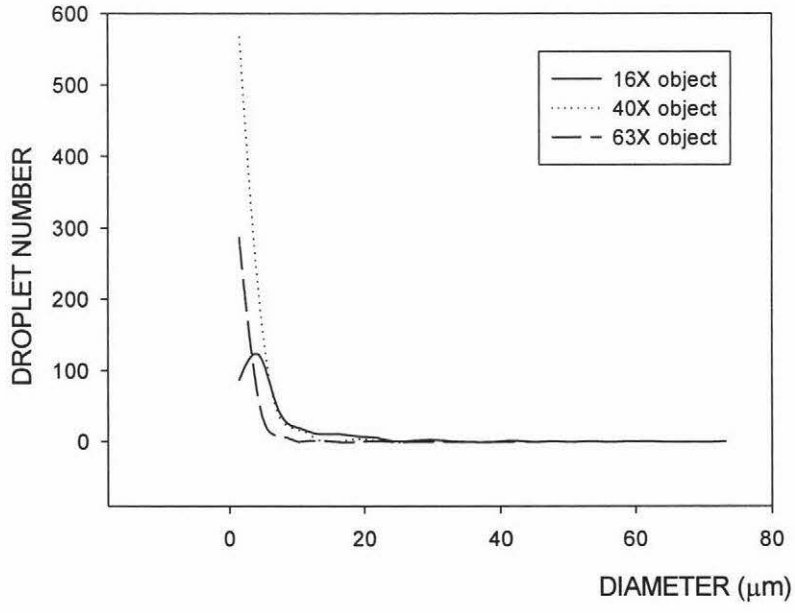

Figure 54. The distribution of water droplet numbers in SPE-1 butter with different magnification.

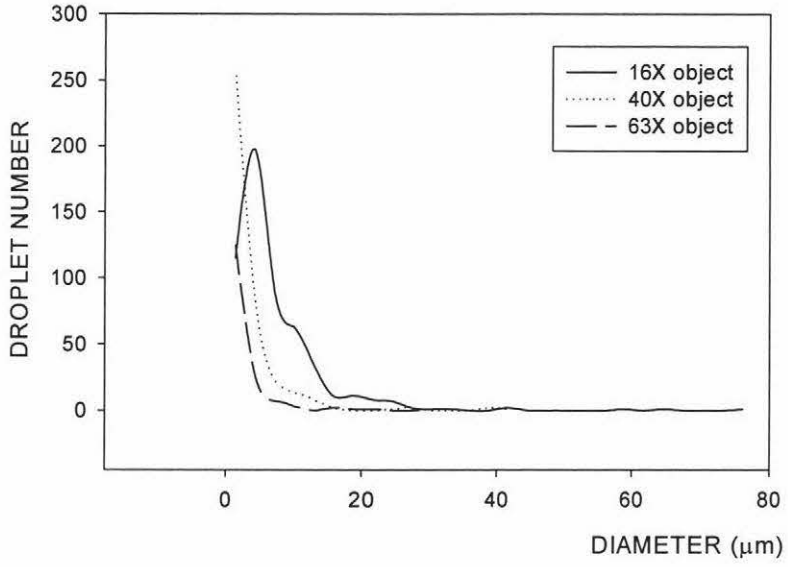

Figure 55. The distribution of water droplet numbers in SPE-2 butter with different magnification.

Limitations of CSLM include:

- Accurate water droplet distribution of butter and an accurate moisture content requires a great number of images of the butter. Moisture contents require the assumption that the observed droplet area is equal to the measure % water in the sample. As the water droplet distribution in the butter is not uniform many images of the butter are needed to represent the bulk properties of the butter. However, they do not represent a full view of the butter.

- For different samples, different magnifications are needed to study their microstructures. For example: for margarine, 40x magnification was used to study its droplet size and moisture content, and excellent results

obtained because the water droplets were middle sizes ($d_{50,3}$ = 5.01 +/- 0.04) and the distribution was uniform. For STD-1 butter and DRI-24 butter, we did not obtain good answers using same magnification.

4.2.4 Z-series experiments

To obtain further understanding of the microstructures of butter and margarine samples, a Z-series of experiment of some samples was obtained. Information from these experiments gives three-dimensional information of the samples (Figure 56, and Figure 57). By knowing the distance between the successive images the sizes of the droplets can be estimated.

In Figure 56, droplet A (in the dashed square) appears in 12 images of SPE-1 butter, its length in the Z direction is more than 8.4 μm (65.36 – 57.00 μm) and its diameter is about 9 μm in the X–Y plane, indicating that droplet A is spherical. However, in Figure 57, droplet B (in the dashed square) appears in 12 images of SPE-2 butter, its length in Z direction is more than 9.0 μm (45.03 – 36.07 μm) but its diameter is smaller than 7.0 μm in X-Y plane. So its shape is that of a prolate ellipsoid. Thus the three dimensional analysis shows more information.

4.2.5 Analytical program of the droplet sizes and droplet numbers in emulsions by computer

Ten CSLM pictures of each sample were obtained. It is necessary to calculate the droplet size and droplet number from these pictures. Also the moisture content in the samples can be estimated.

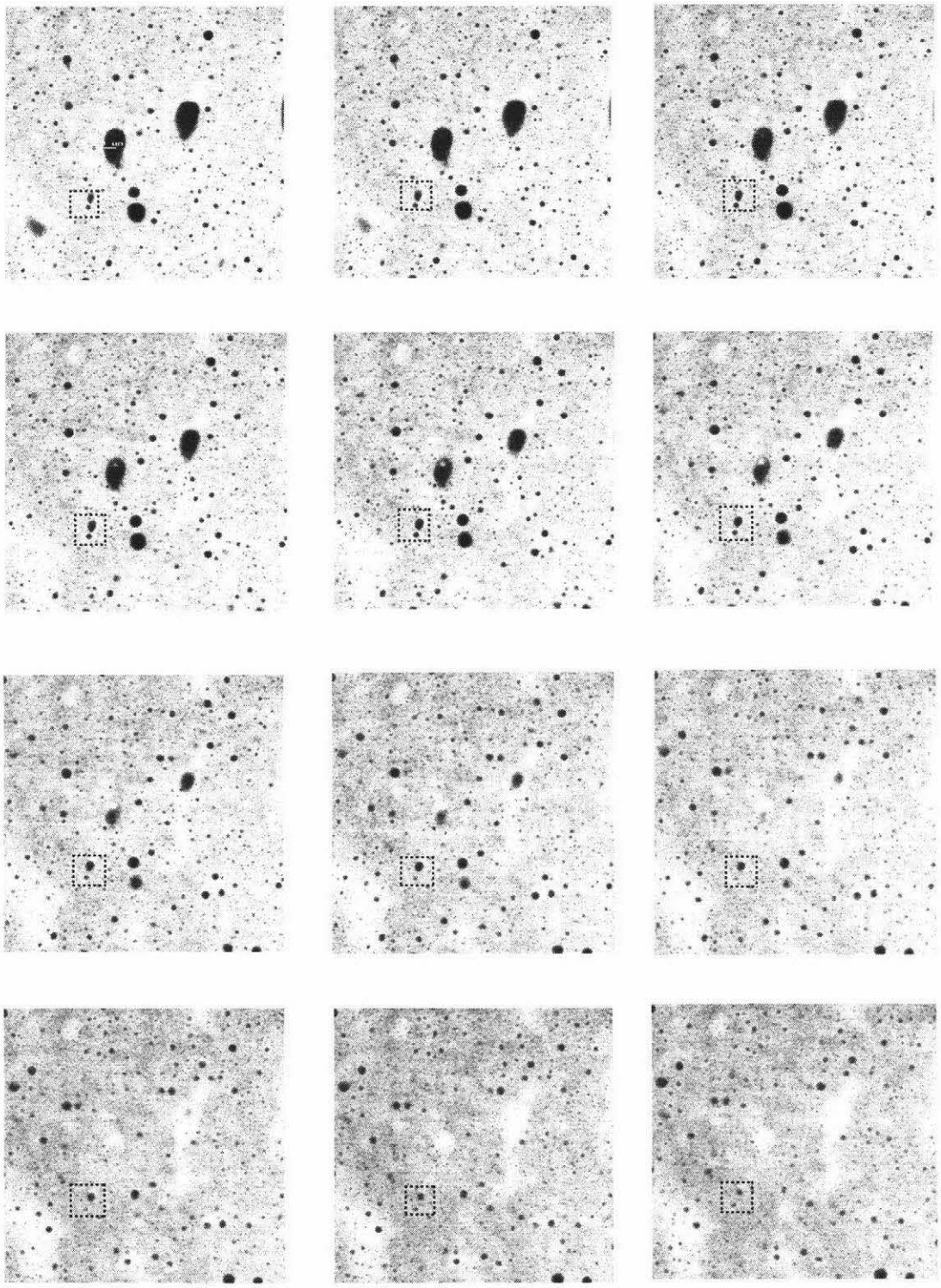

Figure 56 The Z-series experiment of SPE-1 butter. Magnifictaion is 40x object, and scale bar is 20 μm. 12 images from top (65.36 μm) to bottom (57.00 μm).

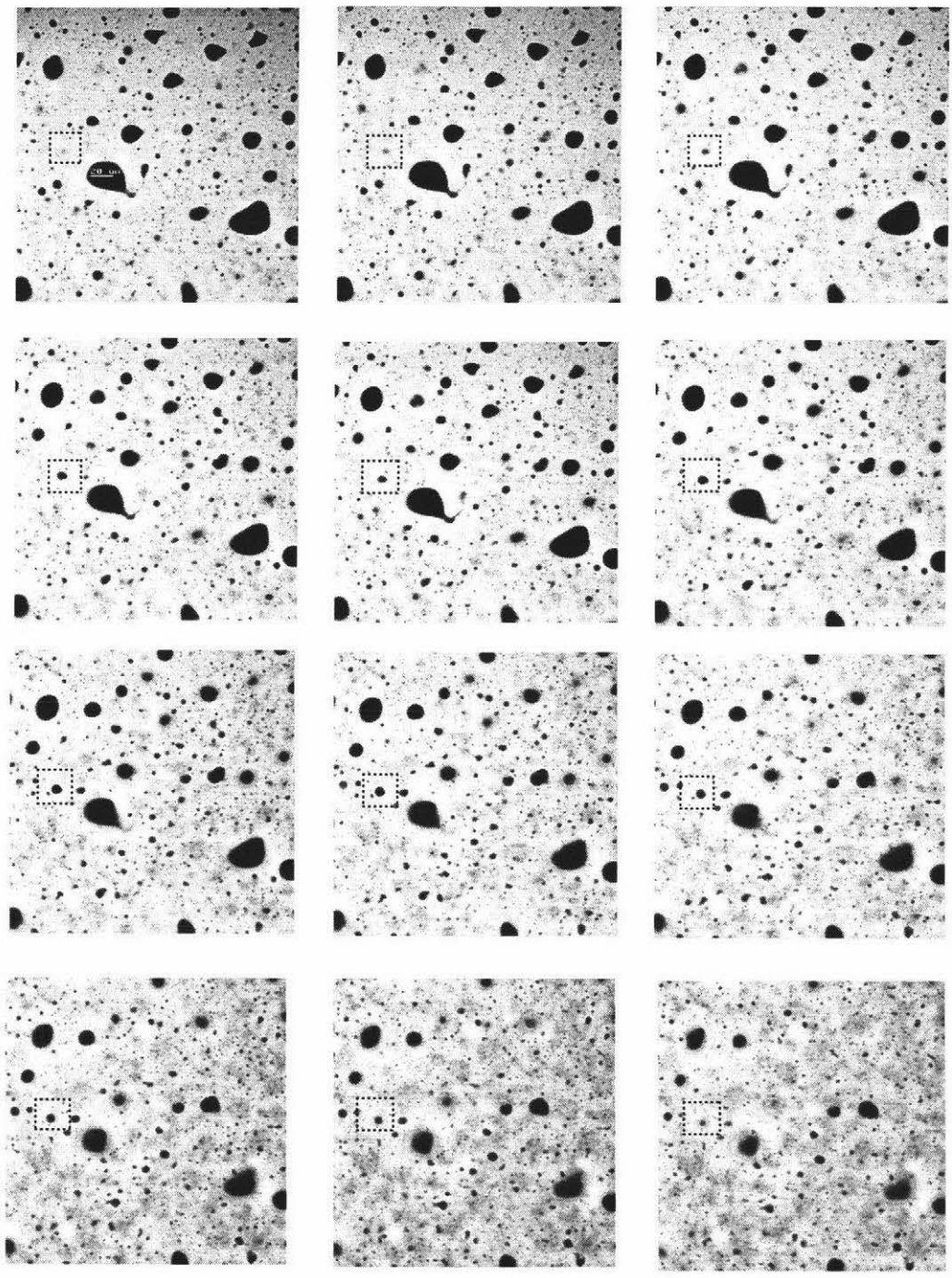

Figure 57 The Z-series experiment of SPE-2 butter. Magnificatrion is 40x object, and scale bar is 20 μm. 12 images from top scetion (45.03 μm) to bottom section (36.07 μm).

The applied software (VIPS) can be used to count the number of droplets in each diameter band. This band is the 2D cut diameter. The data may be unbiased to produce on estimate of the 'actual' (see Table 10) diameter (unbiased number column) by analytical matrix manipulation. However the small number of large droplets lead to negative numbers in the bands adjacent to the large droplets (Table 10). This would only be able to be overcome with hundreds of images to get representative images of all the sizes droplets. All subsequent distributions in this work are based on the biased number column (column 2).

Table 10. The results of using VIPS to determine the droplet sizes and numbers of SPE-1 butter (Scale interval: 2.5 μm; 40x object). The diameter is the midpoint of the 2.5 μm band.

Diameter band (2D cut d)	number	unbiased number
1.25,	4084.0,	3707.20
3.75,	1132.0,	1328.90
6.25,	273.0,	370.59
8.75,	87.0,	115.11
11.25,	44.0,	69.24
13.75,	19.0,	18.81
16.25,	17.0,	23.67
18.75,	12.0,	19.97
21.25,	7.0,	18.46
23.75,	1.0,	0.52
26.25,	1.0,	1.26
28.75,	1.0,	-3.87
31.25,	3.0,	10.43
33.75,	0.0,	-0.11
36.25,	0.0,	-2.61
38.75,	1.0,	1.11
41.25,	1.0,	4.00
43.75,	0.0,	-0.11
46.25,	0.0,	-0.28
48.75,	0.0,	0.11
51.25,	0.0,	-3.30
53.75,	1.0,	4.58
56.25,	0.0,	-0.10
58.75,	0.0,	-0.29
61.25,	0.0,	0.17
63.75,	0.0,	-3.63
66.25,	1.0,	5.17

4.2.6 The distributions of water droplet numbers

After the droplet sizes and droplet numbers are counted, a plot of water droplet numbers versus the water droplet diameters is constructed. In this plot the cut diameters of droplets from CSLM have been converted into the diameters of droplets to compare the result of PFG-NMR. The most possible diameter is 0.87 times the diameters of the droplets (Appendix 4). A statistical meaningful number of the droplet is assumed. Also, the water droplet size distributions in water-in-oil emulsions is assumed to be log-normal because experimental data showed that mathematical function was most suitable to describe particle size distributions of these products. The X-axis is therefore displayed on a log scale.

The results of the sum of 10 images of STD-1 butter and Mar-1 margarine (see Appendix 3) are plotted in Figure 58 and Figure 59.

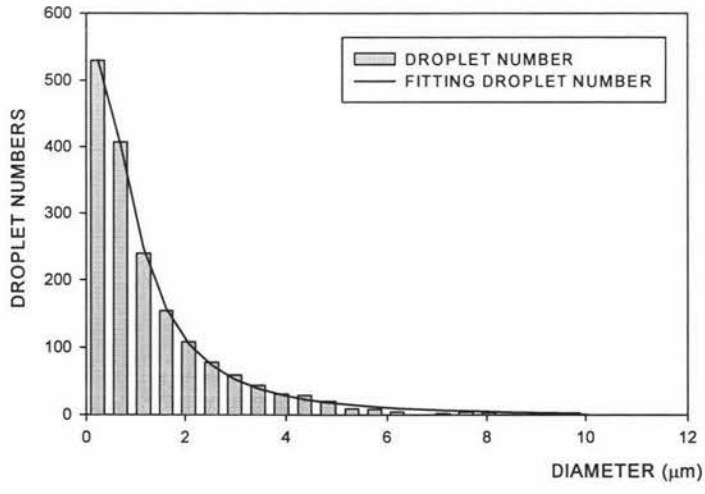

Figure 58. The distribution of water droplet numbers in STD-1 butter by CSLM.

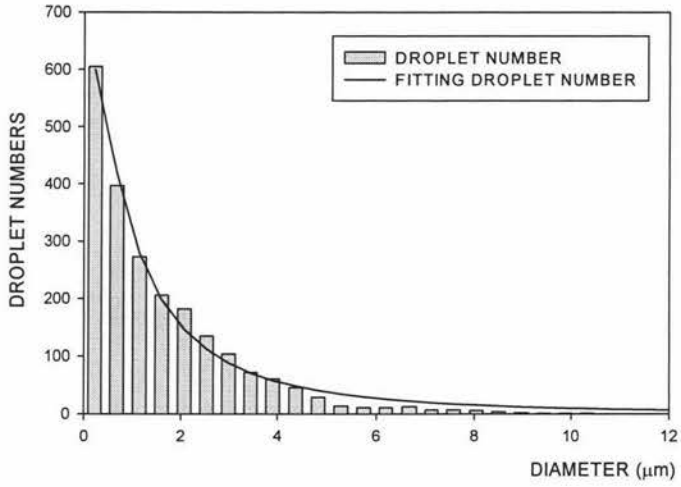

Figure 59. The distribution of water droplet numbers in MAR-1 margarine by CSLM.

From the distributions of water droplet numbers of STD-1 butter (Figure 58) and MAR-1 margarine (Figure 59), it is seen that most of droplets in samples are small size droplets. The answers are same with PFG-NMR results (Figure 24 and Figure 26).

For STD-1 butter, the small size droplets that are below 2 μm in diameter occupy 83.1% in total of droplet number. For MAR-1, the ratio is 75.9%. Comparing STD-1 with MAR-1, most droplets are small sizes in STD-1. But there are some bigger size droplets and middle size droplets in MAR-1.

4.2.7 The distributions of droplet volume

In order to compare the results of confocal scanning laser microscopy with the results of PFG-NMR, the distribution of droplet numbers needs to be

converted into the distribution of droplet volumes. This is done using the equation:

$$V_{\text{droplet}} = (4 / 3) \cdot \pi \cdot (d / 2)^{3} \cdot N$$

where d is the diameter of droplet in the cross area, and N is the number of water droplets with d diameter.

The distributions of water droplet volume of STD-1 butter and MAR-1 margarine are shown in Figure 60 and Figure 61.

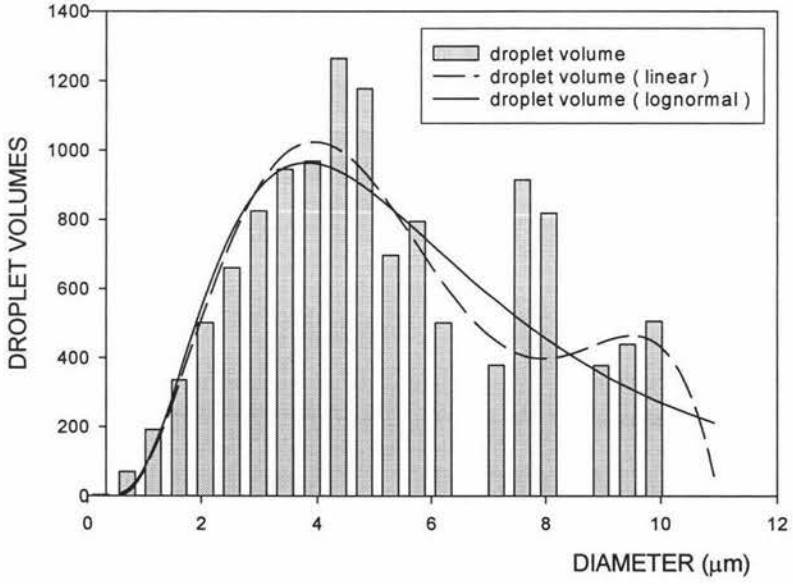

Figure 60. The distribution of water droplet volume of STD-1 butter by CSLM.

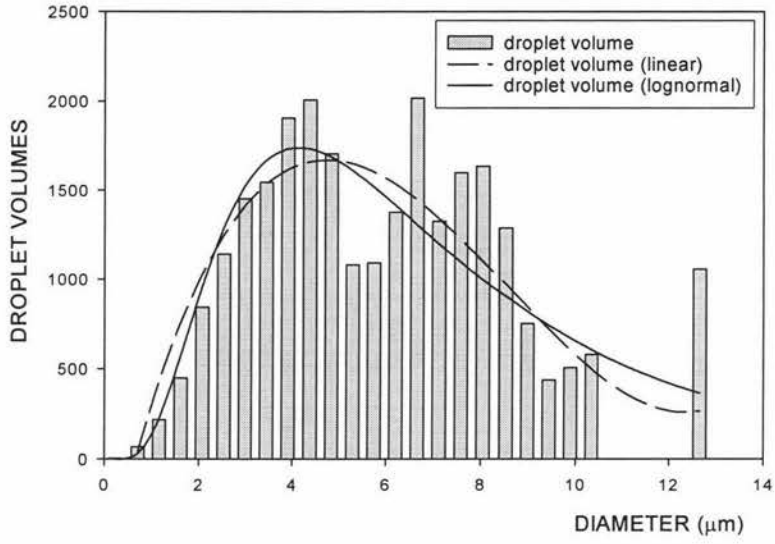

Figure 61. The distribution of water droplet volume of MAR-1 margarine by CSLM.

4.2.8 The measurements of moisture contents

Using confocal images of samples, the moisture contents of samples can be obtained. The assumption is that the area of the image occupied by water droplets is equal to the water content. Moisture contents are listed in Table 11 and Table 12.

Table 11. The moisture contents of SPE-1 butter and SPE-2 butters

Image Number	SPE-1 butter		SPE-2 butter	
	16x	**40x**	**16x**	**40x**
0	8.49	17.20	13.50	18.78
1	11.88	15.38	8.07	17.32
2	14.77	13.06	19.16	19.24
3	9.38	12.55	21.01	15.76
4	16.30	15.11	15.72	16.56
5	14.17	15.56	13.12	20.10
6	10.70	13.19	18.02	20.54
7	14.67	16.54	15.07	22.52
8	12.15	------	17.46	17.11
9	10.13	12.83	13.64	23.90
Mean (STDV)	**12.50 (2.66)**	**14.82 (1.71)**	**15.68 (3.85)**	**19.66 (2.64)**
NZDRI Chemical Analysis	**25.0**		**22.4**	

The moisture content estimate from the CSLM results of the SPE-1 butter and the SPE-2 butter are different from the results of their chemical analysis. Also, the CSLM results with higher magnification (40x object) are

better than that of lower magnification (16x object), due to the loss of some small size droplets in the low magnification images. Conversely, in the large magnification images, some larger size droplets were lost. The results suggest that the smaller droplets are not being picked up. In addition, it is been assumed that droplets are spherical, but there are some irregular droplets in present (Appendix 3-4, SPE-2 butter and Figure 66). So there are certain deviations in the CSLM results of samples and the PFG-NMR results of samples.

In Table 12, STD-1 butter and MAR-1 margarine are compared with the results of their chemical analyses. The moisture content of MAR-1 margarine from CSLM images is quite close the results of its chemical analysis, but there is difference between the CSLM results and the results of chemical analysis in STD-1 butter. The reason for the good agreement with MAR-1 is that the water droplets are bigger and the distribution is uniform. The large standard deviation (Table 11 and 12) also indicate the limitations of this method for the determination of water contents. In STD-1 butter, the water droplet distributions are not uniform and many of the water droplets were small, and there are also some bigger size droplets in STD-1 butter. Some large size droplets may be lost in STD-1 butter because explored cross-area is limited.

Table 12. The moisture contents of STD-1 butter and MAR-1 margarine

Images No.	STD-1 butter	MAR-1 margarine
a	6.78	5.83
b	10.70	11.27
c	8.54	14.28
d	12.16	20.01
e	9.67	17.98
f	5.77	16.79
g	5.87	20.61
h	5.93	20.54
i	10.81	15.78
j	10.01	13.04
Mean (STDV)	**8.93 (2.31)**	**16.70 (3.40)**
NZDRI Chemical Analysis	**14.6**	**15.5**

4.3 Comparisons between the results of the PFG- NMR method and the results of the confocal scanning laser microscopy

4.3.1 Water droplet size by volume distributions

The water droplet size distributions of STD-1 butter obtained using PFG-NMR and CSLM are shown in Figure 62 and the results for MAR-1 margarine are shown in Figure 63.

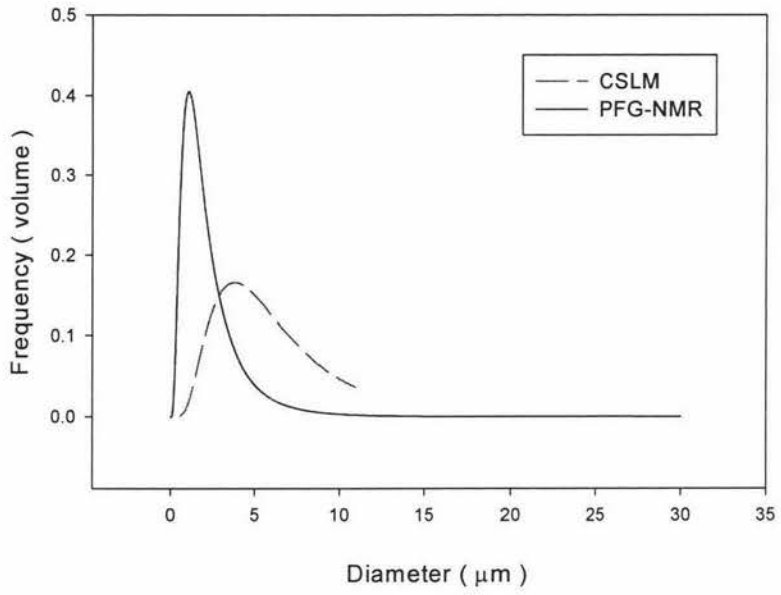

Figure 62. The distribution of water droplets by volume in STD-1 butter obtained from PFG-NMR and CSLM.

In Figure 62, there is a significant difference between the results of PFG-NMR and the results of CSLM. The reason is probably that the ten CSLM pictures of STD-1 butter do not represent the full view of STD-1 butter because most of the droplets are of small size and the droplet distribution is not uniform. To represent the bulk properties of the sample using CSLM, a large number of pictures are required for each sample. The time taken to do this is far too long to make the technique a suitable one for the determination of water droplet size distributions.

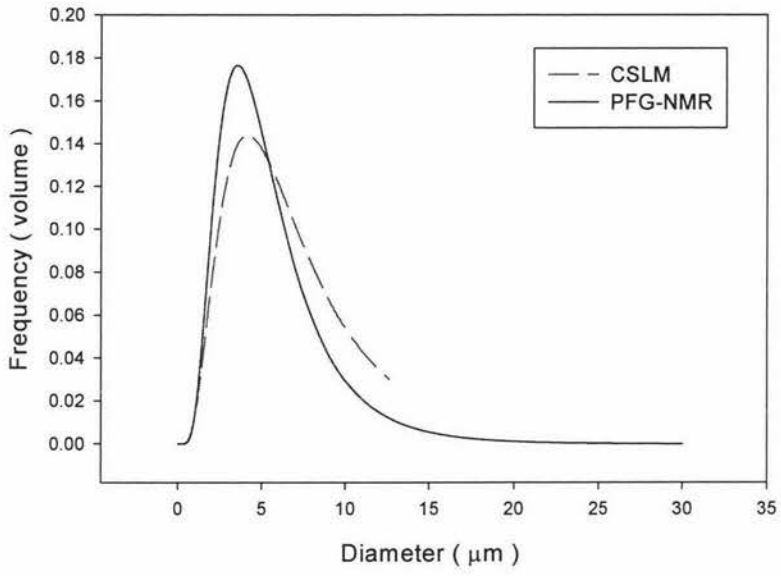

Figure 63. The distribution of water droplet by volumes in MAR-1 margarine obtained from PFG-NMR and CSLM.

In Figure 63, good agreement between the two techniques is apparent. This is because a representative distribution of droplet size is observed at a single magnification in confocal scanning laser microscopy. Also water droplet distributions in MAR-1 margarine are relatively uniform.

4.3.2 Irregular droplets

The NMR results of SPE-1 butter and SPE-2 butter are shown again in Figure 64. The butters have similes moisture content (Table 11) but have significantly different distributions.

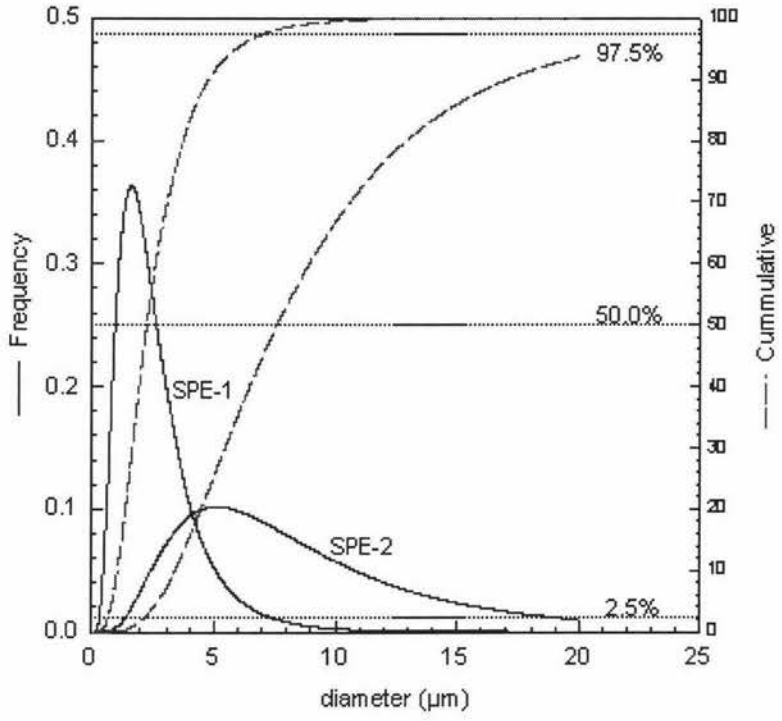

Figure 64. The distributions of water droplet sizes of SPE-1 butter and SPE-2 butter by PFG-NMR method.

In calculating the distribution, it is assumed the droplets are spheres. However, some of the droplets are irregular shapes. This can be seen from the CSLM images. Images for the SPE-1 and SPE-2 butters are shown in Figure 65 and 66 respectively. The droplets in SPE-1 butter are dominantly spherical while in SPE-2 butter there are a large number of irregular shaped droplets. SPE-2 butter is made by the Fritz process which involves more churning of the butter and this leads to the irregular shapes. It would be interesting to test whether the presence of these irregular shapes had any effect on the calculated distribution of water droplets.

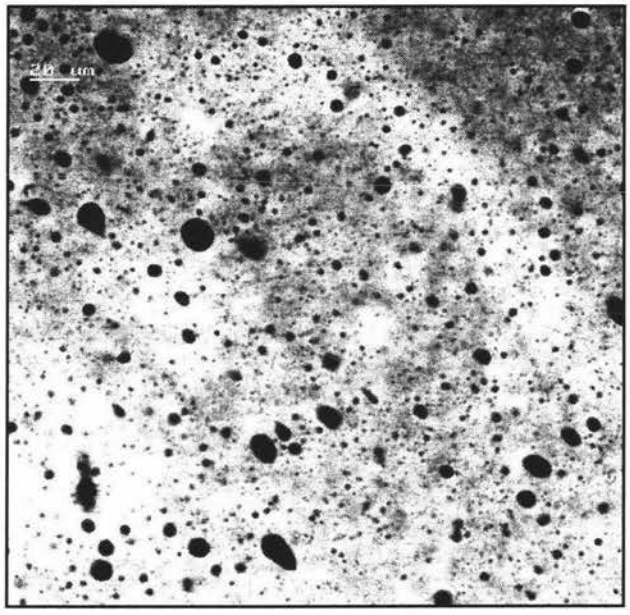

Figure 65. The images of SPE-1 butter by confocal scanning laser microscopy. 40x object. Dark holes are water droplets.

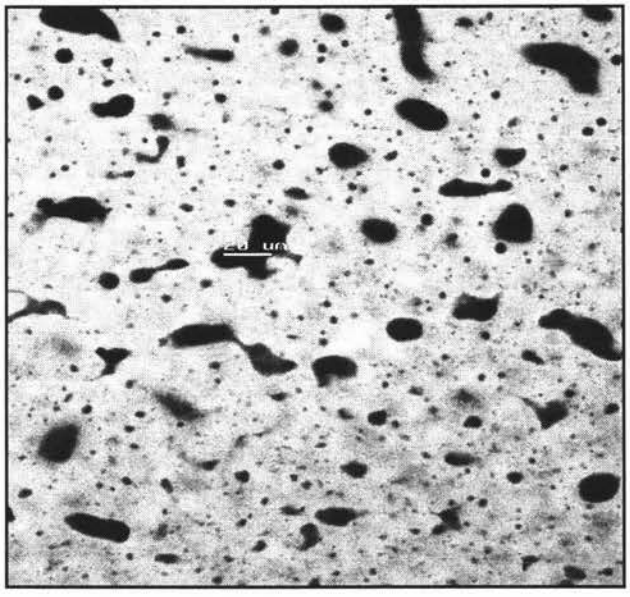

Figure 66. The image of SPE-2 butter by confocal scanning laser microscopy. 40x object. Dark holes are water droplets.

4.4 Comparisons between the results of low resolution NMR and high resolution NMR

When CSLM was used to compare and confirm the results of low resolution PFG-NMR, there were some disadvantages. For example, it is hard to represent the bulk properties of butter sample using several confocal images of the sample because explored area in sample is quite small.

To describe the bulk properties of sample effectively and completely, high resolution NMR (300 *MHz*) was used to confirm the result of low resolution NMR. As we know, high resolution machine has a stronger magnetic field strength. It can give a stronger RF power, so that it can provide a good resolving power and a high sensitivity. It can clearly separate the resonant signals of aqueous phase and fat phase in butter sample. Also, its powerful pulsed gradient unit enables a much larger signal attenuation to be achieved (smaller R values). The comparison between low resolution NMR and high resolution NMR for STD-1 butter was plotted in Figure 67.

In Figure 67, parameter δ^2G^2 was chosen as abscissa in order to achieve a direct comparison between the two methods. All parameters expect δ and G are the same in both the low resolution and high resolution NMR experiments. According to equation (5), for same sample, the experimental results between low resolution NMR and high resolution NMR can be compared although gradients were different between low resolution NMR and high resolution NMR. Because there is a limitation of the δ range ($0 \sim 5$ ms) in the low resolution machine, the R values obtainable are much smaller using this instrument.

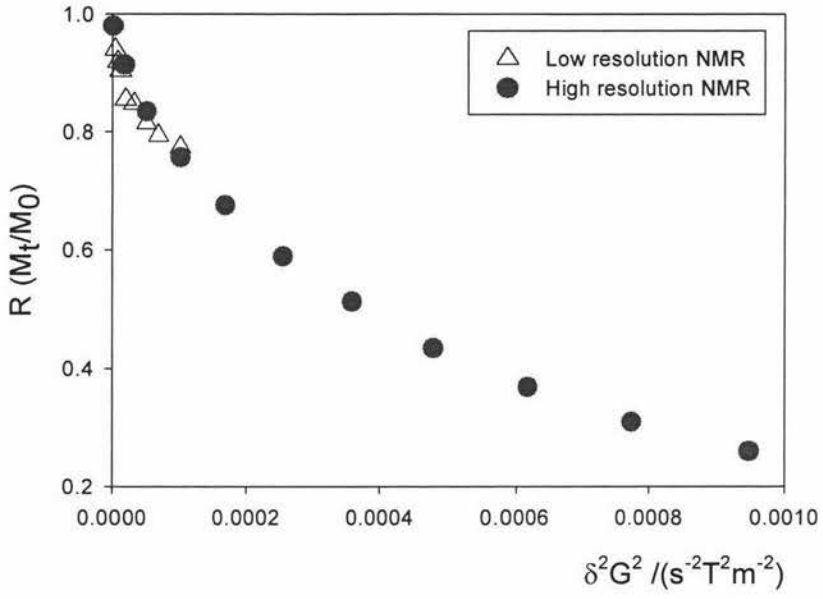

Figure 67. The R versus δ distributions of STD-1 butter between low resolution NMR and high resolution NMR.

The results of comparison in Figure 67 show that the results of two measurements overlapped when δ^2G^2 were below 0.0001. Namely, high resolution NMR and low resolution NMR have same experimental results. Without doubt, the result of high resolution NMR proved the reliability and accuracy of the experimental result of low resolution NMR.

5.0 Conclusions and future work

The PFG-NMR method is a rapid, easy and reliable method to determine the droplet size distribution in emulsions. Especially, it can be used to determine optical dense systems and highly viscous systems.

In the measurement of water droplet size distribution in butter or margarine, the method requires small volume sample and the method is nondestructive. Using new software-"WIN-NMS", a measurement of the water droplet size distribution of butter or margarine can be obtained in 20 minutes from sample preparation to determination. Confirmation of the low resolution methodology was achieved by the use of high resolution NMR. The sample preparations, observations and data analyses consume time and the costs of equipment are expensive.

For butters droplets with a significant proportion of smaller sizes (for example: $d_{50,3}$ = 1.7 μm), a poor fitting curve of the echo height ratio (R) versus PFG width is obtained. This is because the attenuation in the echo height is small. The magnetic strength and RF power in low resolution machine are much small than in high resolution machine and the biggest gradient is 2 T/m. A larger field gradient together with the ability to select larger δ value is required.

One method that could be applied to improve the signal to noise ratio is to increase the number of scans. More time will be needed to do this.

The determination of the droplet size distribution by confocal scanning laser microscope has been shown to have limitation. The small sample area used for analysis gave rise to two problems. 1, Artefacts are due to the random inclusion or exclusion of very large droplets; 2, The inability is to observe both small and large droplets at the same time. Because the explored area is very small in CSLM, to represent the bulk properties of the sample about 100 pictures of each sample are required. The sample preparations, observations and data analyses consume time and the cost of equipment is expensive.

For butters, an agreement can not be got in the measurement of water droplet size distributions and the moisture contents between NMR and CSLM. One reason may be that the droplet distributions were not uniform in the samples and most droplets were irregular. Especially, some irregular droplets with large sizes may be the cause of the big deviation between real distributions and experimental results.

Comparison of the margarine results showed that for samples with a larger proportion of larger droplets the NMR results agreed extremely well with the observed microscopy results. It should also be acknowledged that the NMR is only able to resolve droplets that have a diameter in which the restricted diffusion may be resolved (so there is a lower limit to the resolution of the NMR droplet sizes).

Future work would need to examine the effects caused by irregular droplets in the measurement of water droplet sizes in samples. In addition, further work need to be done on the distribution of water droplet size in butters which contain many small size droplets.

Summary the work presented here has shown that PFG-NMR is a modern, economic, fast method to investigate the properties of dispersed phase in emulsions particularly butters and margarines. It is suitable not only in the laboratory but also in the factory environment. Without doubt, it is a very effective tool to determine the droplet sizes distribution in emulsions.

6.0 References

[1]. Carla P. Rudelle, *Butter – Analysis, Composition and Flavourings*: Index of new information with authors, subjects, research categories and references (1997). 13.

[2]. Gösta Bylund, Dairy Processing Handbook, Tetra Processing Systems. AB, Sweden (1995), 270.

[3]. Michelle Harnett, The rheology of butter (1989), *Ph.D thesis, Massey University*, New Zealand.

[4]. International standard, *Butter – Determination of water dispersion value*. Ref. No: ISO 7586 – 1985 (E).

[5]. G. H. Wilster, *Practical buttermaking*, Eighth edition. (1957), O.S.C. Cooperative Association, Corvallis, Oregon, U.S.A.

[6]. Frederick H. McDowall, *The buttermaker's manual* (1953) Volume I, Wellington, New Zealand University Press. 415.

[7]. Otto F. Hunziker, *The butter industry*, Third edition. (1940), La Grange, Illinois, U.S.A.

[8]. M.M.W. Mooren, M.C.M. Gibnau and M.A. Voorbach, Determination of droplet size distributions in emulsions by pulsed field gradient NMR in Characterization of Food: *Emerging Methods*, ed. by A.G. Gaonker (1995) 151. Elsevier science B.V.

[9]. B. Balinov, etc., Determination of water droplet size in margarines and low-calorie spreads by nuclear magnetic resonance self-diffusion (1994), Vol. **71** (5), *JAOCS*, 513.

[10]. W. Buchheim and P. Dejmek, In *Food Emulsions* (K. Larsson and S. E. Friberg, eds.), Marcel Dekker, Inc., New York, 1990, 203.

[11]. I. Heertje, P. van der Vlist, J.C.C. Blank, H.A.C.M. Hendrickx and G.J. Brakenhoff, Confocal Scanning Laser Microscopy in Food Research : Some Obervations. *Food Microstructure* (1987) **6**, 115~120.

[12]. Brian E. Brooker, The Study of Food Systems Using Confocal Scanning Laser Microscopy, *Microscopy and Analysis* (1991) November, 13.

[13]. B.E. Brooker, Imaging food systems by confocal scanning laser microscopy. In *New Physico-chemical Techniques for the Characterization of complex Food Systems*, (1995) 53. (Ed.E. Dickenson). London: blackie Academic and Professional.

[14]. A. B. McKenna, Food Microstructure: Seeing the unseen at New Zealand Dairy Research Institute, *Food Technologist* (1995) **24** (4), 34.

[15]. I. Heertje, J. Nederlof, H.A.C.M. Hendrickx and E.H. Lucassen–Reynders, The observation of the displacement of emulsifiers by confocal scanning laser microscopy. *Food Structure* (1990) **9,** 305.

[16]. I. Heertje, H. van Aalst, J.C.C. Blonk, A. Don, J. Nederlof and Lucassen – Reynders, Observations on Emulsifiers at the Interface between oil and Water by Confocal Scanning Light Microscopy, *Lebensm.-Wiss. u.-Technol.*, (1996) **29**, 217.

[17]. Peter M. Cooke, Chemical Microscopy, *Anal. Chem.* (1996) **68,** 333R.

[18]. J. C. G. Blonk and H. van Aalst, Confocal scanning light microscopy in food research. *Food Research International* (1993) **22,** 297.

[19]. A.N. Hassan, J.F.Frank, M.A. Farmer, K.A. Schmidt and S.I. Shalabi, Formation of Yogurt Microstructure and Three-Dimensional Visualization as Determined by Confocal Scanning Laser Microscopy, *J. Dairy Sic.* (1995) **78**, 2629.

[20]. Stuart M. Clegg, Adele K. Moore and sylvia A. Jonesa, Low-fat Margarine Spreads as Affected by Aqueous Phase Hydrocolloids, *Journal of Food Science* (1996) **61** (5), 1073.

[21]. Anthony B. McKenna, Examination of whole milk power by confocal scanning laser microscopy, *Journal of Dairy Research* (1997) **64,** 423.

[22]. David Everett, Confocal Scanning Laser Microscopy of Cheese, *Australian Dairy Foods* (1997) December, 41.

[23]. Alastair MacGibbon and Nick Robinson, Milk fat analytical method development, *Food Technology in New Zealand* (1997) February, 20.

[24]. T.F. Conway, R.F. Cohee and R.J. Smith, *Manufacturing Confectioner* (1957) **37,** 27.

[25]. E.O. Stejskal and J.E. Tanner, Spin Diffusion Measurements: Spin Echoes in the Presence of a Time –Dependent Field Gradient, *J. Chem. Phys* (1965) **42,** 288.

[26]. E.O. Stejskal, *J. Chem. Phys.*, (1965 6) **43,** 3597.

[27]. J.E. Tanner and E.O. Stejskal, Restricted Self-Diffusion of Protons in Colloidal Systems by the Pulsed-Gradient, Spin-Echo Method, *J. Chem. Phys* (1968) **49,**1768.

[28]. J.K. Packer and C. Rees, Pulsed NMR Studies of Restricted Diffusion: 1. Droplet Size Distributions in Emulsions, *J. Colloid Interface Sci.* (1972) **40,** 206.

[29]. P. T. Callaghan, K.W. Jolley and J. Lelièvre, *Biophys. J.* (1979) **28,**133.

[30]. P. T. Callaghan, K.W, Jolley and R.S. Humphrey, *J. Colloid Interface Sci.* (1983) **93,** 521.

[31]. G. Fleisher, V.D. Skirda and A. Werner, Eur. *Biophys. J.* (1990) **19,** 25.

[32]. J.C. van den Enden, D. Waddington, H. van Aalst, C.G. van Kralingen and K.J. Packer, Rapid determination of Water Droplet Size Distributions by PFG-NMR, *J. Colloid Interface Sic.* (1990) **140,** 105.

[33]. D.G. Cory and A.N. Garroway, *Magn. Res. Med.*, (1990) **14,** 25.

[34]. I. Lönnqvist, A. Khan and O. Söderman, *J. Colloid Interface Sci.* (1991) **144,** 401.

[35]. J.S. Murday and R.M. Cotts, Self-Diffusion Coefficient of Liquid Lithium, *J. Chem.Phys.* (1968) **48**, 4938.

[36]. O. Söderman, I. Lönnqvist and B. Balinov, *Nato Asi. Ser. C* (1992) **363** (Emulsions: Fundam. Pract. Appr.) 239.

[37]. B. P. Hills and J.E.M. Snaar, *Mol. Phys.* (1992) **76,** 979.

[38]. X. Li, J.C. cox and R.W. Flumerfelt, *AIChE J.* (1992) **38,** 1671.

[39]. B. Balinov and O. Söderman and J.C. Ravey, Diffraction-like Effects Observed in the PGSE Experiment When Applied to a Highly Concentrated Water / Oil Emulsion, *J. Phys. Chem.* (1994) **98,** 393.

[40]. J.P. Renou, J. Kopp, P. Garellier, G. Monin and G. Kosak-Reiss, *Meat Sci.* (1989) **26,** 101.

[41]. P. G. Mottis, *Nuclear Magnetic Resonance Imaging in Medicine and Biology* (1986), Oxford University Press, Oxford.

[42]. M. A. Foster, N.J.F. Dodd, F.D. Rolls and R.R. Price, *Nuclear magnetic Resonance Imaging* (1983), W.B. Saunders, Philadelphia.

[43]. R.R. Ernst, Quart. *Rev. Biophys.* (1987) **19**, 183.

[44]. J.M. Pope and V. Sarafis, *Chem. Australia* (1990) **57**, 221.

[45]. P.S. Belton, I.J. Colquhun and B.P. Hills, Applications of NMR to Food Science in *Annual Report on NMR Spectroscopy* (1993) Vol. **26,**1.

[46]. B. P. Hills, Magnetic Resonance Imaging in Food Science. In *New Physico-Chemical Techniques for the Characterization of Complex Food Systems*, ed. by Eric Dickinson (1995), 319. London: Blackie Academic and Professional.

[47]. R. Raun, K. Chang, P.L. Chen, R.G. Fulcher and E.D. Bastian, A Magnetic Resonance Imaging Technique for Quantitative Mapping of Moisture and Fat in a Cheese Block. *J. Dairy Sci.* (1998) **80,** 9.

[48]. C.P. Slichter, *Principles of Magnetic Resonance*, (1989) Springer–Verlag, New York.

[49]. Daniel Canet, *Nuclear Magnetic Resonance–Concepts and Methods*, (1996) John Wiley & Sons, England.

[50]. P. T. Callaghan, *Principles of Nuclear Magnetic Resonance Microscopy*. Oxford University Press, Oxford, 1991.

[51]. P. T. Callaghan, D. MacGowan, K.J. Packer and F. O. Zelaya, *J. Magn. Reson.* (1990) **90,** 177.

[52]. P. T. Callaghan, A. Coy, D. MacGowan, K.J. Packer and F. O. Zelaya, *Nature* (1991) **351,** 467.

[53]. R.M. Cotts, *Nature* (1991) **351,** 443.

[54]. P. T. Callaghan, A. Coy, T.P.J. Halpin, D. MacGowan, K.J. Packer and F. O. Zelaya, *J. Chem. Phys.* (1992) **97** (1), 651.

[55]. M.J. Gidlry, A.J. McArthur, A.H. Darke and S. Ablett, High Resolution Nuclear Magnetic Resonance Spectroscopy of solid and Semi-Solid Food Components in *New Physico-Chemical Techniques for the Characterization of Complex Food Systems*, ed. by Eric Dickinson (1995), 296.

[56]. Elvino Brosio and Renato Barbieri, Nuclear Magnetic Resonance in the Analysis of Dairy Products, *Reviews in Analytical Chemistry* (1996) **15** (4), 273.

[57]. A.M. Gil, P.S. Belton and B. P. Hills, Applications of NMR to Food Science in *Annual Report on NMR Spectroscopy* (1993) Vol. **32,**2.

[58]. Douglas A. Skoog and James J. Leary, *Principles of Instrumental Analysis*, 4th Edition (1992), Harcourt Brace College Publishers, 314.

[59]. Bruker, NMS User's Manual: Bruker Analytsche Messtechnik (1996).

[60]. P. T. Callaghan, *Aust. J. Phys.* (1984) **37**, 359.

[61]. Erwin Kreyszig, *Advanced Engineering Mathematics*. (Seventh Edition), John Wiley $ Sons, INC. (1996) 225~240.

[62]. M. Minsky, Microscopy Apparatus, *United States Patent* 3,013,467. Dec.1961.

[63]. M. Petran, M. Hadravsky, D. Egger and R. Galambos, *J. Opt. Soc. Am*, (1968) **58,** 661.

[64]. C.J.R. Sheppard, J.N. Cannaway, D. Walsh and T. Walson, Scanning optical microscope for the inspection of electronic devices. *Microcircuit Engineering Conference* (1978), Cambridge.

[65]. G.J. Brakenhoff, Imaging modes of confocal scanning light microscopy. *J. Microsc.* (1979) **117**, 233.

[66]. Shotton, D. M., *J. Cell Sci.* (1989) **94,** 175.

[67]. Wilson, T., *Trends Neurosci.* (1989) **12,** 486.

[68]. James Richard Stephenson, Proton NMR Studies of Butter, B.Sc. (Honours) report, Massey University 1996.

[69] Ming Lu, Distribution of Water Droplet Sizes in Butters, P.G.Diploma report, Massey University 1997.

7.0 Appendix

Appendix 1. The Hahn spin-echo experiment and the Hahn spin-echo experiment with pulsed field gradient

1. Hahn spin-echo experiment

If all the nuclei are in the same field (i.e. in a completely homogeneous field) then the NMR signal after a 90^0 pulse decays exponentially with time constant T_2 according to the equation:

$$\boldsymbol{M}_t = \boldsymbol{M}_0 \cdot exp\,(-\,t\,/\,T_2)$$

In practice, the perfect field condition is almost never achieved. The field is much more often inhomogeneous. For example, some nuclei "see" a higher field ($B_0 + \Delta B$) and some a lower field ($B_0 - \Delta B$) than the average B_0. Thus, within the sample there are nuclei with various resonance frequencies (ω, $\omega+\Delta\omega$, $\omega-\Delta\omega$). After the 90^0 pulse is switched off all nuclei have the same phase. However, after a time t, phase differences are present as a result of the different precession speeds. These differences reduce the signal since this depends on the vector sum of the magnetic moments of all the rotating nuclei and the maximum signal is only obtained when all the individual components are parallel.

If the field distribution is rectangular (i.e. there is a linear field gradient across the sample) then the signal is described to a first approximation by

$$\boldsymbol{M}_t = \boldsymbol{M}_0 \cdot [\,sin\,(\,\gamma \cdot \Delta B \cdot t\,)\,/\,\gamma \cdot \Delta B \cdot t\,]$$

Where ΔB is the largest deviation of the field from the average value.

Provided that the individual nuclei do not change their positions there is a fixed relationship between their phases. In other words, the dephasing of the magnetization is, under the above condition, a reversible process. With a 180^0 pulse applied, after a time τ one can reverse the motion of the spins and cause the nuclear moments to refocus after a time 2τ. They then dephase again. This process is referred to as a ' spin-echo ' or ' Hahn-echo '.

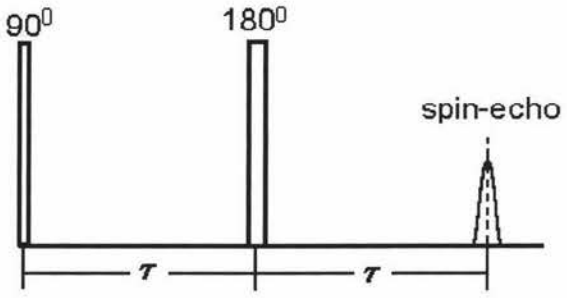

We assume that protons are in the magnetic field B_0 and the net magnetisation M is along the Z-axis. The 90^0 pulse puts M in the direction of the Y-axis (A). Under the influence of some inhomogeneity of the magnetic field magnetisation starts to " fan out " in the X-Y plane at that moment (B). This is because M is composed of many magnetic moments which do not all have the same velocity. There are moments with a lower and moments with higher rotation speed than the average and they get out of phase, we call this " fanning-out ".

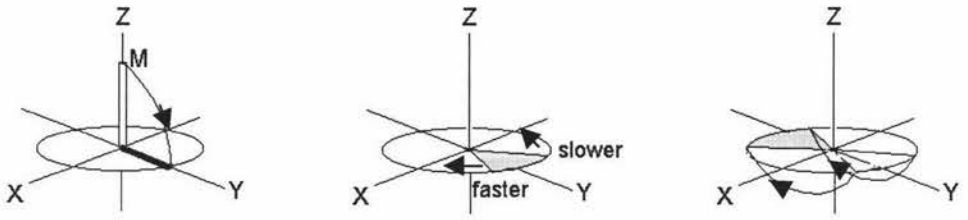

A B C

Suppose we have arrived at time τ, then we apply the 180^0 pulse. All signals will therefore rotate 180^0 round the X-axis and hence also get into the X-Y plane again (C). The protons that moved faster during fanning-out than the average, move clockwise and still do this after 180^0 pulse. Likewise the slower ones will still move anti-clockwise after the 180^0 pulse (D). Then a situation is reached in which the protons will refocus, the fan closes (E).

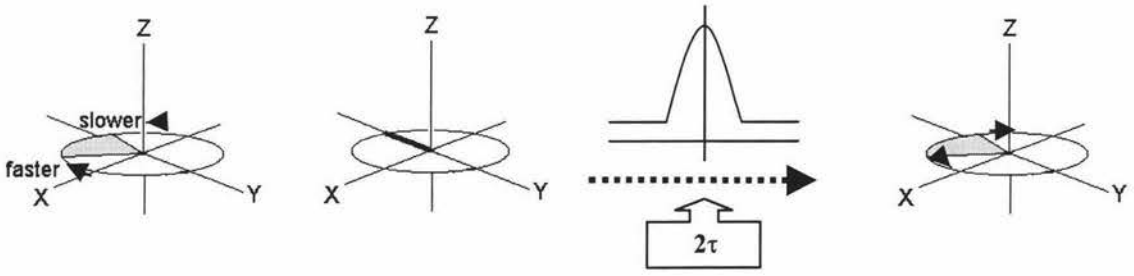

D E F G

Our observation of the signals is directed along the Y-axis and we see this refocussing as an echo-signal on our oscilloscope. At time 2τ refocussing is completed and the top of echo has been reached (F). After time 2τ there is fanning-out again and we see that signal height decreases again (G).

2. Hahn spin-echo experiment with field gradient pulse

What a field gradient is, has already been stated in the introduction. If we apply such a gradient for a short time, we speak of field gradient pulses (fgp). A Miniso operating at 20 MHz proton-resonance has a permanent magnet with a strength of about 0.5 T. A gradient in the magnet field strength is expressed in Tesla per meter (T / m).

The field gradient in our Minispce operates round the positive Z-axis. This means that gradient pulses can move a vector in the X-Y plane over specific angle (A). It should be borne in mind that the angle increases with the gradient strength or if the fgp takes a longer time. In the B, three axes of the rotating frame in combination with the phenomenon that exists along each axis.

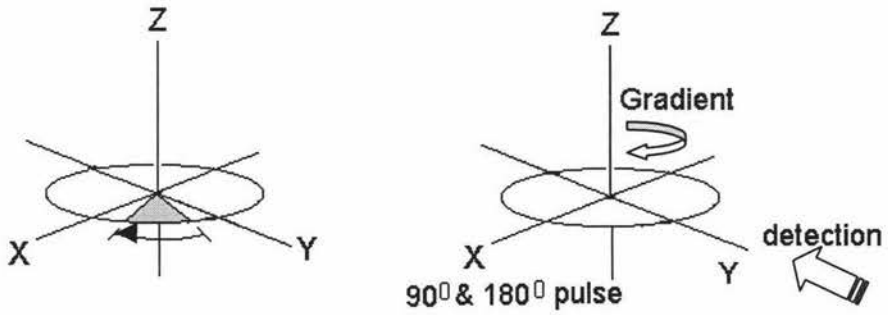

A B

The pulse-sequence of the Hahn spin-echo experiment with field gradient pulses look as follows:

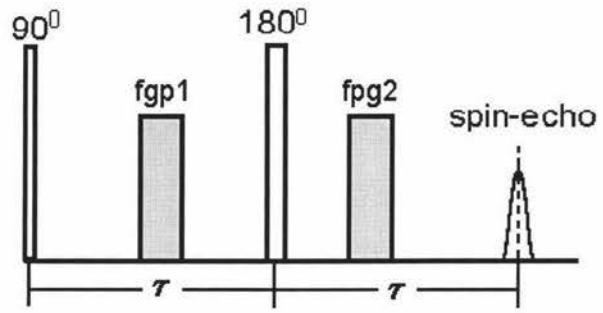

The first field gradient pulse is between the 90^0 and 180^0 pulses. The second has been put after the 180^0 pulse, but of course before the point of time when we expect the echo signal. Using the pulse sequence shown above we are able to determine diffusion coefficients. However, for the sake of clarity of the story we assume in the explanation below that there is no diffusion.

The pulse sequence starts at the 90^0 pulse (C) and we have seen a few times already that the vector is tipped over to the Y-axis and starts to fan out in the X-Y plane (D). Because the " fan " consists of many vectors we can focus our attention on one of them for use in the further explanation (E).

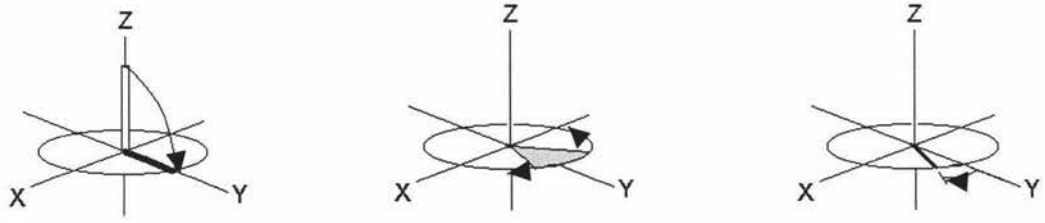

C D E

Now as an example, observe the three axes systems that are present in various places in the sample. Of each " fan " we consider only that vector which has succeeded in gaining a lead of some 30^0 over its average co-vectors at the time fgp1 starts. The three (F, G, H) are present in various places in the magnetic field and are subject to various gradient strengths. The result will be that when

fgp1 is finished they all point into a different direction, because they have rotated round the Z-axis through various angles.

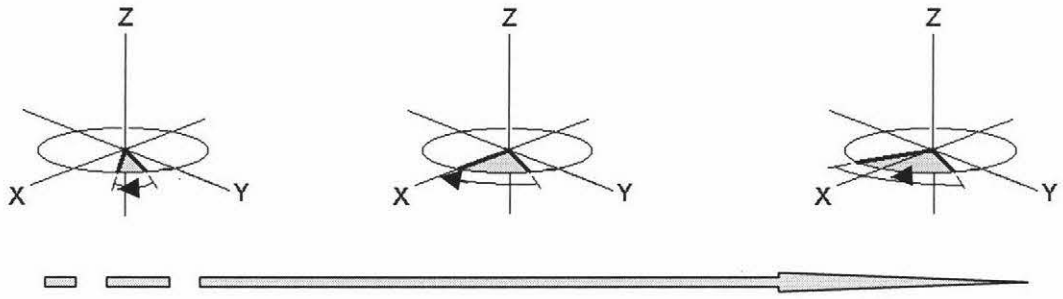

Gradient puls 1

F G H

At the 180^0 pulse which follows now they are rotated round the X-axis through an angle of 180^0 (I, J, K) and then enter the positions shown.

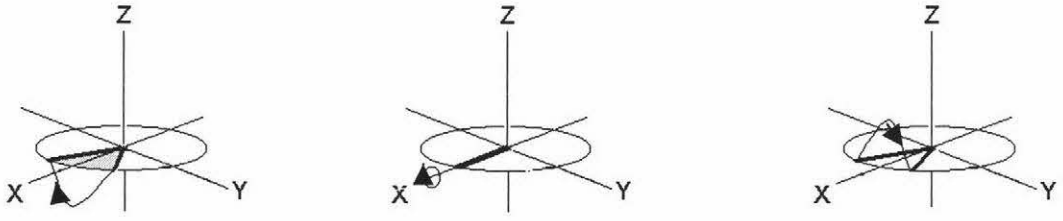

I J K

The second field gradient pulse will displace the vectors through the same angle as fgp1 did. Then they get into a position of 30^0 before the Y-axis (L, M, N). The advance with respect to the other vectors meanwhile goes on (and went on) normally and at time 2τ they will all be situated on the Y-axis. Because the same story applies to the vectors that lagged behind, the result is that also these lie on the Y-axis at time 2τ. At time 2τ the " fan " closes which we detect as an echo.

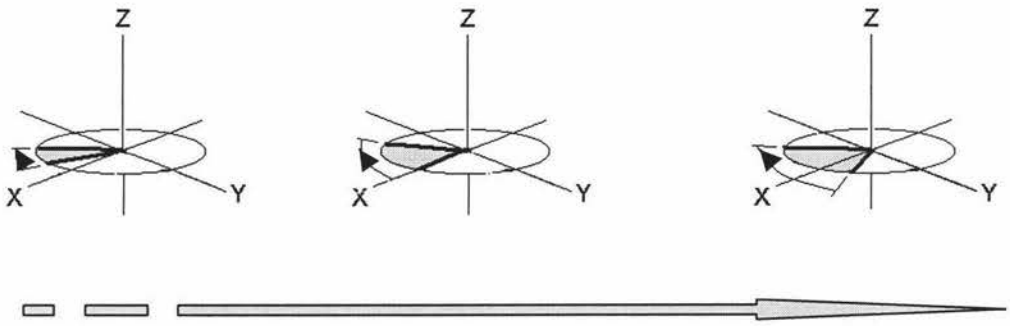

Gradient Pulse 2

L M N

We have seen now that if the protons experience the same gradient strength at the second fgp, there will be another complete focussing. This means that if the end having the same height as when this experiment had been done without field gradient pulses. So we do not detect an echo weakening if the protons do not change place.

What happens if we do enable the water molecules to take part in diffusion is only a short story. In the drawing below two axes systems have been drawn which are present in different places in the sample. In the following example these two will change places and then we see what happens. The Hahn spin-echo experiment has already started, the 90^0 pulse has done its duty. The vectors have already fanned out in the X-Y plane and our attention is focussed on the one vector in each " fan " which is 30^0 ahead of the average vector. In the drawing below these vectors which are ahead have been drawn " open ". Under the influence of fgp1 they are both displaced in the X-Y plane through different angles.

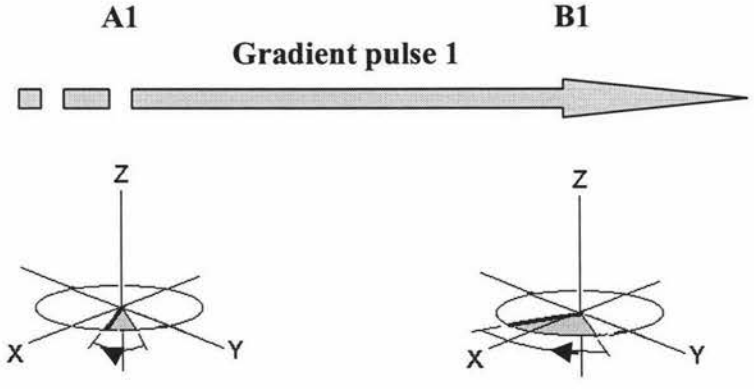

Before it is the turn of fgp2, in the drawing below the 180^0 pulse does its job. Up to the story is the same as the previous one, if we had not agreed upon the two systems would change place.

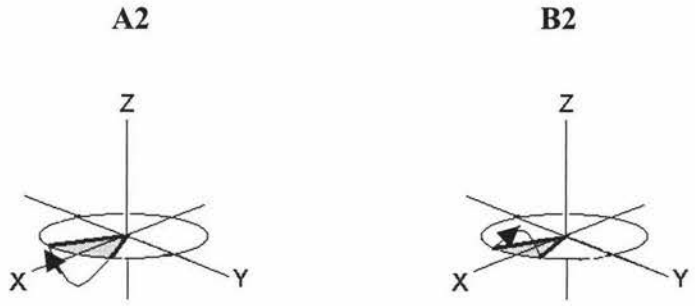

If fgp2 does its job, each axes system in its new position experiences a different gradient strength than during fgp1. So the vectors will turn through an angle different from the one before. The drawing shows the situation after fgp2.

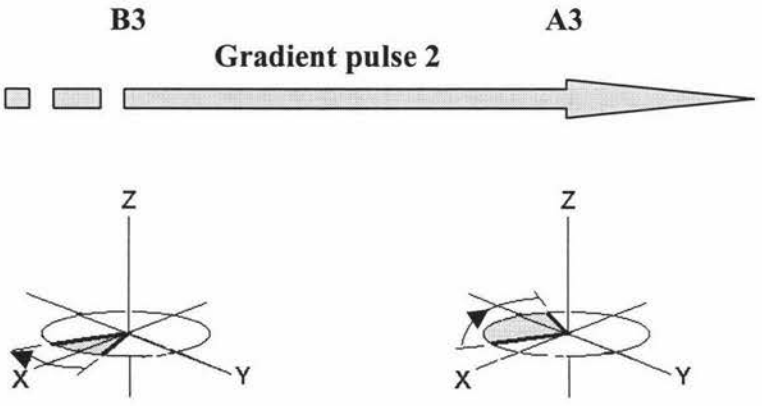

During the entire process the vectors have continued getting ahead. When this is completed the situation at time 2τ is as shown in the drawing. Because we are only able to detect along the Y-axis only their projections on the Y-axis contribute to the echo height. In the drawing below the diffusion we see an attenuated echo on the oscilloscope.

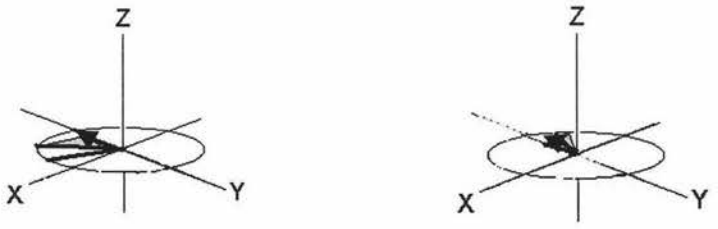

APPENDIX

Appendix 2. Self-diffusion coefficients from aqueous phases of samples

1. Water (0.125% $CuSO_4 \cdot 5H_2O$ in deionized water)

Sample	Amp. of Gradinet	D(10E-9*m*m/s)	Mean
06 / 06 / 1997			
W - 50 - 1 - 1	50	1.32841	
W - 50 - 1 - 2		1.33141	1.3299
W - 100 - 1 - 1	100	1.31962	
W - 100 - 1 - 2		1.30327	1.3115
11 / 06 / 1997			
W - 50 - 1 - 1	50	1.31847	
W - 50 - 1 - 2		1.33079	1.3246
W - 100 - 1 - 1	100	1.30800	
W - 100 - 1 - 2		1.30997	1.3089
12 / 01 / 1998			
W - 50 - 1 - 1	50	1.30870	
W - 50 - 1 - 2		1.29943	1.3041
W - 100 - 1 - 1	100	1.33210	
W - 100 - 1 - 2		1.32616	1.3291
13 / 01 / 1998			
W - 50 - 1 - 1	50	1.31096	
W - 50 - 1 - 2		1.33252	1.3217
W - 100 - 1 - 1	100	1.30946	
W - 100 - 1 - 2		1.32281	1.3161
06 / 04 / 1998			

W - 50 - 1 - 1	50	1.28809	
W - 50 - 1 - 2		1.33031	
W - 50 - 1 - 3		1.32248	
W - 50 - 1 - 4		1.32426	1.3132
W - 100 - 1 - 1	100	1.33585	
W - 100 - 1 - 2		1.33182	
W - 100 - 1 - 3		1.32633	
W - 100 - 1 - 4		1.32714	1.3303
23 / 04 1998			
W - 50 - 1 - 1	50	1.30828	
W - 50 - 1 - 2		1.29363	1.3010
W - 100 - 1 - 1	100	1.32660	
W - 100 - 1 - 2		1.32070	1.3237
27 / 04 1998			
W - 50 - 1 - 1	50	1.26624	
W - 50 - 1 - 2		1.30179	1.2990
W - 100 - 1 - 1	100	1.32505	
W - 100 - 1 - 2		1.32653	1.3258

2. Aqueous Phase extracted from STD - 1 butter

Sample	**Amp. of Gradinet**	**D(10E-9*m*m/s)**	**Mean**
06 / 06 / 1997			
STD - 1 - 50 - 1 - 1	50	0.85437	
STD - 1 - 50 - 1 - 2		0.87075	0.8521
STD - 1 - 50 - 2 - 1		0.84342	
STD - 1 - 50 - 2 - 2		0.83974	

STD - 1 - 100 - 1 - 1	100	0.81695	
STD - 1 - 100 - 1 - 2		0.83209	0.8236
STD - 1 - 100 - 2 - 1		0.83299	
STD - 1 - 100 - 2 - 2		0.82224	
12 / 01 / 1998			
STD - 1 - 50 - 1 - 1	50	0.80430	
STD - 1 - 50 - 1 - 2		0.76076	0.7825
STD - 1 - 100 - 1 - 1	100	0.76891	
STD - 1 - 100 - 1 - 2		0.77072	0.7748
13 / 01 / 1998			
STD - 1 - 50 - 1 - 1	50	0.76685	
STD - 1 - 50 - 1 - 2		0.80871	0.7878
STD - 1 - 100 - 1 - 1	100	0.77377	
STD - 1 - 100 - 1 - 2		0.77932	0.7766

3. Aqueous Phase extracted from DRI-16 butter

Sample	**Amp. of Gradinet**	**D(10E-9*m*m/s)**	**Mean**
12 / 01 /1998			
DRI -16 - 50 - 1 - 1	50	0.83746	
DRI -16 - 50 - 1 - 2		0.87030	0.8539
DRI -16 - 100 - 1 - 1	100	0.85716	
DRI -16 - 100 - 1 - 2		0.86336	0.8602
13 / 01 / 1998			
DRI -16 - 50 - 1 - 1	50	0.95590	
DRI -16 - 50 - 1 - 2		0.89109	0.9235
DRI -16 - 100 - 1 - 1	100	0.86520	
DRI -16 - 100 - 1 - 2		0.87316	0.8692

4. Aqueous Phase extracted from MAR - 1 margarine

Sample	Amp. of Gradinet	D(10E-9*m*m/s)	Mean
06 / 06 1997			
MAR - 1 - 50 - 1 - 1	50	1.05757	
MAR - 1 - 50 - 1 - 2		1.08405	
MAR - 1 - 50 - 2 - 1		1.04324	
MAR - 1 - 50 - 2 - 2		1.04626	1.0578
MAR -1 - 100 - 1 - 1	100	1.03707	
MAR -1 - 100 - 1 - 2		1.04635	
MAR -1 - 100 - 2 - 1		1.01697	
MAR -1 - 100 - 2 - 2		1.01601	1.0291
06 / 04 1998			
MAR - 1 - 50 - 1 - 1	50	1.14393	
MAR - 1 - 50 - 1 - 2		1.12833	1.1245
MAR - 1 - 50 - 2 - 1		1.14286	
MAR - 1 - 50 - 2 - 2		1.12775	
MAR -1 - 100 - 1 - 1	100	1.15399	
MAR -1 - 100 - 1 - 2		1.15766	1.1462
MAR -1 - 100 - 2 - 1		1.15251	
MAR -1 - 100 - 2 - 2		1.14212	

5. Fresh Milk

Sample	Amp. of Gradinet	D(10E-9*m*m/s)	Mean
11 / 06 / 1997			
F-milk - 50 - 1 - 1	50	1.05811	
F-milk - 50 - 1 - 2		1.07019	1.0436
F-milk - 50 - 2 - 1		1.03725	
F-milk - 50 - 2 - 2		1.00900	

F-milk - 100 - 1 - 1	100	1.03111	
F-milk - 100 - 1 - 2		1.03560	1.0407
F-milk - 100 - 2 - 1		1.05836	
F-milk - 100 - 2 - 2		1.03781	

8. Mixed Milk*

Sample	**Amp. of Gradinet**	**D(10E-9*m*m/s)**	**Mean**
11 / 06 / 1997			
F-milk - 50 - 1 - 1	50	1.24659	
F-milk - 50 - 1 - 2		1.15113	1.1681
F-milk - 50 - 2 - 1		1.14905	
F-milk - 50 - 2 - 2		1.12578	
F-milk - 100 - 1 - 1	100	1.10330	
F-milk - 100 - 1 - 2		1.09175	1.1029
F-milk - 100 - 2 - 1		1.11493	
F-milk - 100 - 2 - 2		1.10171	

* The sample of skim milk powder comes from NZMAF

APPENDIX

Appendix 3. The images of samples by Laser Scanning Confocal Microscopy

1. STD - 1 butter

(1). 63 X object, Nile Red in propylene glycol, Copper dish.

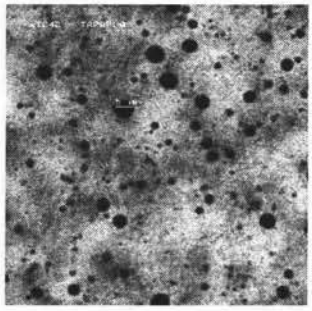

X1242A

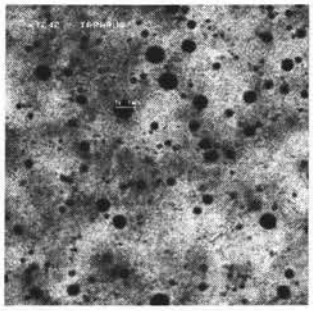

X1242B

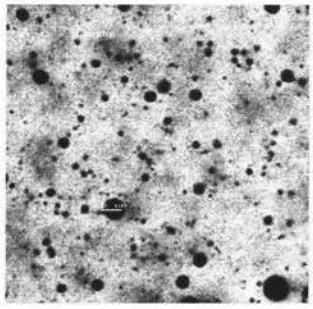

X1242C

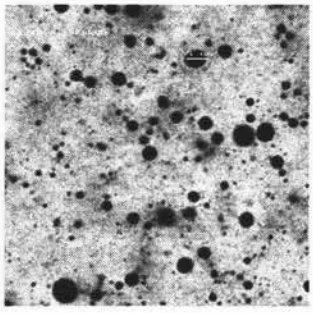

X1242D

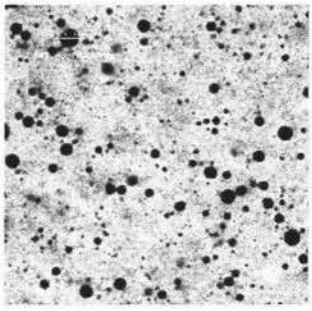

X1242E

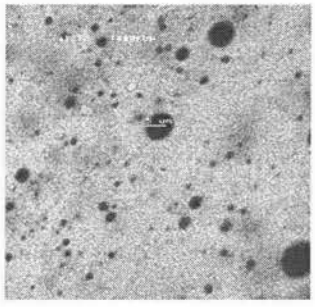

X1242F

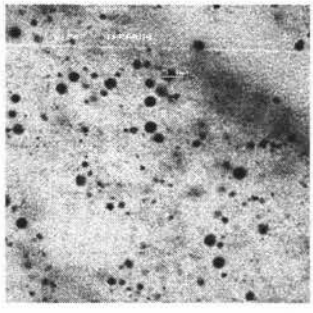

X1242G

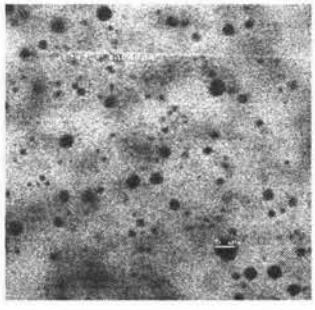

X1242H

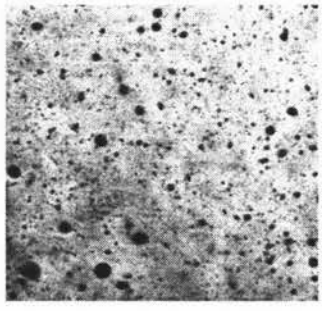

X1242I

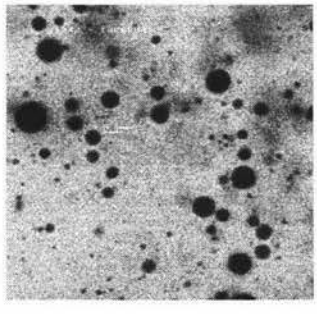

X1242J

(2). 40 X object, Nile Blue in propylene glycol, Copper dish.

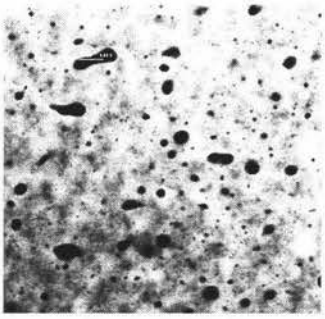

X1307B10

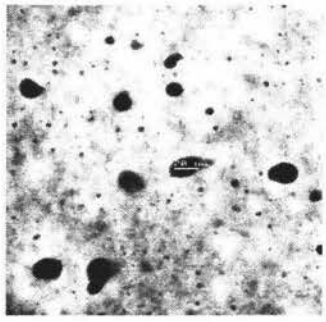

X1307B20

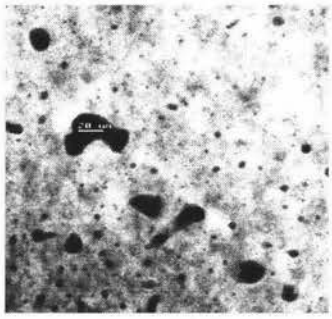

X1307B30

(3). 40 X object, Nile Red in propylene glycol, Copper dish.

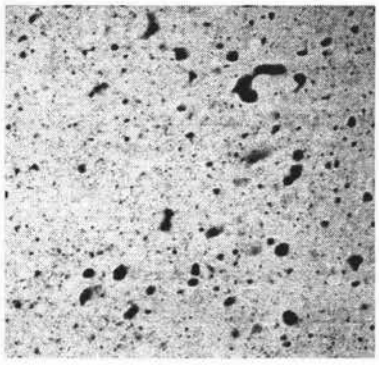

X1307R1

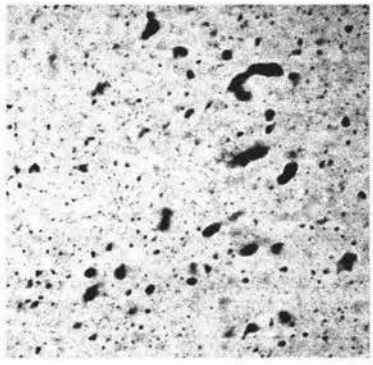

X1307R2

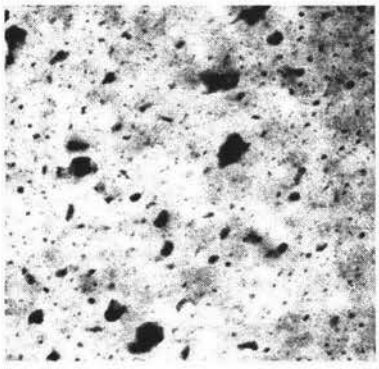

X1307R3

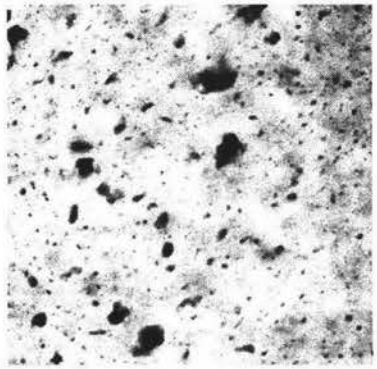

X1307R4

(4). 40 X object, Nile Red in propylene glycol, Copper dish and sample were dipped in dye solution to stain the sample.

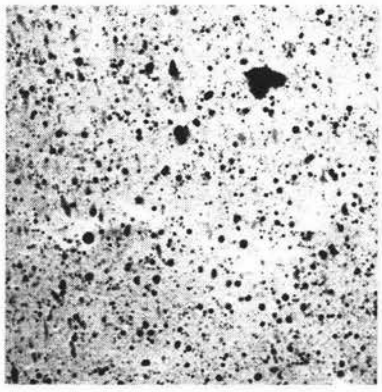

X1307B10

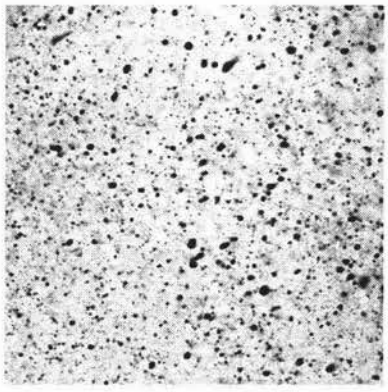

X1307B20

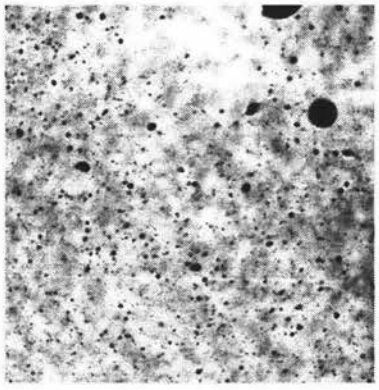

X1307B30

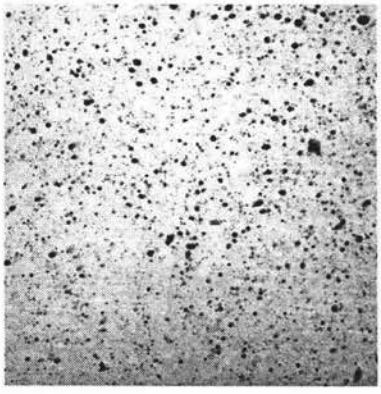

X1307B40

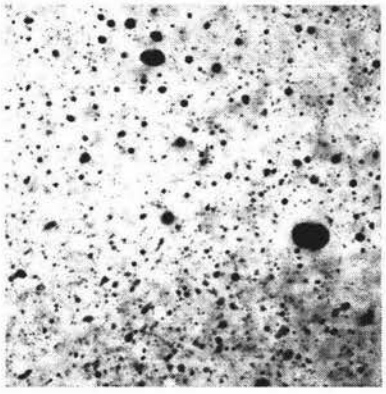

X1307B50

APPENDIX

Appendix 3. The images of samples by Laser Scanning Confocal Microscopy

2. DRI-24 butter

(1). 63 X object, Nile Red in propylene glycol, Copper dish.

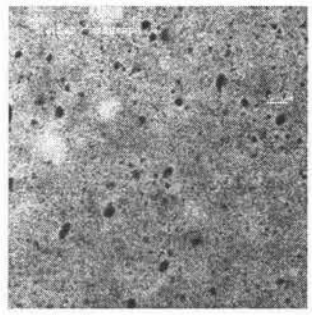

X1243A

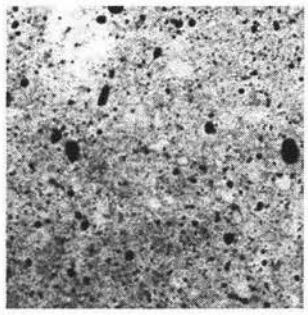

X1243B

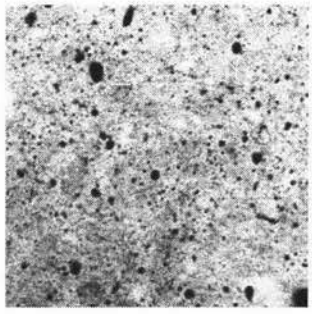

X1243C

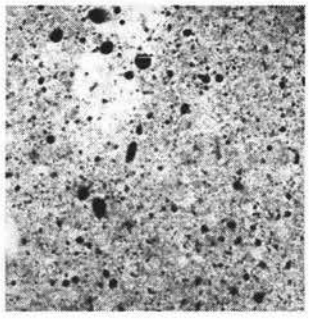

X1243D

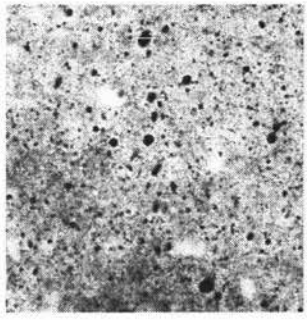

X1243E

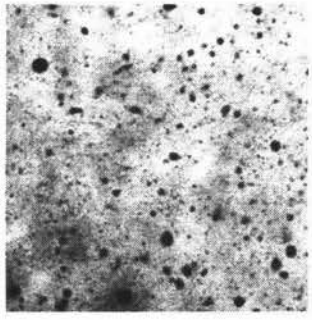

X1243F

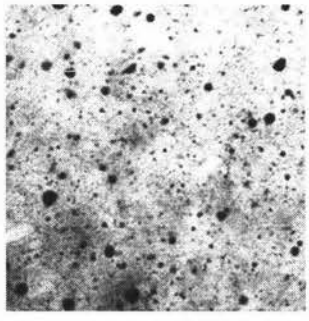

X1243G

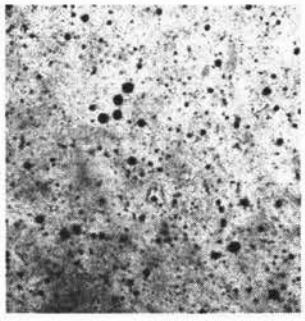

X1243H

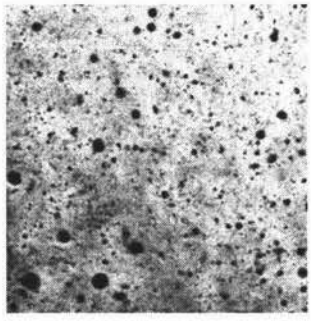

X1243I

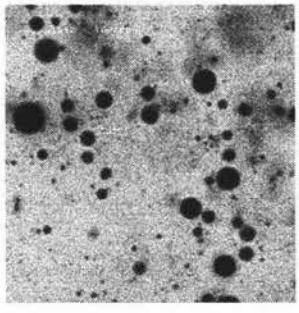

X1243J

(2). 40 X object, Nile Red in propylene glycol, Copper dish and sample were dipped in dye solution to stain the sample.

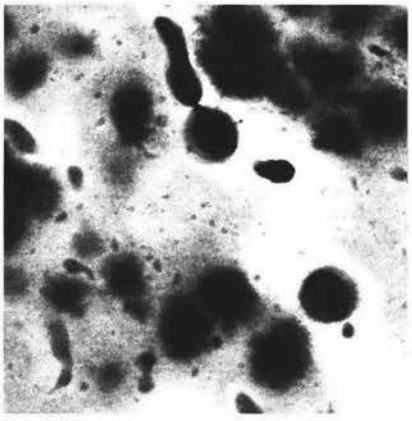

X1308R10

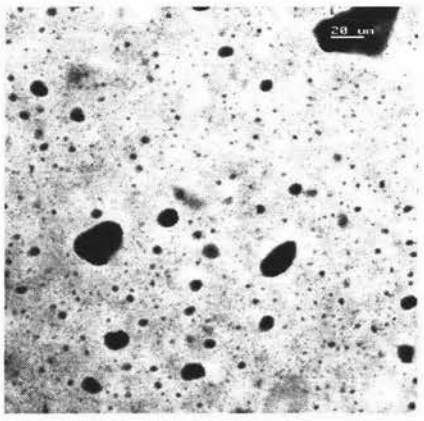

X1308R20

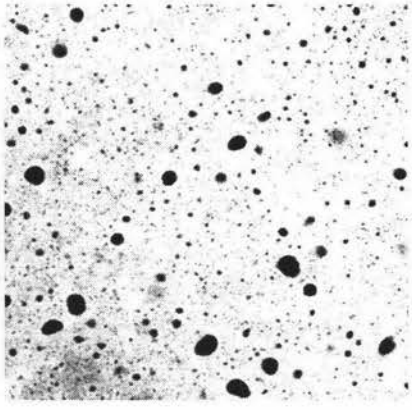

X1308R30

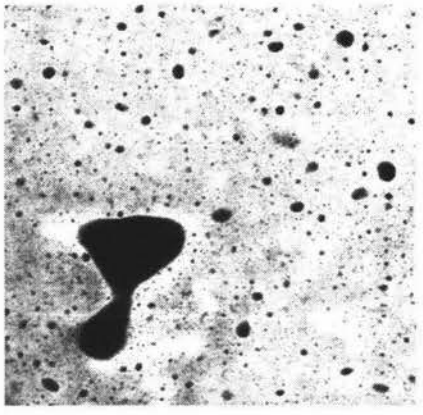

X1308R40

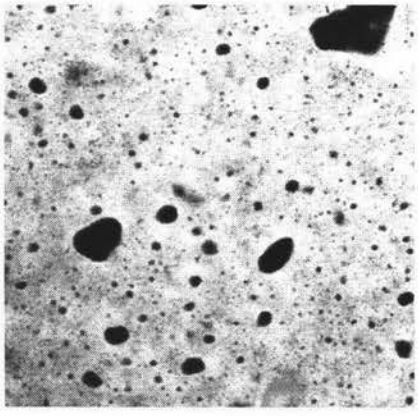

X1308R50

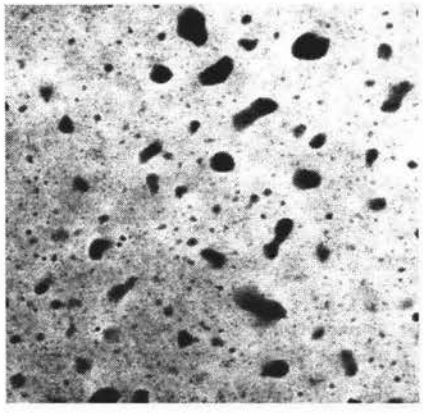

X1308R60

APPENDIX

Appendix 3. The images of samples by Laser Scanning Confocal Microscopy

3. MAR-1 margarine

63 X object, Nile Red in propylene glycol, Copper dish.

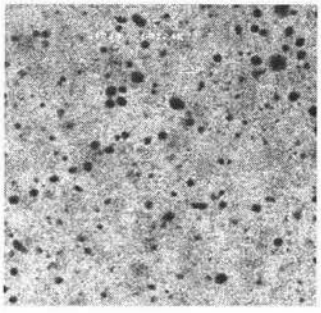

X1244A

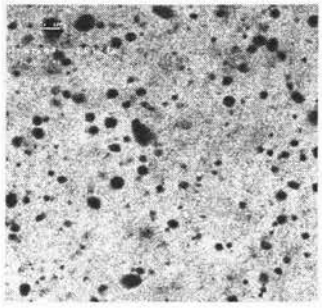

X1244B

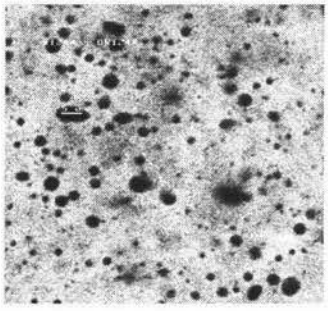

X1244

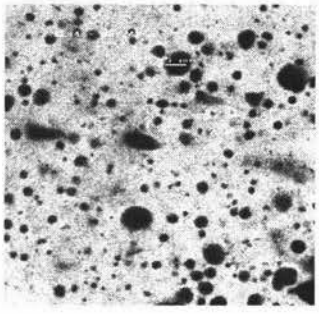

X1244D

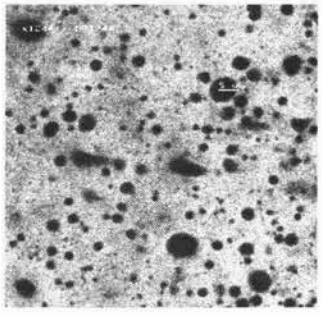

X1244E

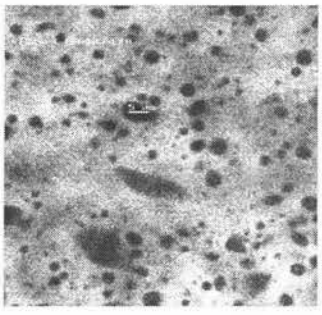

X1244F

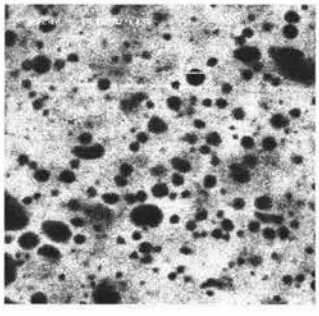

X1244G

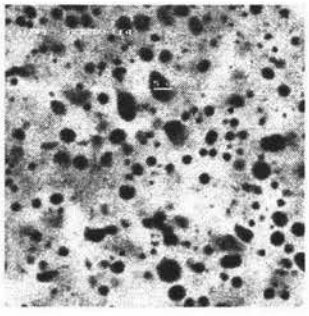

X1244H

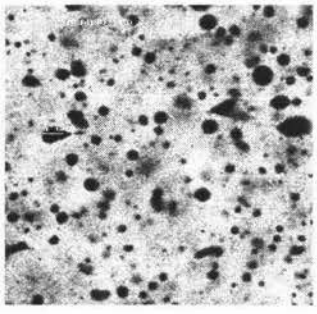

X1244I

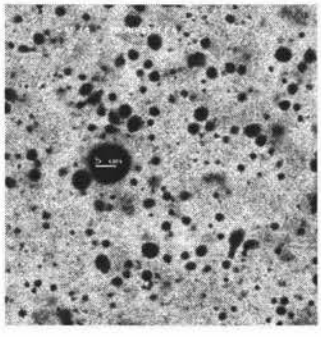

X1244J

APPENDIX

Appendix 3. The images of samples by Laser Scanning Confocal Microscopy

4. STD - 2 butter

(1). 16 X object, Nile Red in propylene glycol, Copper dish.

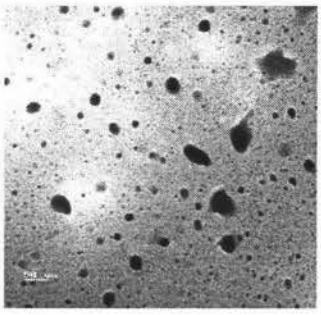

X1393N00

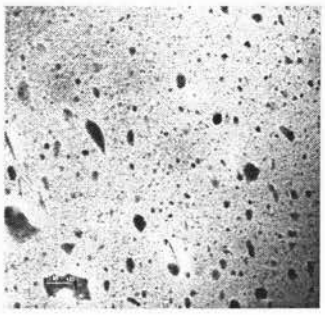

X1393N10

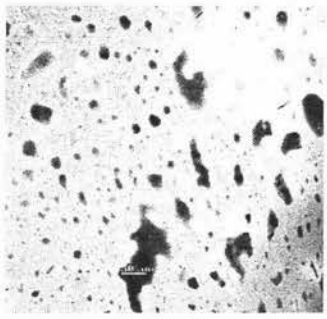

X1393N20

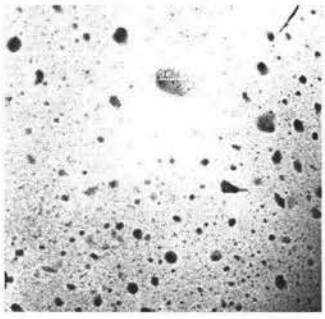

X1393N30

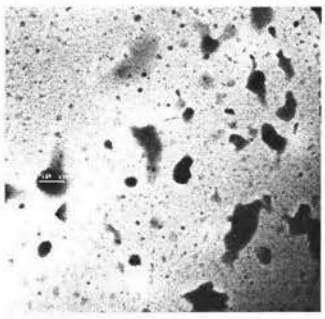

X1393N40

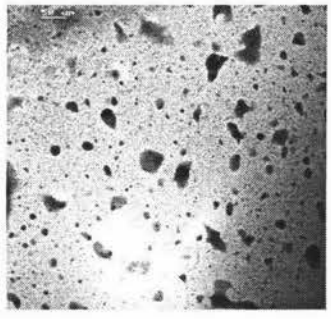

X1393N50

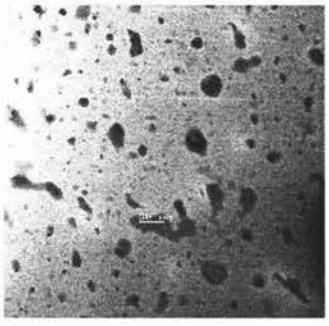

X1393N60

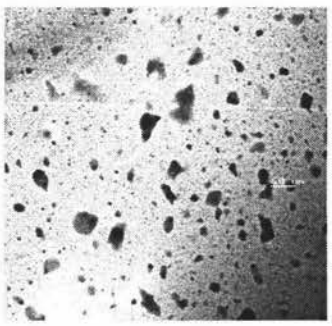

X1393N70

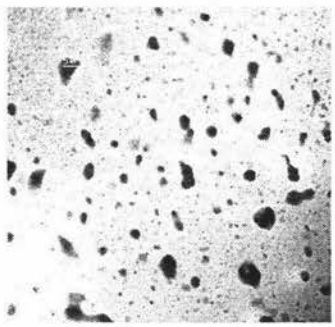

X1393N80

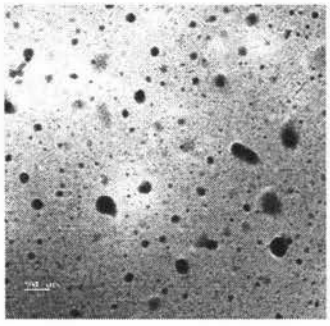

X1393N90

(2). 40 X object, Nile Red in propylene glycol, Copper dish.

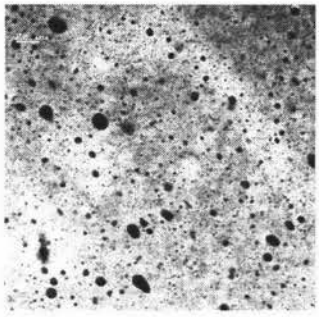

X1393B00

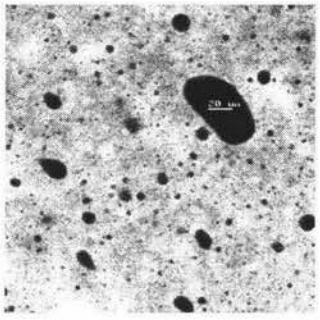

X1393B10

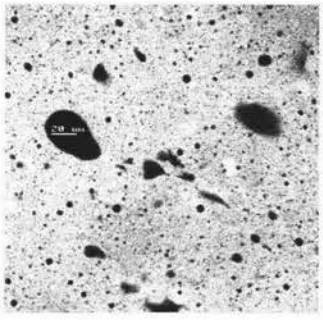

X1393B20

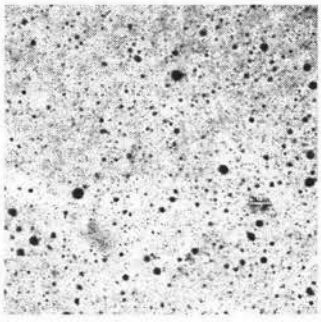

X1393B30

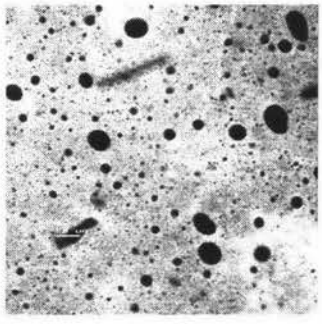

X1393B40

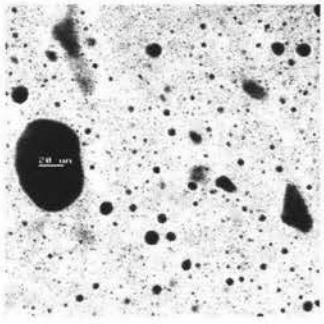

X1393B50

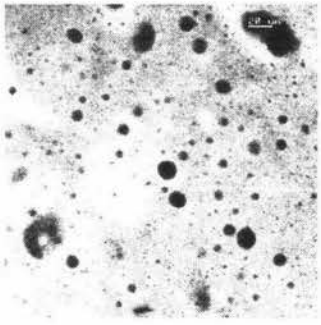

X1393B60

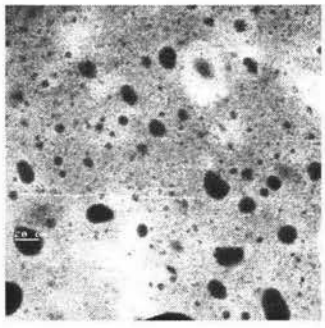

X1393B70

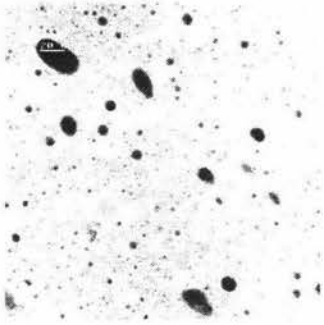

X1393B80

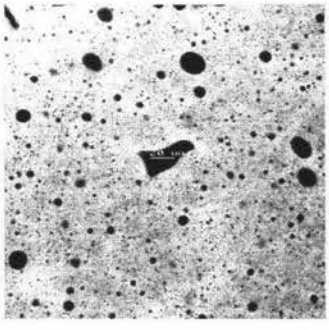

X1393B90

APPENDIX

Appendix 3. The images of samples by Laser Scanning Confocal Microscopy

5. SPE-2 butter

(1). 16 X object, Nile Red in propylene glycol, Copper dish.

X1394N00

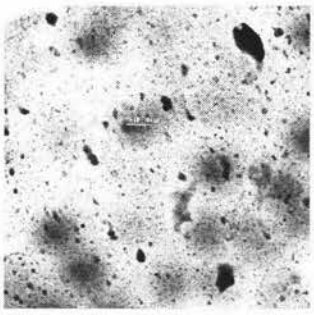

X1394N10

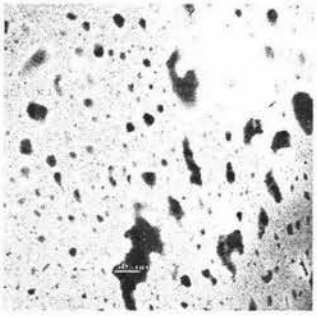

X1394N20

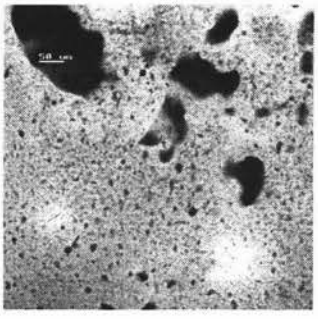

X1394N30

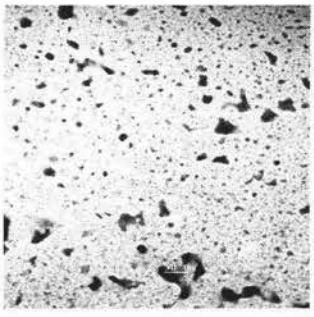

X1394N40

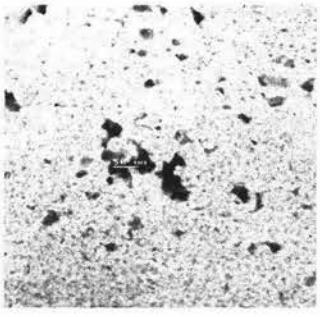

X1394N50

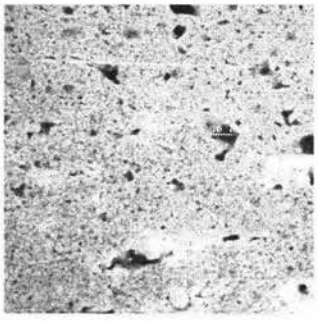

X1394N60

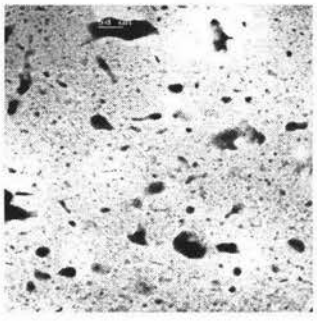

X1394N70

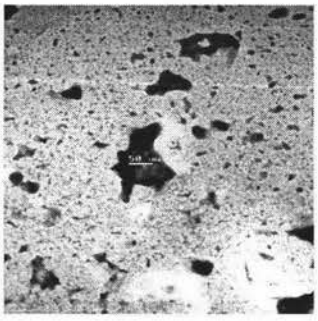

X1394N80

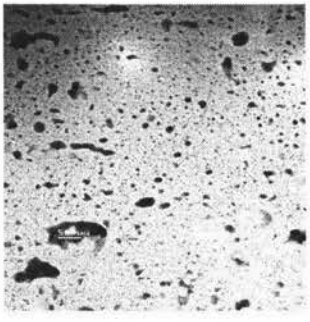

X1394N90

(2). 40 X object, Nile Red in propylene glycol, Copper dish.

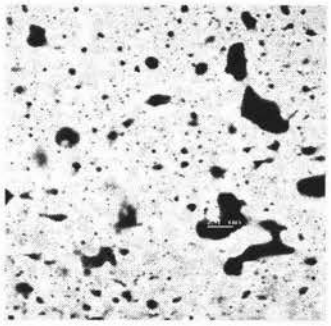

X1394B00

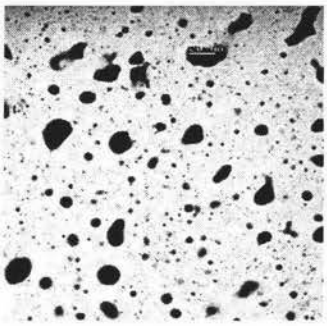

X1394B10

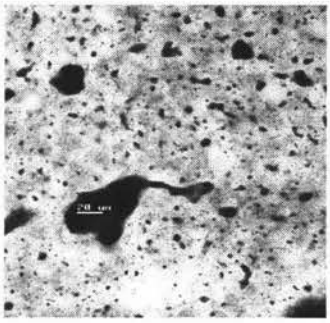

X1394B20

X1394B30

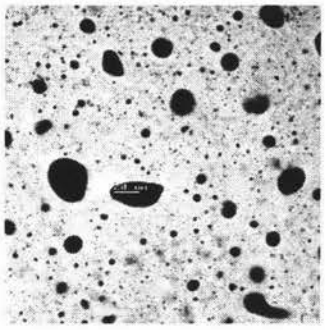

X1394B40

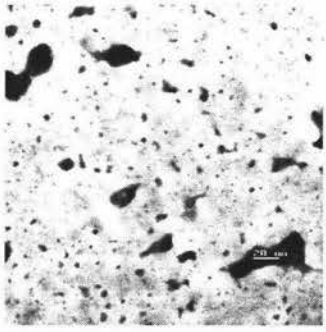

X1394B50

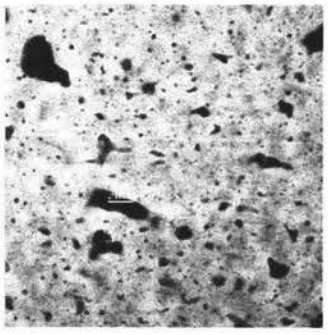

X1394B60

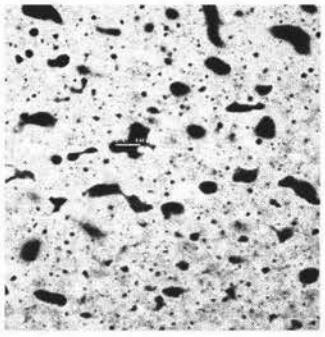

X1394B70

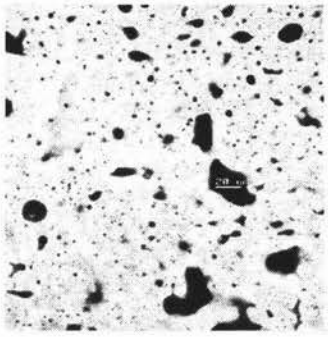

X1394B80

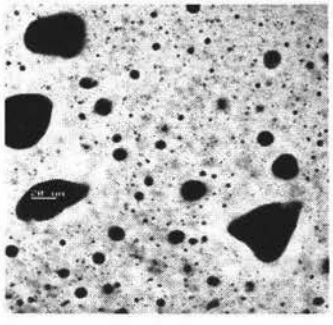

X1394B90

APPENDIX

Appendix 4. Conversion between the cut diameters and the diameters of water droplets

The cut diameter of water droplets of a sample is obtained from CSLM. To compare it with the distribution of water droplet sizes of the sample from PFG-NMR, cut diameters of the droplets need to be conversed in to diameters of water droplets. The calculation is shown in the following.

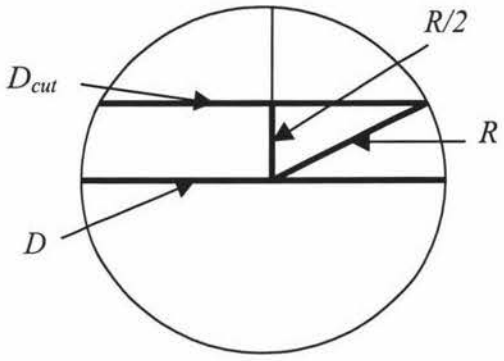

A droplet

Where D_{cut} is the mean cut diameter of the droplet, D is diameter of the droplet, and R is a radius of the droplet.

$$(D_{cut}/2)^2 + (R/2)^2 = R^2$$

$$D_{cut} = 2\,(R^2 - (R/2)^2)^{1/2} = 2\,(3R^2/4)^{1/2} = (3)^{1/2}\,R = ((3)^{1/2}/2)\,D = 0.87\,D$$

After the calculation, distribution of the droplet numbers has been assumed the statistical meaningful number of droplets. When the numbers of droplets with larger diameter are calculated, bigger deviation may be given because the number of bigger droplets is small.